Order Number 9108126

Integral formulations with special kernels for a composite panel with an elliptical hole or a crack

Kamel, Michael, Ph.D.

City University of New York, 1990

U·M·I
300 N. Zeeb Rd.
Ann Arbor, MI 48106

A

INTEGRAL FORMULATIONS WITH SPECIAL KERNELS FOR A COMPOSITE PANEL WITH AN ELLIPTICAL HOLE OR A CRACK

by

MICHAEL KAMEL

A dissertation submitted to the Graduate Faculty in Engineering in partial fulfillment of the requirements for the degree of Doctor of Philosophy, The City University of New York.

1990

This manuscript has been read and accepted for the Graduate Faculty in Engineering in satisfaction of the dissertation requirement for the degree of Doctor of Philosophy.

June 19, 1990
Date

Benjamin Been-Ming Liaw
Professor Been-Ming Liaw
Chair of Examining Committee

6/19/1990
Date

Gerard G. Lowen
Professor Gerard G. Lowen
Executive Officer

Professor Been-Ming Liaw

Professor Steven C. Cowin

Professor Feridun Delale

Professor Mumtaz K. Kassir

Professor Ali M. Sadegh

Professor Toshio Nakamura
(SUNY at Stony Brook)

Supervisory Committee

The City University of New York

ABSTRACT

INTEGRAL FORMULATIONS WITH SPECIAL KERNELS FOR A COMPOSITE PANEL WITH AN ELLIPTICAL HOLE OR A CRACK

by

Michael Kamel

Advisor: Professor Been-Ming Liaw

Complex variable method is used to obtain the fundamental solutions for an infinite anisotropic plate with an elliptical hole. The plate is loaded by an arbitrarily positioned point force and/or concentrated moment. Fracture analysis is performed by setting the length of the minor axis of the ellipse equal to zero so that the elliptical hole is reduced into a crack. Using the principle of superposition, any set of general loadings applied anywhere in the domain can be analyzed with the proposed fundamental solutions. A boundary integral equation approach then is developed incorporating the derived fundamental solutions. This approach is used to determine stress intensity factors for cracks in a linearly elastic, anisotropic plate in the presence of a curvilinear boundary. Among others, the problems of cracks emanating from a curvilinear hole in an anisotropic plate, cracks in anisotropic solid disks, and interaction between a crack and a hole in an anisotropic plate are considered. Numerical results are obtained for various loading conditions in each case and are compared with known solutions where available.

The boundary integral equation developed here extends only over that portion of the boundary not including the surface of the crack,

since the boundary conditions on the crack surface have been already incorporated into the fundamental solutions. Thus, excellent accuracy can be obtained and the labor involved in preparing the computer algorithm is minimized as compared with other numerical methods which require to model the crack as part of the boundary. The fundamental solutions obtained here are for a plane, homogeneous, anisotropic body containing a single elliptical hole or a crack. Problems involving more than one hole or crack or more than one material could, in principle, be solved by dividing the region into homogeneous sections, each enclosing only one hole or crack. The continuity conditions are then enforced along the dividing boundaries.

The excellent accuracy obtained for the numerous example problems considered, paves the way for further applications of the proposed fundamental solutions. The possible avenues of future applications are numerous. Of the foreseeable application areas, problems related to laminated anisotropic panels, the study of fracture process zone (FPZ) ahead of a crack-tip in a composite plate, and the analysis of stiffened composite panels containing cracks or holes seem well suited. Many of these possible new applications can be of significant value to the structural analysts.

ACKNOWLEDGMENTS

The author would like to express his sincere gratitude and appreciation to his advisor, Professor Been-Ming Liaw, for his guidance and assistance in all phases of this work. He is grateful to the members of his Advisory and Examining Committees, Professors Steven C. Cowin, Feridun Delale, Mumtaz K. Kassir, Ali M. Sadegh, and Toshio Nakamura, for their interest and helpful suggestions. Last but not least, the author would like to gratefully acknowledge Professor Gerard G. Lowen, Executive Officer, Associate Dean, and a dear friend, for his support through-out the author's course of study at the City College of the City University of New York.

TABLE OF CONTENTS

Page

LIST OF TABLES

LIST OF FIGURES

NOMENCLATURE

a,A	Semi-major axis of ellipse or semi-crack length
a_{ij}	(i,j=1,2,6) Components of the compliance matrix (plane stress)
b,B	Semi-minor axis of ellipse
b_{ij}	(i,j=1,2,6) Components of the compliance matrix (plane strain)
K_I,K_{II}	Mode I and mode II stress intensity factors
M	Concentrated moment
P,Q	Vertical and horizontal components of point force
s_1,s_2	Complex roots of the characteristic equation of anisotropy
u,v	Horizontal and vertical components of Displacement
U	The Airy's stress function
x,y	Cartesian coordinates
z^0	The point of application of point force or concentrated moment
z_1,z_2	Additional planes of transformation due to anisotropy
Φ_1,Φ_2	Components of the fundamental solution
σ_{ij}	Stress components in Cartesian coordinates (i,j=x,y)
ζ_j	The corresponding conformally mapped point for z_j (j=1,2)

CHAPTER I

INTRODUCTION

I.1 GENERAL OBJECTIVES

In recent years there has been a steady increase in the application of fiber reinforced composites in primary and secondary aircraft and space vehicle components. Due to their high strength-to-weight and high stiffness-to-weight ratios compared to conventional metallic materials, composites are being used in both strength and stiffness critical structures formerly built with costly metallic alloys. Their attractive properties have also prompted the application of modern composites into other areas of engineering design, such as ground transportation, medical equipment and prostheses, and sporting goods.

Like their isotropic counterparts, components made of composites contain manufacturing defects, i.e. micro-cracks, and man-made elliptical or circular holes created for joining or other purposes. But unlike their isotropic counterparts, since the use of modern composite materials has prevailed only during the past two decades, behavior of these composite components are still not completely understood, especially when they contain stress raisers, such as holes or cracks. This is also due to the fact that composites are heterogeneous in nature and behave in an anisotropic manner so that their formulations are much more involved and complicated than their isotropic counterparts. Stress and failure analysis has, therefore, become an increasingly important issue for design engineers who attempt to use composites. In this dissertation, composite panels

with holes and/or cracks will be studied by complex-variable, integral equation method.

The formulation of plane anisotropic elasticity was given decades ago by Lekhnitskii [1,2] and has been used by many to solve problems involving anisotropic materials. But these solutions, in general, are applicable only to a set of simple geometries (e.g. an infinite plate with an elliptical or a circular hole) and loading conditions (e.g. uniform tension or pure shear). Still there are a large number of fundamentally important problems which either have not been solved because of their complicated loading conditions or unusual geometries, or if they have been solved, their methods of solution are too difficult to follow and too restricted to be generalized. The purpose of this study is to:

(i) derive a set of general fundamental solutions which includes the presence of the hole or the crack,

(ii) to develop a boundary integral formulation incorporating these fundamental solutions,

(iii) identify some of the problems solvable using the integral formulation and to obtain some numerical results for each problem considered, and

(iv) specify some other possible areas of application for the proposed solutions.

After reviewing the basic formulation of anisotropic elasticity in Chapter II, the above mentioned fundamental solutions are derived analytically in Chapter III. The fundamental solutions are for an infinite anisotropic plate containing an elliptical hole or a crack subjected to an arbitrarily positioned point force and/or concentrated moment.

One of the most basic problem areas in numerical fracture mechanics deals with the behavior of a sharp crack in the presence of other boundaries, due to the potential numerical difficulty arisen from the stress singularity at the crack tip. Since the presence of the crack has already been considered in the proposed fundamental solutions, crack problems can be solved easily and effectively once a procedure is found to deal with the additional boundary. This is accomplished through the application of the Boundary Integral Equation technique (BIE) which is formulated in Chapter IV. In BIE, approximation is made on the boundary of the domain rather than the entire field as with the Finite Element Method (FEM). This leads to a coefficient matrix which is of much lower order than that obtained in FEM. BIE is particularly advantageous when the domain is infinitely or semi-infinitely extended. The main limitation of this technique is known to be its inaccuracy near the boundary under consideration. This is due to the fact that the boundary is discretized into elements and error is known to be higher near the discretization. The BIE formulation studied here uses the proposed fundamental solutions of Chapter III as its Green's functions. This incorporates the presence of the crack into the kernel of the integral equations so that very good results are obtained near the hole or the crack. In Chapter V, typical problems involving a crack in the presence of other boundaries are considered and solved using the BIE formulation of Chapter IV.

It should remain clear that the present study is meant to show only a small number of example problems which can be solved using the proposed fundamental solutions and certainly not all the possible applications. The group of application problems considered here

(i.e. a sharp crack in the presence of other boundaries in a composite panel), is presented just to show the diversified applications of the proposed fundamental solutions.

I.2 REVIEW OF OTHER FUNDAMENTAL SOLUTIONS

In the following, a general background and a review of the published works relating to the aforementioned fundamental solutions are presented. The problem of stress concentration around an elliptical hole in an infinite anisotropic plate has been generally formulated using complex-variable method decades ago by Lekhnitskii [1,2] and Savin [3]. Approximate stress analyses have also been conducted by Konish and Whitney [4] for an orthotropic plate containing a circular hole, by Tan [5] for a laminated composite with an elliptical opening, and by Ueng and Lin [6] for two interacting elliptical holes inside a composite laminate. But these approximate analyses can only apply to some special loading cases, such as the uniaxial stretching. Various Green's functions for perforated or cracked plates have also been obtained. Collinear cuts in an isotropic plate was studied by Erdogan [7]. Sih et al. [8], and Embly [9] gave solutions for a normal concentrated force acting on a crack in an orthotropic plate. The fundamental solution for an anisotropic plate containing a straight crack was derived by Snyder and Cruse [10] and also by Clements and Haselgrove [11] using Muskhelishvili's [12] singular integral equation approach. Ang [13] extended the approach to solve the case of multiple interacting cracks within an isotropic plate. However this approach can only apply to plane problems involving line-type discontinuities, such as cracks and contact interfaces.

The corresponding fundamental solutions derived in this study however, are for a generally anisotropic plate weakened by an elliptical cutout or a crack and subjected to an arbitrarily positioned concentrated force and/or moment. Through the application of the principle of superposition the solutions due to any general in-plane loading can be obtained using the proposed fundamental solutions. As pointed out by Ang [13], any numerical simulation, based on a fundamental solution which already includes the presence of cracks or openings, does not require to model the discontinuities any more and thus avoids any numerical difficulties which are associated with modeling the stress singularities at the crack tips or high stress concentrations near cutouts. Based on this fact, Sadegh [14] derived the corresponding isotropic solution for the point load case and Denda [15] considered the interaction of a dislocation or a point force and an elliptical hole in a plane anisotropic medium.

CHAPTER II

BASIC EQUATIONS OF COMPLEX VARIABLE ANISOTROPIC ELASTICITY

The development of the complex representation of the solution of plane problems for fully anisotropic elastic materials is given by Lekhnitskii [1,2]. The problem has also been treated by Savin [3], Milne-Thomson [16], and Green and Zerna [17]. As it is known, the only distinction between the formulation of isotropic and anisotropic elasticity is due to the Hooke's law. The generalized Hooke's law relating stresses and strains for a plane anisotropic problem in a state of plane stress can be expressed in the form:

$$\epsilon_i = \sum_{j=1}^{6} a_{ij}\sigma_j, \qquad (i,j = 1,2,6). \tag{2.1}$$

In the above formula, a_{ij} is the symmetric compliance matrix (i.e. $a_{ij} = a_{ji}$). In terms of engineering constants its components are given by:

$$a_{11}=1/E_{11},\quad a_{12}=-\nu_{12}/E_{11}=-\nu_{21}/E_{22},\quad a_{22}=1/E_{22},\quad a_{66}=1/G_{12}, \tag{2.2}$$

where E_{ii}, ν_{ij}, and G_{ij} represent the moduli of elasticity, poisson's ratio, and the shear moduli of the material in the corresponding directions, respectively. For plane strain case, the elastic constants a_{ij} are simply replaced by b_{ij} where,

$$b_{ij} = a_{ij} - \frac{a_{i3}\,a_{j3}}{a_{33}}, \qquad (i,j = 1,2,6). \tag{2.3}$$

As in the case of isotropic elasticity, the equilibrium equations will be satisfied if the stresses are expressed in terms of the Airy's stress function (U) as:

$$\sigma_{xx} = \frac{\partial^2 U}{\partial y^2}, \quad \sigma_{yy} = \frac{\partial^2 U}{\partial x^2}, \quad \tau_{xy} = \frac{\partial^2 U}{\partial x \partial y}. \tag{2.4}$$

Then, the basic equation of the two-dimensional anisotropic elasticity, as obtained by Lekhnitskii [1], takes the form:

$$a_{22}\frac{\partial^4 U}{\partial x^4} - 2a_{26}\frac{\partial^4 U}{\partial x^3 \partial y} + (2a_{12}+a_{66})\frac{\partial^4 U}{\partial x^2 \partial y^2} - 2a_{16}\frac{\partial^4 U}{\partial x \partial y^3} + a_{11}\frac{\partial^4 U}{\partial y^4} = 0, \tag{2.5}$$

which is a general form of the well-known biharmonic equation. The general solution of Eq. (2.5) depends on the roots of the constant coefficient characteristic equation:

$$a_{11}s^4 - 2a_{16}s^3 + (2a_{12}+a_{66})s^2 - 2a_{26}s + a_{22} = 0. \tag{2.6}$$

For the case of unequal roots this solution is of the form:

$$U(x,y) = F_1(x+s_1y) + F_2(x+s_2y) + F_3(x+s_3y) + F_4(x+s_4y), \tag{2.7}$$

where F_j (j=1 to 4) are arbitrary analytic functions and s_j (j=1 to 4) are the complex roots of Eq. (2.6). Through energy consideration, Lekhnitskii [1] showed that the roots of Eq. (2.6) can not be real, i.e. they have to be either complex or pure imaginary numbers. By defining the complex roots:

$$s_1 = s_1' + is_1'', \quad s_2 = s_2' + is_2'', \quad s_3 = s_1' - is_1'', \quad s_4 = s_2' - is_2'', \tag{2.8}$$

with $(s_1'', s_2'' > 0; s_1'' \neq s_2'')$, and,

$$z_1 = x + s_1 y, \quad z_2 = x + s_2 y, \tag{2.9}$$

the real function U of Eq. (2.7) takes the form:

$$U(x,y) = F_1(z_1) + F_2(z_2) + \overline{F_1(z_1)} + \overline{F_2(z_2)}. \tag{2.10}$$

Introducing

$$dF_1/dz_1=\Phi_1(z_1), \quad dF_2/dz_2=\Phi_2(z_2), \tag{2.11}$$

and inserting Eq. (2.10) into (2.4), the general expressions for the stress components in terms of the stress functions (Φ_1 and Φ_2) are given as:

$$\sigma_{xx} = 2Re[s_1^2\Phi_1'(z_1)+s_2^2\Phi_2'(z_2)], \tag{2.12a}$$

$$\sigma_{yy} = 2Re[\Phi_1'(z_1)+\Phi_2'(z_2)], \tag{2.12b}$$

$$\tau_{xy} = -2Re[s_1\Phi_1'(z_1)+s_2\Phi_2'(z_2)]. \tag{2.12c}$$

The displacement components are then readily obtained as:

$$u = 2Re[p_1\Phi_1(z_1)+p_2\Phi_2(z_2)] + \text{rigid-body displacements}, \tag{2.13a}$$

$$v = 2Re[q_1\Phi_1(z_1)+q_2\Phi_2(z_2)] + \text{rigid-body displacements}. \tag{2.13b}$$

In the above, p_j and q_j (j=1,2) are complex constants defined as:

$$p_j = p_j'+ip_j'' = a_{11}s_j^2+a_{12}-a_{16}s_j, \tag{2.14a}$$

$$q_j = q_j'+iq_j'' = (a_{12}s_j^2+a_{22}-a_{26}s_j)/s_j. \tag{2.14b}$$

Therefore, the solution of two-dimensional anisotropic elasticity reduces to the determination of the stress functions Φ_1 and Φ_2 such that they satisfy the boundary conditions of the specific problem under consideration. These complex functions are used as Green's functions and constitute the fundamental solutions.

The boundary conditions which the fundamental solutions must satisfy are different for the first and second fundamental problems. For the first fundamental problem, i.e. when stresses are prescribed on the boundary, the final expressions for the boundary conditions are of the form:

$$\Phi_1(z_1)+\overline{\Phi_1(z_1)}+\Phi_2(z_2)+\overline{\Phi_2(z_2)} = -\int_0^s Y_n ds = f_1, \tag{2.15a}$$

$$s_1\Phi_1(z_1)+\bar{s}_1\overline{\Phi_1(z_1)}+s_2\Phi_2(z_2)+\bar{s}_2\overline{\Phi_2(z_2)} = \int_0^s X_n ds = f_2, \tag{2.15b}$$

where s is an arc measured along the boundary. In the above, X_n and Y_n are the horizontal and vertical components of the normal resultant of the forces acting along the boundary, i.e.

$$X_n = \sigma_{xx}\cos(n,x)+\tau_{xy}\cos(n,y), \tag{2.16a}$$

$$Y_n = \tau_{xy}\cos(n,x)+\sigma_{yy}\cos(n,y), \tag{2.16b}$$

and n is the positive normal to the boundary (positive direction corresponds to one for which the area remains on the left of the integration path).

For the second fundamental problem, i.e. when displacements are known on the boundary, the boundary conditions are expressed as:

$$p_1\Phi_1(z_1)+\overline{p_1\Phi_1(z_1)}+p_2\Phi_2(z_2)+\overline{p_2\Phi_2(z_2)} = g_1(s), \tag{2.17a}$$

$$q_1\Phi_1(z_1)+\overline{q_1\Phi_1(z_1)}+q_2\Phi_2(z_2)+\overline{q_2\Phi_2(z_2)} = g_2(s), \tag{2.17b}$$

where g_1 and g_2 are known values of the displacement components.

Fracture analysis for cracked anisotropic plates can be performed once the fundamental solutions are obtained by setting the length of the semi-minor axis of the elliptical hole equal to zero. To apply Linear Elastic Fracture Mechanics (LEFM) concepts to fiber reinforced composites, the material is modeled as a homogeneous, linearly elastic, anisotropic continuum. Experimental evidence [18] indicates that the homogeneous model is justified for cracks of sufficient size such that the zone of elastic singularity near the

crack tip contains a sufficient number of fibers. The effect of neglecting material heterogeneity has been discussed by Cruse et al. [18].

As shown by Sih and Liebowitz [19], the mode I and mode II stress intensity factors (K_I and K_{II}) for a crack of length 2a centered at the origin of the z-plane can be evaluated from the following formulae:

At the right crack tip (x=+a):

$$\Psi_j = K_I + \frac{K_{II}}{s_k}$$

$$= 2\sqrt{2\pi}\left(\frac{s_k - s_j}{s_k}\right) \lim_{z_j \to +a} (z_j - a)^{1/2} \Phi_j'(z_j), \qquad (2.18a)$$

At the left crack tip (x=-a):

$$\Psi_j = K_I + \frac{K_{II}}{s_k}$$

$$= 2\sqrt{2\pi}\left(\frac{s_k - s_j}{s_k}\right) \lim_{z_j \to -a} -i(z_j + a)^{1/2} \Phi_j'(z_j), \qquad (2.18b)$$

where (j=1,2; k=2,1) and,

$$\Phi_j'(z_j) = \frac{\Phi_j'(\zeta_j)}{z_j'(\zeta_j)}, \qquad (j = 1,2). \qquad (2.19)$$

It can be proved easily that for $|\zeta_j| \leq 1$,

$$\lim_{z_j \to +a} \{[z_j(\zeta_j) - a]^{1/2} / z_j'(\zeta_j)\} = -\frac{1}{\sqrt{2a}}, \qquad (2.20a)$$

and

$$\lim_{z_j \to -a} \{[z_j(\zeta_j) + a]^{1/2} / z_j'(\zeta_j)\} = -\frac{i}{\sqrt{2a}}. \qquad (2.20b)$$

Then, the stress intensity factors can be obtained as:

$$K_I = \Psi_1' + \Psi_1''\left(\frac{s_2'}{s_2''}\right) - \Psi_2' + \Psi_2''\left(\frac{s_1'}{s_1''}\right), \tag{2.21a}$$

and

$$K_{II} = -\Psi_1''\left(\frac{s_2'^2+s_2''^2}{s_2''}\right) - \Psi_2''\left(\frac{s_1'^2+s_1''^2}{s_1''}\right), \tag{2.21b}$$

where Ψ_j' and Ψ_j'' are the real and the imaginary components of Ψ_j in Eq. (2.18), respectively. The expressions for the stress and displacement fields near the crack tip in terms of mode I and mode II stress intensity factors are given in Appendix E.

CHAPTER III

DERIVATION OF THE FUNDAMENTAL SOLUTIONS

In this section the fundamental solutions for an infinite anisotropic plate with an elliptical hole or a crack subjected to an arbitrarily located point force and/or concentrated moment are derived. These solutions are also valid when the loading is moved directly on the boundary of the hole. To check the proposed result, the fundamental solutions for the case where the loading is directly applied on the elliptical hole are derived and given in Appendix A. As will be demonstrated in Appendix A, explicit and more simplified solutions can be obtained when the loading is applied on the boundary. Numerical results and discussions for direct applications of the fundamental solutions are presented in Appendix C, where an infinite anisotropic plate containing an elliptical hole or a crack under various loading conditions are considered. Wherever possible, the results are checked against known solutions to establish the validity and accuracy of the proposed fundamental solutions.

III.1 POINT LOAD SOLUTION

Consider a concentrated force $F=Q+iP$ acting at a point $z^0=x_0+iy_0$ in an infinite anisotropic plate containing an elliptical hole, $x^2/a^2 + y^2/b^2 = 1$, as shown in Fig. 3.1(a). Applying the principle of superposition the problem of Fig. 3.1(a) is equivalent to the sum of two cases: the concentrated force acting in an infinite anisotropic plate without the hole as shown in Fig. 3.1(b) and an infinite anisotropic plate containing the elliptical hole, as shown in Fig. 3.1(c), loaded with the reverse of the surface tractions

resulting from the case of Fig. 3.1(b). Thus, the complex potentials for the case of Fig. 3.1(a) can be expressed as:

$$\Phi_j(z_j) = \Phi_j^o(z_j) + \Phi_j^*(z_j), \qquad (j = 1,2), \qquad (3.1)$$

where $\Phi_j^o(z_j)$ and $\Phi_j^*(z_j)$ (j=1,2) are the complex potentials corresponding to the cases of Fig. 3.1(b) and 3.1(c), respectively.

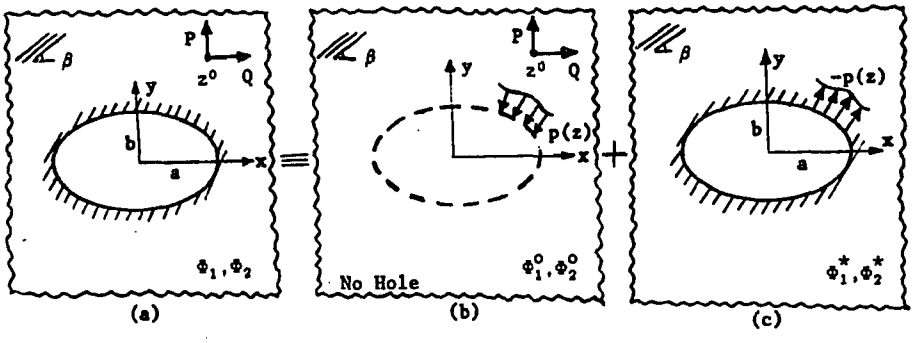

Figure 3.1. Principle of superposition applying to the fundamental solution for a point force.

For the problem of Fig. 3.1(b), we have [3,16]:

$$\Phi_j^o(z_j) = B_j \ln(z_j - z_j^0), \qquad (j = 1,2), \qquad (3.2)$$

where

$$B_j = \frac{1}{4\pi D}(D_{j1}Q + D_{j2}P), \qquad (j = 1,2). \qquad (3.3)$$

In the above,

$$D = -\frac{a_{11}a_{22}s_1''s_2''}{(s_1'^2+s_1''^2)(s_2'^2+s_2''^2)}[(s_2'-s_1')^4 + 2(s_2'-s_1')^2(s_2''^2+s_1''^2)+(s_2''^2-s_1''^2)^2], \qquad (3.4)$$

and

$$D_{ji} = D'_{ji}+iD''_{ji}, \qquad (j,i = 1,2), \qquad (3.5)$$

with

$$D'_{i1} = p''_2(q'_i-q'_2)-q''_2(p'_i-p'_2), \qquad (3.6a)$$

$$D''_{i1} = -D''_{2i} = p''_i q''_2-p''_2 q''_i, \qquad (3.6b)$$

$$D'_{i2} = s''_2(p'_i q'_2-p'_2 q'_i)+p''_2(q'_i s'_2-q'_2 s'_i)+q''_2(s'_i p'_2-s'_2 p'_i), \qquad (3.6c)$$

$$D''_{i2} = s'_2(p''_i q''_2-p''_2 q''_i)+p'_2(q''_i s''_2-q''_2 s''_i)+q'_2(s''_i p''_2-s''_2 p''_i), \qquad (3.6d)$$

$$D'_{2i} = -p''_i(q'_i-q'_2)+q''_i(p'_i-p'_2), \qquad (3.6e)$$

$$D'_{22} = -s''_i(p'_i q'_2-p'_2 q'_i)-p''_i(q'_i s'_2-q'_2 s'_i)-q''_i(s'_i p'_2-s'_2 p'_i), \quad \text{and} \qquad (3.6f)$$

$$D''_{22} = -s'_i(p''_i q''_2-p''_2 q''_i)-p'_i(q''_i s''_2-q''_2 s''_i)-q'_i(s''_i p''_2-s''_2 p''_i). \qquad (3.6g)$$

To solve the problem of Fig. 3.1(c) we use the conformal mapping:

$$z_j = d_{j1}\zeta_j + d_{j2}\frac{1}{\zeta_j}, \qquad (j = 1,2), \qquad (3.7)$$

where

$$d_{j1} = \tfrac{1}{2}(a+is_j b), \quad \text{and} \quad d_{j2} = \tfrac{1}{2}(a-is_j b), \qquad (j = 1,2), \qquad (3.8)$$

to map the anisotropic medium outside the elliptical hole on the z_j-planes (j=1,2) into the interior of a unit circle: $t=\exp(i\theta)$ on $\zeta_j=\xi+s_j\eta$ planes (j=1,2). Ignoring the integration constants which make contributions only to the rigid-body displacements, the corresponding complex potentials can then be obtained by using Schwarz formulae [3]:

$$\Phi_j^*(\zeta_j) = \frac{i}{4\pi(s_j-s_k)}\int_\gamma [s_k f_1(t)-f_2(t)]\frac{t+\zeta_j}{t-\zeta_j}\frac{1}{t}dt, \qquad (3.9)$$

where (j=1,2; k=2,1). In the above f_1 and f_2 are defined by Eq. (2.15) and for the present problem are given by:

$$f_1 = -2\mathrm{Re}[\Phi_1^o(z_1)+\Phi_2^o(z_2)]$$

$$= -B_1 \ell n(z_1-z_1^o)-\bar{B}_1 \ell n(\bar{z}_1-\bar{z}_1^o)-B_2 \ell n(z_2-z_2^o)-\bar{B}_2(\bar{z}_2-\bar{z}_2^o), \qquad (3.10a)$$

and

$$f_2 = -2\mathrm{Re}[s_1\Phi_1^o(z_1)+s_2\Phi_2^o(z_2)]$$

$$= -s_1B_1 \ell n(z_1-z_1^o)-\bar{s}_1\bar{B}_1 \ell n(\bar{z}_1-\bar{z}_1^o)$$

$$-s_2B_2 \ell n(z_2-z_2^o)-\bar{s}_2\bar{B}_2(\bar{z}_2-\bar{z}_2^o). \qquad (3.10b)$$

Substituting Eq.s (3.10a,b) into (3.9) we get:

$$\Phi_j^*(\zeta_j) = \frac{i}{4\pi(s_j-s_k)}[(s_k-s_j)B_j \int_\gamma \ell n(z_j-z_j^o)\frac{t+\zeta_j}{t-\zeta_j}\frac{dt}{t}$$

$$+(s_k-\bar{s}_k)\bar{B}_j \int_\gamma \ell n(\bar{z}_j-\bar{z}_j^o)\frac{t+\zeta_j}{t-\zeta_j}\frac{dt}{t}$$

$$+(s_k-\bar{s}_k)\bar{B}_k \int_\gamma \ell n(\bar{z}_k-\bar{z}_k^o)\frac{t+\zeta_j}{t-\zeta_j}\frac{dt}{t}], \quad (j=1,2;\ k=2,1). \qquad (3.11)$$

Using Eq. (3.7), we can write:

$$z_j-z_j^o = \frac{[d_{j1}(t-t_{j1}^i)(t-t_{j1}^o)]}{t}, \qquad (j=1,2), \qquad (3.12a)$$

$$\bar{z}_j-\bar{z}_j^o = \frac{[\bar{d}_{j2}(t-t_{j2}^i)(t-t_{j2}^o)]}{t}, \qquad (j=1,2), \qquad (3.12b)$$

where

$$t_{j1}^i, t_{j1}^o = \frac{z_j^o \pm [(z_j^o)^2-4d_{j1}d_{j2}]^{1/2}}{2d_{j1}}, \qquad (j=1,2), \qquad (3.13a)$$

and

$$t_{j2}^i, t_{j2}^o = \frac{\bar{z}_j^o \pm [(\bar{z}_j^o)^2-4\bar{d}_{j1}\bar{d}_{j2}]^{1/2}}{2\bar{d}_{j1}}, \qquad (j=1,2). \qquad (3.13b)$$

The sign convention in Eqs. (3.13a,b) should be selected so that t^i_{jk} and t^o_{jk} (j,k=1,2) locate inside and outside the unit circle of ζ_j-plane (j=1,2), respectively. Thus, t^i_{ji} and t^o_{ji} represent the inner and outer complex roots of the equation:

$$z_j - z^o_j = d_{j1}\zeta_j + d_{j2}\frac{1}{\zeta_j} - z^o_j = 0, \qquad (j = 1,2), \qquad (3.14a)$$

or

$$\bar{z}_j - \bar{z}^o_j = \bar{d}_{j2}\zeta_j + \bar{d}_{j1}\frac{1}{\zeta_j} - \bar{z}^o_j = 0, \qquad (j = 1,2), \qquad (3.14b)$$

on the unit circle.

Substituting (3.12) into (3.11) results in a group of integrals which can be solved using the theorems of Cauchy integrals. The first group of integrals are of the type:

$$\ell n(c_j) \int_\gamma \frac{t+\zeta_j}{t-\zeta_j}\frac{dt}{t} = \ell n(c_j)\left[2\pi i\left(\frac{\sigma+\zeta_j}{\sigma}\right)_{\sigma\to\infty}\right] = \text{Constant}, \qquad (3.15a)$$

where γ represents contour integration along the unit circle and c_j (j=1,2) are constants relating to d_{11} and $\overline{d_{12}}$. The second group of integrals are evaluated as follows:

$$\int_\gamma \ell n(t-t_i)\frac{t+\zeta_j}{t-\zeta_j}\frac{dt}{t} = 2\int_\gamma \frac{\ell n(t-t_i)}{t-\zeta_j}\,dt - \int_\gamma \frac{\ell n(t-t_i)}{t}\,dt, \qquad (3.15b)$$

where t_i represents t^i_{j1} or t^i_{j2} (j=1,2). To evaluate the first integral in Eq. (3.15b), let:

$$I_1 = \int_\gamma \frac{\ell n(t-t_i)}{t-\zeta_j}\,dt,$$

then, $$\frac{dI_1}{d\zeta_j} = \int_\gamma \frac{\ell n(t-t_i)}{(t-\zeta_j)^2}\,dt = -\int_\gamma \ell n(t-t_i)\,d\left(\frac{1}{t-\zeta_j}\right)$$

$$= -\left[\frac{\ell n(t-t_i)}{t-\zeta_j}\right]_\gamma + \int_\gamma \frac{dt}{(t-\zeta_j)(t-t_i)} = -\frac{2\pi i}{t_i-\zeta_j}.$$

Therefore, $I_1 = 2\pi i\ \ell n(t_i-\zeta_j)$, $(j=1,2)$. (3.15c)

To evaluate the second integral in (3.15b), let $t = \frac{1}{\omega}$, $dt = -\frac{d\omega}{\omega^2}$. Then,

$$\int_\gamma \frac{\ell n(\omega-t_i)}{\omega}\, d\omega = -\int_\gamma \omega\ \ell n(\tfrac{1}{\omega}-t_i)\frac{d\omega}{\omega^2} = -\int_\gamma \frac{\ell n(1/\omega-t_i)}{\omega}\, d\omega$$

$$= -\int_\gamma \frac{i\pi}{\omega}\, d\omega - \int_\gamma \frac{\ell n(t_i-1/\omega)}{\omega}\, d\omega.$$

Here, the first integral is a constant and the second integral is found to be [12]:

$$\frac{1}{2\pi i}\int_\gamma \frac{\ell n(t_i-1/\omega)}{\omega-z}\, d\omega = \ell n(t_i) = \text{constant}.$$

Therefore, the second integral in Eq. (3.15b) also is a constant. Substituting (3.15c) into (3.15b) we arrive at:

$$\int_\gamma \ell n(t-t_i)\frac{t+\zeta_j}{t-\zeta_j}\frac{dt}{t} = 4\pi i\ \ell n(t_i-\zeta_j) + \text{constant}. \qquad (3.15d)$$

The next integral is of the same form as (3.15b) with t_i replaced by t_o, i.e. the inner roots replaced by outer ones. Following the same procedure we get:

$$\int_\gamma \ell n(t-t_o)\frac{t+\zeta_j}{t-\zeta_j}\frac{dt}{t} = 4\pi i\ \ell n(\zeta_j-t_o) + \text{constant}, \quad (j=1,2). \qquad (3.15e)$$

Finally, the last integral to be considered here is also of the same format as the one in (3.15b) with $(t-t_i)$ replaced by t. The same procedure as above leads to:

$$\int_\gamma \ell n(t)\frac{t+\zeta_j}{t-\zeta_j}\frac{dt}{t} = 4\pi i\ \ell n(t-\zeta_j) + \text{constant}, \quad (j=1,2). \tag{3.15f}$$

The complex potentials $\Phi_j^*(\zeta_j)$ (j=1,2) are then obtained from (3.11) as:

$$\Phi_j^*(\zeta_j) = -B_j \ell n(\zeta_j - t_{j1}^o) - \bar{B}_j\left(\frac{s_k-\bar{s}_j}{s_k-s_j}\right)\ell n(\zeta_j - t_{j2}^o)$$

$$-\bar{B}_k\left(\frac{s_k-\bar{s}_k}{s_k-s_j}\right)\ell n(\zeta_j - t_{k2}^o), \qquad (j=1,2;\ k=2,1). \tag{3.16}$$

The complete fundamental solution for the original problem of Fig. (3.1a) can then be obtained by substituting Eqs. (3.2) and (3.16) into Eq. (3.1). It should be noted that the above derivation remains valid for the case of a crack except that the length of the semi-minor axis, b, in Eq. (3.8) should be set zero. Then mode I and mode II stress intensity factors (K_I and K_{II}), can be evaluated using Eq. (2.21) with:

$$\Psi_j = \Psi_j' + i\Psi_j'' = \frac{2}{s_k}\sqrt{\frac{\pi}{a}}\left[B_j\left(\frac{s_k-s_j}{\pm 1-t_{j1}^o}\right)+\bar{B}_j\left(\frac{s_k-\bar{s}_j}{\pm 1-t_{j2}^o}\right)\right.$$

$$\left.+\bar{B}_k\left(\frac{s_k-\bar{s}_k}{\pm 1-t_{k2}^o}\right)\right], \qquad (j=1,2;\ k=2,1). \tag{3.17}$$

Here the "+" and "-" signs are for the right (x=+a) and the left (x=-a) crack tips, respectively.

This concludes the derivation of the fundamental solution for an anisotropic plate containing an elliptical hole or a crack subjected to an arbitrarily located point force.

III.2 CONCENTRATED MOMENT SOLUTION

Consider a concentrated moment M acting at a point $z^0=x_0+iy_0$ in an infinite anisotropic plate containing an elliptical hole, $x^2/a^2 + y^2/b^2 = 1$, as shown in Fig. 3.2(a). As for the point load case in Sec. III.1, the principle of superposition can be applied here to get the equivalent problems of Figs. 3.2(b,c) and to yield Eq. (3.1).

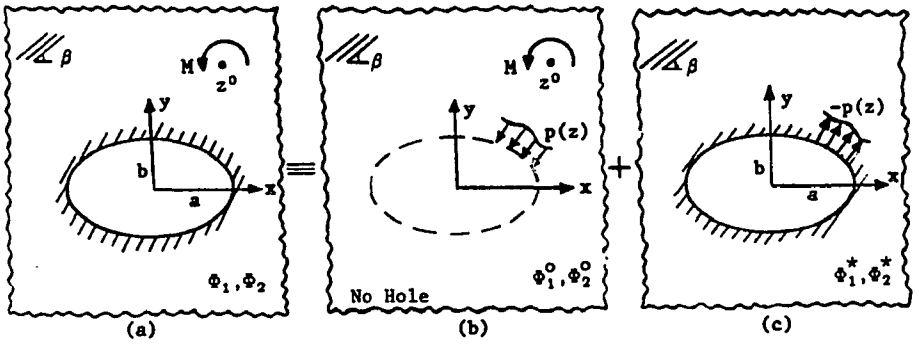

Figure 3.2. Principle of superposition applying to the fundamental solution for a concentrated moment.

Unlike the point load case, $\Phi_j^0(z_j)$ $(j = 1,2)$ for the concentrated moment is not given in the open literature but can be obtained as follows. Consider an anisotropic plate containing a central circular hole of radius ρ whose edge is subjected to a uniform shear τ. The fundamental solution for this problem is given by Savin [3]. Taking the limit as the radius ρ approaches zero, replacing $2\pi\rho^2\tau$ by a concentrated moment M, and shifting the origin to an arbitrary location $z^0=x_0+iy_0$, the corresponding fundamental solution for a concentrated moment applied at z^0 in an anisotropic plate without a hole is obtained as:

$$\Phi_j^o(z_j)=C_j\left(\frac{1}{z_j-z_j^o}\right), \qquad (j=1,2), \qquad (3.18)$$

where

$$C_j=\left(\frac{M}{8\pi}\right)\frac{(1-is_j)(1+is_k)}{(s_k-s_j)}, \qquad (j=1,2;\ k=2,1). \qquad (3.19)$$

In the above, $z^o=x_o+s_jy_o$ are the transformed coordinates for the loading point $z^o=x_o+iy_o$.

To obtain the fundamental solution for the second component of the superposition, we follow the same procedure outlined for the point load case. Here instead of the integrals evaluated in Eqs. (3.15), the integrals involved are of the type:

$$\int_\gamma\left(\frac{1}{(t-t_i)(t-t_o)}\right)\frac{t+\zeta_j}{t-\zeta_j}\,dt = \int_\gamma\left(\frac{1}{(t-t_i)(t-t_o)}\right)\left(1+\frac{2\zeta_j}{t-\zeta_j}\right)dt$$

$$= \left(\frac{1}{t_i-t_o}\right)\int_\gamma\left(\frac{1}{t-t_i}-\frac{1}{t-t_o}\right)\left(1+\frac{2\zeta_j}{t-\zeta_j}\right)dt$$

$$= \left(\frac{1}{t_i-t_o}\right)\left[\int_\gamma\left(\frac{1}{t-t_i}\right)dt+\int_\gamma\frac{\left(\frac{2\zeta_j}{t-t_i}\right)}{t-\zeta_j}dt-\int_\gamma\left(\frac{1}{t-t_o}\right)dt\right.$$

$$\left.+\int_\gamma\frac{\left(\frac{2\zeta_j}{t-t_o}\right)}{t-\zeta_j}dt\right] = \left(\frac{4\pi i}{t_o-t_i}\right)\frac{\zeta_j}{\zeta_j-t_o}+\text{Constant}. \qquad (3.20)$$

The integrals in Eq. (3.20) were again evaluated using Cauchy's integral theorem [12]. The fundamental solution corresponding to the second component of the superposition is thus obtained as:

$$\Phi_j^*(\zeta_j) = -\frac{C_j}{d_{j1}}\left(\frac{1}{t_{j1}^o-t_{j1}^i}\right)\left(\frac{\zeta_j}{\zeta_j-t_{j1}^o}\right)-\frac{\bar{C}_j}{\bar{d}_{j2}}\left(\frac{s_k-\bar{s}_j}{s_k-s_j}\right)\left(\frac{1}{t_{j2}^o-t_{j2}^i}\right)\left(\frac{\zeta_j}{\zeta_j-t_{j2}^o}\right)$$

$$-\frac{\bar{C}_k}{\bar{d}_{k2}}\left(\frac{s_k-\bar{s}_k}{s_k-s_j}\right)\left(\frac{1}{t^o_{k2}-t^i_{k2}}\right)\left(\frac{\zeta_j}{\zeta_j-t^o_{k2}}\right), \quad (j = 1,2;k = 2,1). \quad (3.21)$$

Similarly, the obtained fundamental solution for the concentrated moment case will remain valid when the elliptical hole is degenerated into a crack by setting the length of the semi-minor axis of the ellipse (b) equal to zero in Eq. (3.8). Then, mode I and mode II stress intensity factors can be obtained by substituting:

$$\Psi_j = \Psi'_j+i\Psi''_j = -\frac{2}{a}\left[C_j\left(\frac{t^o_{j1}}{t^o_{j1}-t^i_{j1}}\right)\left(\frac{s_k-s_j}{(\pm1-t^o_{j1})^2}\right)+\bar{C}_j\left(\frac{t^o_{j2}}{t^o_{j2}-t^i_{j2}}\right)\left(\frac{s_k-\bar{s}_j}{(\pm1-t^o_{j2})^2}\right)\right.$$

$$\left.+\bar{C}_k\left(\frac{t^o_{k2}}{t^o_{k2}-t^i_{k2}}\right)\left(\frac{s_k-\bar{s}_k}{(\pm1-t^o_{k2})^2}\right)\right], \quad (j=1,2;k=2,1), \quad (3.22)$$

into Eq. (2.21). Interestingly, it will be proved in Appendix A that when the concentrated moment is moved directly on the face of the crack the stress intensity factors will become independent of material anisotropy and turn out to be identical to those of the isotropic case.

CHAPTER IV

INDIRECT BOUNDARY INTEGRAL FORMULATION

The Boundary Integral Equation method (BIE) has been proven to be an effective and efficient numerical scheme in solving mechanics problems of complex nature. In BIE, approximation is made on the boundary of the body rather than in the entire field as with the finite element method. The resulting system of equations is therefore of a smaller size than with the finite element method. But, this is offset by the fact that the coefficient matrix is fully occupied instead of the banded matrix as obtained in finite element method. However, the boundary integral method is quite advantageous when it is required to find unknowns at only a few points, i.e. near a crack tip, as opposed to over the entire field and can be applied to infinite and semi-infinite domains directly.

The technique is based upon a suitable fundamental solution to the field equations of elasticity. The fundamental solution is used to derive a set of integral equations relating boundary values of displacement or traction corresponding to a well-posed boundary value problem. These integral equations can then be solved using approximate techniques such as modeling the boundary by constant displacement or constant traction segments. The accuracy of the method has been established for two and three-dimensional crack problems in isotropic materials in [20] and for two-dimensional crack problems in anisotropic materials in [10]. As reported in [20], the accuracy of the method is mainly dependent upon correct modeling of the crack.

In this study, the BIE is developed using the previously derived fundamental solutions (Ch. III) which satisfy boundary conditions on the crack automatically, thus avoiding the problem of modeling the crack boundary. The Indirect BIE being developed is intended to introduce additional boundaries, such as an outer boundary of a disk or the boundary of a curvilinear hole. In the Indirect BIE, the integral equations are expressed entirely in terms of the unit singular solution (fundamental solution) of the original differential equations distributed at a specific density over the boundary of the region. This is as opposed to the Direct BIE, where the integral equations are expressed in terms of the actual physical variables (i.e. displacements and tractions). The Indirect BIE provides a particularly clear and simple physical illustration of the solution scheme [21], and therefore is adopted here. The fundamental solutions derived in Chapter III constitute the required unit singular solutions. Since all the cases that we intend to solve with the aid of BIE involve cracks, the fundamental solutions for an anisotropic plate containing a crack are considered directly. It should be clear that the same approach remains valid when the crack is replaced by an elliptical hole.

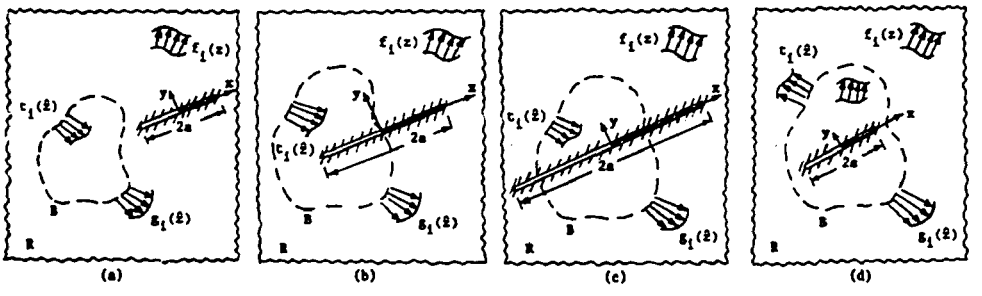

Figure 4.1. Application of BIE to the fundamental solution of a cracked anisotropic plate to introduce an additional curvilinear boundary.

Consider an infinite anisotropic plane containing a crack of length 2a as shown in Figs. 4.1(a), (b), (c), and (d). The boundary B, which is of a curvilinear shape, denotes the additional boundary to be introduced by BIE. Note that the crack can be outside of B (as in Fig. 4.1(a)), intersecting B at one or two locations (as in Fig. 4.1(b) or (c)), or be contained in B (as in Fig. 4.1 (d)). The case where the crack is outside of B (Fig. 4.1(a)), represents the problem of interaction between a curvilinear hole and a crack in an anisotropic plate. That of Fig. 4.1(b), could represent the case of a crack emanating from a curvilinear hole or an edge crack in a curvilinearly shaped anisotropic solid disk depending on the chosen direction for the positive normal (positive direction corresponds to one for which the area remains on the left). It should be noted that if B is taken to be a hole, the segment of the crack which falls inside of B will have no effect on the solution since it is outside of the domain. Whereas if B is taken to represent a solid disk, only the left segment of the crack should be considered. The case where the crack intersects B in two locations (Fig. 4.1(c)), can only represent a curvilinear hole with two cracks emanating from the edge. Again for this case the segment of the crack which falls inside of B can be disregarded. Finally, when the crack locates inside of B (Fig. 4.1(d)), represents a curvilinearly shaped anisotropic solid disk with an internal crack.

Let us denote the domain (including the crack) as R, and assume that B is loaded by a distribution of surface traction: $t_i(\hat{z})$ (i=1,2 and $\hat{z}=\hat{x}+i\hat{y}$) and the domain R by a body force: $f_i(z)$ (i=1,2 and $z=x+iy$). It is clear that the boundary B is still an imaginary contour. To change B into a real boundary, it is assumed to be

subjected to a fictitious line load $g_i(\hat{z})$ (i=1,2) so that the combination of $f_i(z)$ and $g_i(\hat{z})$ generates tractions along the imaginary contour B equal to $t_i(\hat{z})$, the prescribed tractions. Using the standard procedure of BIE [21], one can show that the traction $t_i(\hat{z})$ at any point $\hat{z}$ along the imaginary contour B is:

$$t_i(\hat{z}) = \frac{1}{2}g_i(\hat{z}) + \int_B T_{ijk}(\hat{z},\hat{\rho})n_j(\hat{z})g_k(\hat{\rho})ds(\hat{\rho}) + \int_R T_{ijk}(\hat{z},\rho)n_j(\hat{z})f_k(\rho)dv(\rho), \qquad (i,j,k = 1,2), \quad (4.1)$$

where $n_j(\hat{z})$ is the outward normal vector at point $\hat{z}$ along B and $T_{ijk}(\hat{z},\hat{\rho})$ (or $T_{ijk}(\hat{z},\rho)$) are the influence coefficients corresponding to the stress components σ_{ij} (i,j=1,2) at $\hat{z}$ due to a unit force acting in k-direction (k=1,2) at a point $\hat{\rho}$ (or ρ) in an infinite anisotropic plate weakened by a crack of length 2a. It should be noted that the strong -1 singularity in the first integral of Eq. (4.1) has been removed using the "jump" condition (as expressed in the $\frac{1}{2}g_i(\hat{z})$ term) and the integral is taken at its Cauchy principal value [21]. A brief review of the "jump" condition is given in Appendix F. The summation convention is used in Eq. (4.1), which is the proposed BIE. By differentiating the complex stress functions $\Phi_j(z_j)$ (obtained in Ch. III) with respect to z_j and using Eqs. (2.12 a, b, c), we can get the influence coefficients.

Equation (4.1) is a complex Fredholm integral equation of the second kind and can be solved numerically. The boundary B is first divided into N intervals of length Δs_n (n=1,2,...,N). Within a

typical n^{th} interval distribution of the fictitious load $g_i(\hat{z})$ is assumed to be constant and can be represented by its value at the midpoint $\hat{z}_n$ of the interval. Let us denote the fictitious load and the traction at this midpoint as g_{in} and t_{in}, respectively. If we evaluate the last integral in Eq. (4.1) at the midpoints of the N intervals and call the resultant vector t^*_{in}, then Eq. (4.1) becomes:

$$\hat{t}_{in} = t_{in} - t^*_{in} = \frac{1}{2}g_{in} + \sum_{m=1}^{N} g_{im}\int_{\Delta s_m} T_{ijk}(\hat{z}_n,\hat{\rho}_m)n_j(\hat{z}_n)ds(\hat{\rho}_m), \quad (n=1,2,\ldots,N). \quad (4.2)$$

Both the last integral in Eq. (4.1) and the integral in Eq. (4.2) can be evaluated by standard numerical integration schemes, such as the Gauss-Legendre or the Gauss-Chebyshev quadrature. Equation (4.2) is a system of 2N simultaneous linear algebraic equations which can be solved by any standard equation solver, such as the Gauss elimination. As stated above, once the fictitious loads g_{in} (n=1,2,...,N) are found, the complex stress functions $\Phi_j(z_j)$ (j=1,2) corresponding to the problems stated above can be obtained by applying the applied and the fictitious loads to the equivalent problems of Fig. 4.1.

CHAPTER V

APPLICATIONS OF THE BIE

In this chapter, numerical results and discussions are presented for the application of the BIE formulation of Chapter IV to various engineering problems involving cracks in the presence of other boundaries. The results, whenever possible, are checked with some known solutions available in open literature. On average, subdivision of the curvilinear boundary being introduced by BIE into 40 to 60 elements resulted in values to within 3% difference as compared with known solutions. Further discussions and a case study of the effect of variation of element size for an example problem are presented in Appendix G.

Unless stated otherwise, numerical computations were performed using AS4 3501-6 Graphite/Epoxy, with engineering constants: E_1=129.92 GPa, E_2=10.12 GPa, G_{12}=6.27 GPa, and ν_{12}=0.28. The problems considered were assumed to be in a state of plane stress in which the fiber direction is oriented at an angle β with respect to the positive x-axis. Relations to transform the elements of the compliance matrix (a_{ij} (i,j=1,2,6) of Eq. (2.1)) from the geometrical coordinates to the principal material coordinates in terms of the fiber angle β are given in Appendix D. In some of the computations the isotropic counterparts were also calculated by setting: E_1=0.9999E_2=99.99 GPa, ν_{12}=ν=0.25, and G_{12}=G= $\frac{E}{2(1+\nu)}$. The elliptical hole of the fundamental solution is: $x^2/a^2 + y^2/b^2 = 1$, and the curvilinear boundary due to BIE is assumed to be either elliptical: $x^2/A^2 + y^2/B^2 = 1$ or circular: $x^2 + y^2 = R^2$.

V.1 CRACKS EMANATING FROM A CURVILINEAR HOLE IN AN ANISOTROPIC PLATE UNDER GENERAL LOADINGS

V.1.1 Background

The problem of holes in composite plates have attracted many research activities. Particularly many efforts are made toward stress analyses of laminated composites with circular or elliptical openings [4,5,24] which may be designed for fluid passage or other purposes and are subjected to various types of loadings. Very often fracture initiates from these stress concentrations [25,26] and the presence of these cutouts enhances crack propagation since the stress intensity factors are, in general, increased due to the crack-hole interaction. Therefore understanding the behavior of cracks emanating from a cutout in an anisotropic plate is very important for a better design of laminated composites.

For isotropic materials under various loading conditions (e.g. uniaxial or biaxial tension, pure shear, or internal pressure, etc.), numerous techniques, such as conformal mapping-collocation [27-30], boundary collocation [31], and Mellin transform [32-34] have been used to study extensively the problems of a single radial crack, two symmetrical radial cracks, two collinear radial cracks of different lengths, or an array of radial cracks emanating from a circular hole. Fracture analyses have also been performed for cracks originating from a fastener hole which is only partially pressurized [35-38], for a crack initiating from a circular hole at an arbitrary angle [39], and for cracks extending from a hole of general shape (e.g., elliptical, rectangular or hypocycloidal) [31,40-43].

Contrary to the extensive studies on the isotropic material case, only very few researches on the problem of crack emanating from a hole in an anisotropic material have been reported. Waddroups,

Eisenmann and Kaminski [24] first investigated the failure of finite-dimensional laminated composites with circular cutouts using Bowie's [27] solution for a cracked circular hole in an infinite isotropic medium. Wang and Yau [44] studied, by finite element method, the mixed-mode problems of cracks emanating from a circular hole in unidirectional fiber reinforced composites. The mode I and mode II stress intensity factors were obtained by using conservative laws of elasticity, such as the J- and the M-integrals. Recently Cheong and Hong [45] used the modified mapping-collocation (MMC) technique developed by Bowie and Neal [46] to solve the problem of a pair of symmetrical radial cracks initiating from a circular hole in an orthotropic plate subjected to uniaxial tension and pure shear.

In this section, numerical values for stress intensity factors are evaluated for cracks emanating from a circular or an elliptical hole in an infinite anisotropic plate subjected to arbitrary loadings. The BIE formulation of Chapter IV is used to satisfy the traction boundary conditions on the hole. This approach is similar to the ones adopted by Snyder and Cruse [10] and by Clements and Haselgrove [11] to solve a finite cracked anisotropic plate. To avoid singularities, the nodes of the elements of the curvilinear hole which locate on the crack mouth were shifted a small distance ($O(10^{-7}R)$, where R is the radius of the hole) away from the crack.

V.1.2 Numerical Results and Discussions

Table 5.1.1 shows a radial crack of length a emanating from a circular hole of radius R contained in an infinite isotropic medium. The crack is loaded by either a pair of horizontal forces Q or a pair of vertical forces P acting on the upper and lower crack faces at a

distance d measured from the crack mouth. Normalized mode I and mode II stress intensity factors are computed at various d/a ratios for a/R equal to 1, 5, or 50. Except when the loading point is very close to the crack mouth, i.e., d/a=0.05, the mode I results are within 2% difference in comparison with those reported by Shivakumar and Forman [30] who used Bowie's [27] transformation to map the exterior of the cracked hole onto the exterior of a unit circle and solved the problem by the truncated conformal mapping technique. In Ref. [30] the normalized stress intensity factors, F_I and F_{II}, were always found to be equal. In this study, however, it is found that F_I and F_{II} are equal only when the crack is extremely long (say, $a/R > 1000$) or short (say, $a/R < 0.001$). Otherwise F_{II} is consistently larger than F_I.

The mixed-mode stress intensity factors shown in Table 5.1.2 are due to a horizontal force Q, a vertical force P, or a concentrated moment M applied on the upper face of a crack which has a length a and emanates in the x-direction from a circular hole of radius R. In this computation the crack length a is assumed to be equal to the radius R. The loading point is located at a distance d measured from the hole-crack intersection. In all three cases the effect of anisotropy on the stress intensity factors is more prominent when the loading point is close to the crack mouth. For the case due to the horizontal force Q, consistent higher K_{II} and lower K_I are found for the case with smaller fiber angle β. For the vertical force case, again, K_{II} is higher when β is small, but higher K_I is obtained when β equals 0 or 90°. No coherent dependency on anisotropy can be found for the concentrated moment case. It is interesting to note that the

stress intensity factors for the case of β=45° are approximately equal to those of the isotropic case. This may be due to the fact that when β equals 45°, the effect of anisotropy evens up along the directions parallel and normal to the crack.

Stress intensity factors for a radial crack of length a emanating from a circular hole of radius R subjected to a uniaxial tension σ or a uniform shear τ are shown in Fig. 5.1.1. Although the loading and geometry are symmetrical, small but not negligible K_{II} for the uniaxial tension case and K_I for the uniform shear case are observed for the β=45° case which possesses asymmetrical anisotropy. This observation is true for all the examples illustrated hereon. As a/R approaches infinite, the normalized stress intensity factors become 0.707, indicating that the presence of the circular hole can be ignored. For the uniaxial tension case the effect of anisotropy can be neglected, especially when a/R is relatively large. As shown in Fig. 5.1.1, the present isotropic solution is in excellent agreement with those reported by Hsu [29], Shivakumar and Forman [30], and Tweed and Rooke [32]. For the uniform shear case, anisotropy is very influential on stress intensity factors, particularly when the a/R ratio is relatively small. The present isotropic solution agrees very well with Hsu's [29] result except when a/R equals 4 where the tabulated results in Ref. [29] has a sudden drop, indicating that a typographical error might have appeared in Ref. [29]. The present solution, however, differs substantially from that reported by Shivakumar and Forman [30], whose solution is very close to the line crack solution for $a \geq 2R$. Thus they implied that the presence of the hole had no significant effect on stress intensity factors due to pure shear. This of course is not

true when the crack length a and the radius R are comparable. This difference may result from the above-mentioned underestimation of F_{II} in Ref. [30].

Table 5.1.3 shows the stress intensity factors for the above cracked hole loaded by an internal pressure p. The crack faces are assumed to be either "dry" (λ=0) or "saturated" (λ=1). Principle of superposition can be applied to obtain the results corresponding to any degree of "humidity". As depicted in Table 5.1.3, K_I for the "saturated" case is about twice of that for the "dry" case when the crack is relatively short. As the crack grows, the non-dimensionalized K_I decreases drastically to zero for the "dry" case (since it is similar to a line crack opened up by a pair of centrally loaded forces), or gradually approaches to 0.707 for the "saturated" case (since it is equivalent to a line crack subjected to an internal pressure). In general, the effect of anisotropy is not very significant except when the crack is very short.

Next we consider an edge crack emanating from an elliptical hole in its major-axis direction. The length ratio of the semi-minor and semi-major axes of the elliptical hole is B/A=0.5. Stress intensity factors due to uniaxial tension σ or uniform shear τ are shown in Table 5.1.4. The isotropic results agree reasonably well with the solutions given by Isida, Chen and Nisitani [40], who solved the problem by the body force method. For the uniaxial tension case the effect of anisotropy can be neglected except when the crack is very short. The anisotropy has stronger effect on the uniform shear case. This is consistent with the circular hole results (Fig. 5.1.1). Comparing Table 5.1.4 with Fig. 5.1.1, it is seen that the case of

circular hole can be used to approximate this elliptical hole case when a/A is greater than 1.0. The dimensionless K_I for the uniform tension case and K_{II} for the uniform shear case again approach 0.707 as the crack-hole length ratio a/A increases, thus indicating that the presence of the hole can be ignored when the crack is long.

Figure 5.1.2 shows the stress intensity factors due to uniaxial or biaxial tension σ acting on an infinite anisotropic plate with two symmetrical radial cracks, each of length a, emanating from a circular hole of radius R. The anisotropy has almost no effect for the biaxial tension case but exerts stronger influence on the uniaxial tension case when the cracks are relatively short. The mode II stress intensity factor, which exists only for the β=45° case, is larger in the uniaxial tension case than in the biaxial tension case. This is understandable since the degree of anisotropy with respect to the loading tends to be decreased under the all-around biaxial tension. The corresponding isotropic results are in excellent agreement with the solutions obtained by Bowie [27] and Newman [31]. As the cracks grow, the normalized K_I value in both cases approach 1.0 and the problems again reduce to a line crack under uniaxial or biaxial tension.

Figure 5.1.3 is for a double-cracked hole loaded by an internal pressure p, where only the "saturated" cracks were considered. As shown in Fig. 5.1.3, the effect of anisotropy on K_I can be neglected and the isotropic case agrees very closely with Newman's [31] solution.

Finally for the purpose of further verification we study the problem solved recently by Cheong and Hong [45] using the MMC

technique [46] for the above double-cracked hole embedded in an infinite anisotropic plane subjected to a uniaxial tension σ or a pure shear τ. The composite that they used is E-Glass/Epoxy (E_1=53.74 GPa, E_2=17.91 GPa, G_{12}=8.96 GPa and ν_{12}=0.25.) As shown in Fig. 5.1.4, the comparison is reasonably well, however, the difference is larger than the above-mentioned comparison for the isotropic counterparts, especially when the crack is relatively short.

Table 5.1.1. A pair of concentrated forces acting on a radial crack emanating from a circular hole (isotropic case).

		Ref.[30]	PRESENT	
d/a	a/R	F_I=F_{II}	F_I	F_{II}
0.05	1	1.383	1.262	1.882
0.10	1	1.403	1.428	1.298
0.20	1	1.482	1.501	1.656
0.30	1	1.593	1.599	1.844
0.40	1	1.727	1.730	1.996
0.50	1	1.903	1.905	2.163
0.60	1	2.145	2.145	2.381
0.70	1	2.500	2.499	2.703
0.80	1	3.095	3.092	3.257
0.90	1	4.425	4.421	4.535
0.05	5	0.847	0.896	1.071
0.10	5	0.916	0.934	1.221
0.20	5	1.056	1.063	1.349
0.30	5	1.213	1.217	1.466
0.40	5	1.395	1.398	1.610
0.50	5	1.617	1.619	1.798
0.60	5	1.901	1.903	2.052
0.70	5	2.299	2.299	2.420
0.80	5	2.937	2.936	3.029
0.90	5	4.319	4.315	4.378
0.05	50	0.436	0.420	0.563
0.10	50	0.555	0.548	0.644
0.20	50	0.765	0.762	0.825
0.30	50	0.971	0.969	1.017
0.40	50	1.191	1.189	1.228
0.50	50	1.444	1.443	1.474
0.60	50	1.757	1.755	1.781
0.70	50	2.181	2.179	2.200
0.80	50	2.844	2.843	2.859
0.90	50	4.255	4.252	4.263

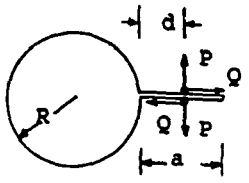

$F_I = K_I/(P/\sqrt{\pi a})$ $F_{II} = K_{II}/(Q/\sqrt{\pi a})$

Table 5.1.2. A horizontal point force, a vertical point force, or a concentrated moment acting on a radial crack emanating from a circular hole.

	ISOTROPIC		$\beta = 0°$		$\beta = 45°$		$\beta = 90°$	
d/a	K_I/K_o	K_{II}/K_o	K_I/K_o	K_{II}/K_o	K_I/K_o	K_{II}/K_o	K_I/K_o	K_{II}/K_o
0.05	0.111	0.931	0.029	1.033	0.135	0.945	0.255	0.874
0.10	0.104	0.983	-0.010	1.060	0.122	0.955	0.246	0.901
0.20	0.073	1.018	-0.034	1.093	0.114	0.973	0.215	0.926
0.30	0.065	1.047	-0.041	1.120	0.113	1.004	0.208	0.958
0.40	0.065	1.087	-0.043	1.156	0.114	1.052	0.208	1.005
0.50	0.067	1.147	-0.043	1.212	0.115	1.122	0.209	1.075
0.60	0.070	1.239	-0.041	1.298	0.117	1.225	0.211	1.178
0.70	0.074	1.388	-0.039	1.440	0.118	1.384	0.213	1.337
0.75	0.076	1.499	-0.038	1.547	0.118	1.501	0.214	1.454
0.80	0.077	1.654	-0.036	1.697	0.118	1.662	0.215	1.615
0.85	0.079	1.887	-0.035	1.924	0.118	1.900	0.216	1.853
0.90	0.080	2.284	-0.034	2.314	0.117	2.302	0.217	2.258
0.95	0.080	3.195	-0.035	3.216	0.115	3.219	0.216	3.177

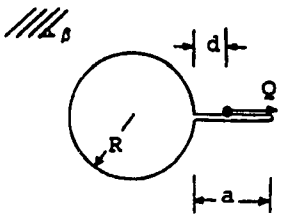

$K_o = Q/\sqrt{\pi a}$

	ISOTROPIC		$\beta = 0°$		$\beta = 45°$		$\beta = 90°$	
d/a	K_I/K_o	K_{II}/K_o	K_I/K_o	K_{II}/K_o	K_I/K_o	K_{II}/K_o	K_I/K_o	K_{II}/K_o
0.05	0.631	-0.276	0.718	-0.677	0.555	-0.325	0.607	-0.095
0.10	0.675	-0.275	0.766	-0.647	0.588	-0.310	0.638	-0.089
0.20	0.733	-0.244	0.816	-0.560	0.643	-0.277	0.691	-0.078
0.30	0.790	-0.214	0.864	-0.483	0.703	-0.250	0.752	-0.070
0.40	0.860	-0.189	0.924	-0.421	0.775	-0.228	0.827	-0.065
0.50	0.949	-0.169	1.004	-0.372	0.868	-0.208	0.921	-0.061
0.60	1.070	-0.153	1.117	-0.332	0.992	-0.191	1.048	-0.058
0.70	1.248	-0.141	1.287	-0.299	1.172	-0.176	1.230	-0.055
0.75	1.374	-0.136	1.409	-0.285	1.300	-0.168	1.359	-0.054
0.80	1.545	-0.131	1.575	-0.272	1.471	-0.161	1.532	-0.053
0.85	1.794	-0.127	1.819	-0.259	1.722	-0.153	1.783	-0.053
0.90	2.210	-0.123	2.230	-0.248	2.139	-0.145	2.201	-0.052
0.95	3.144	-0.120	3.158	-0.239	3.074	-0.136	3.138	-0.051

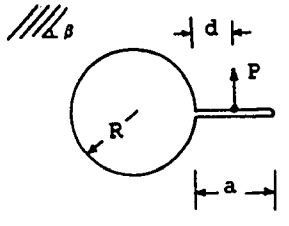

$K_o = P/\sqrt{\pi a}$

	ISOTROPIC		$\beta = 0°$		$\beta = 45°$		$\beta = 90°$	
d/a	K_I/K_o	K_{II}/K_o	K_I/K_o	K_{II}/K_o	K_I/K_o	K_{II}/K_o	K_I/K_o	K_{II}/K_o
0.05	1.231	-0.391	1.539	0.273	0.789	0.161	0.804	0.063
0.10	0.692	0.218	0.644	0.784	0.589	0.342	0.538	0.126
0.20	0.543	0.327	0.451	0.854	0.560	0.286	0.559	0.093
0.30	0.618	0.280	0.527	0.690	0.651	0.228	0.668	0.065
0.40	0.776	0.222	0.689	0.549	0.809	0.179	0.832	0.047
0.50	1.026	0.175	0.941	0.442	1.055	0.138	1.079	0.035
0.60	1.438	0.139	1.354	0.363	1.464	0.100	1.487	0.028
0.70	2.209	0.113	2.125	0.303	2.233	0.053	2.255	0.023
0.75	2.896	0.102	2.810	0.280	2.919	0.019	2.941	0.021
0.80	4.034	0.094	3.943	0.262	4.057	-0.034	4.078	0.021
0.85	6.184	0.088	6.087	0.252	6.209	-0.128	6.230	0.023
0.90	11.306	0.091	11.195	0.269	11.334	-0.353	11.356	0.036
0.95	31.806	0.163	31.659	0.512	31.847	-1.250	31.870	0.137

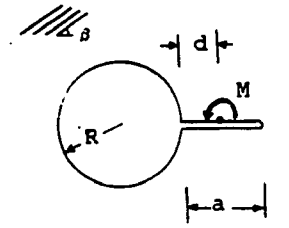

$K_o = M/a\sqrt{\pi a}$

Table 5.1.3. A radial crack emanating from a circular hole under internal pressure.

		ISOTROPIC	$\beta = 0°$	$\beta = 45°$		$\beta = 90°$
a / R	λ	K_I/K_o	K_I/K_o	K_I/K_o	K_{II}/K_o	K_I/K_o
0.1	0	0.967	1.058	0.926	0.172	1.062
0.5	0	0.574	0.620	0.581	0.055	0.551
1.0	0	0.368	0.389	0.373	0.009	0.357
1.5	0	0.264	0.274	0.269	-0.001	0.261
2.0	0	0.199	0.206	0.203	-0.006	0.195
2.5	0	0.158	0.162	0.161	-0.007	0.156
3.0	0	0.130	0.132	0.132	-0.007	0.128
4.0	0	0.093	0.094	0.095	-0.006	0.092
5.0	0	0.071	0.072	0.073	-0.005	0.070
6.0	0	0.057	0.057	0.058	-0.004	0.056
7.0	0	0.046	0.047	0.047	-0.004	0.046
8.0	0	0.039	0.039	0.040	-0.003	0.038
9.0	0	0.033	0.033	0.034	-0.003	0.033
10.0	0	0.029	0.029	0.029	-0.002	0.028
20.0	0	0.011	0.011	0.012	-0.001	0.011
1000.0	0	0.000	0.000	0.000	0.000	0.000
0.1	1	1.960	2.059	1.987	0.265	1.994
0.5	1	1.488	1.569	1.503	0.064	1.430
1.0	1	1.235	1.290	1.229	-0.032	1.207
1.5	1	1.105	1.143	1.104	-0.045	1.095
2.0	1	1.025	1.053	1.026	-0.047	1.015
2.5	1	0.972	0.993	0.974	-0.044	0.966
3.0	1	0.935	0.951	0.936	-0.041	0.930
4.0	1	0.885	0.894	0.886	-0.035	0.880
5.0	1	0.853	0.860	0.854	-0.030	0.849
6.0	1	0.831	0.836	0.831	-0.026	0.827
7.0	1	0.814	0.819	0.814	-0.024	0.811
8.0	1	0.802	0.805	0.802	-0.021	0.798
9.0	1	0.791	0.794	0.792	-0.019	0.789
10.0	1	0.784	0.787	0.783	-0.017	0.780
20.0	1	0.747	0.748	0.746	-0.009	0.745
1000.0	1	0.708	0.708	0.708	0.000	0.708

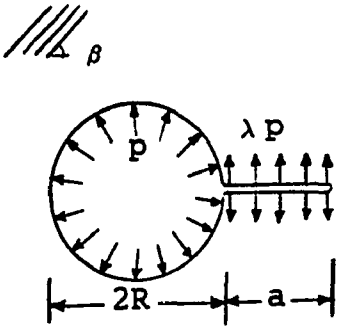

$K_o = p\sqrt{\pi a}$

Table 5.1.4. An edge crack emanating from an elliptical hole under uniaxial tension or pure shear.

	ISOTROPIC	Ref.[40]	$\beta = 0°$	$\beta = 45°$		$\beta = 90°$
a / A	K_I/K_∞	K_I/K_∞	K_I/K_∞	K_I/K_∞	K_{II}/K_∞	K_I/K_∞
0.1	3.248	3.256	2.914	3.508	0.852	3.362
0.2	2.471	2.460	2.375	2.569	0.347	2.437
0.5	1.638	1.640	1.651	1.638	0.036	1.639
1.0	1.253	1.248	1.277	1.254	-0.026	1.268
2.0	1.014	-	1.024	1.013	-0.032	1.021
3.0	0.922	-	0.927	0.921	-0.027	0.926
4.0	0.873	-	0.876	0.872	-0.023	0.876
5.0	0.842	-	0.845	0.842	-0.019	0.844
8.0	0.794	-	0.796	0.794	-0.013	0.795
10.0	0.780	-	0.779	0.777	-0.011	0.778
20.0	0.745	-	0.744	0.743	-0.006	0.743
1000.0	0.708	-	0.708	0.708	0.000	0.708

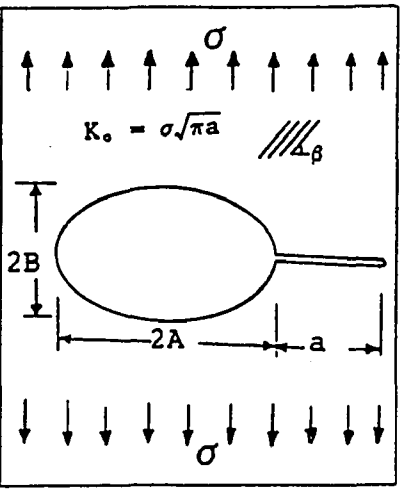

	ISOTROPIC	Ref.[40]	$\beta = 0°$	$\beta = 45°$		$\beta = 90°$
a / A	K_{II}/K_∞	K_{II}/K_∞	K_{II}/K_∞	K_I/K_∞	K_{II}/K_∞	K_{II}/K_∞
0.1	1.212	1.175	0.604	-0.598	1.193	1.883
0.2	1.463	1.443	0.834	-0.007	1.733	1.841
0.5	1.483	1.471	1.095	0.055	1.606	1.567
1.0	1.309	1.300	1.195	0.030	1.337	1.301
2.0	1.100	-	1.124	0.012	1.088	1.073
3.0	0.996	-	1.051	0.008	0.981	0.972
4.0	0.935	-	0.995	0.006	0.922	0.914
5.0	0.895	-	0.954	0.005	0.883	0.877
8.0	0.831	-	0.877	0.003	0.822	0.818
10.0	0.807	-	0.847	0.003	0.800	0.797
20.0	0.759	-	0.781	0.002	0.755	0.753
1000.0	0.708	-	0.709	0.000	0.708	0.708

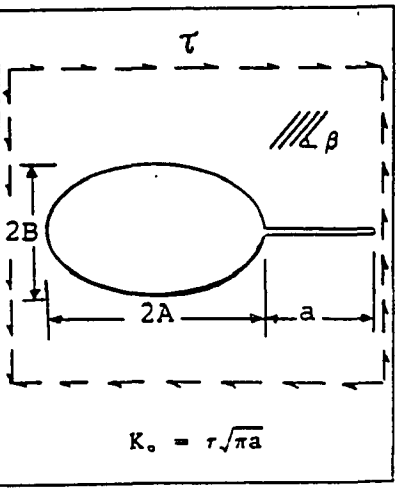

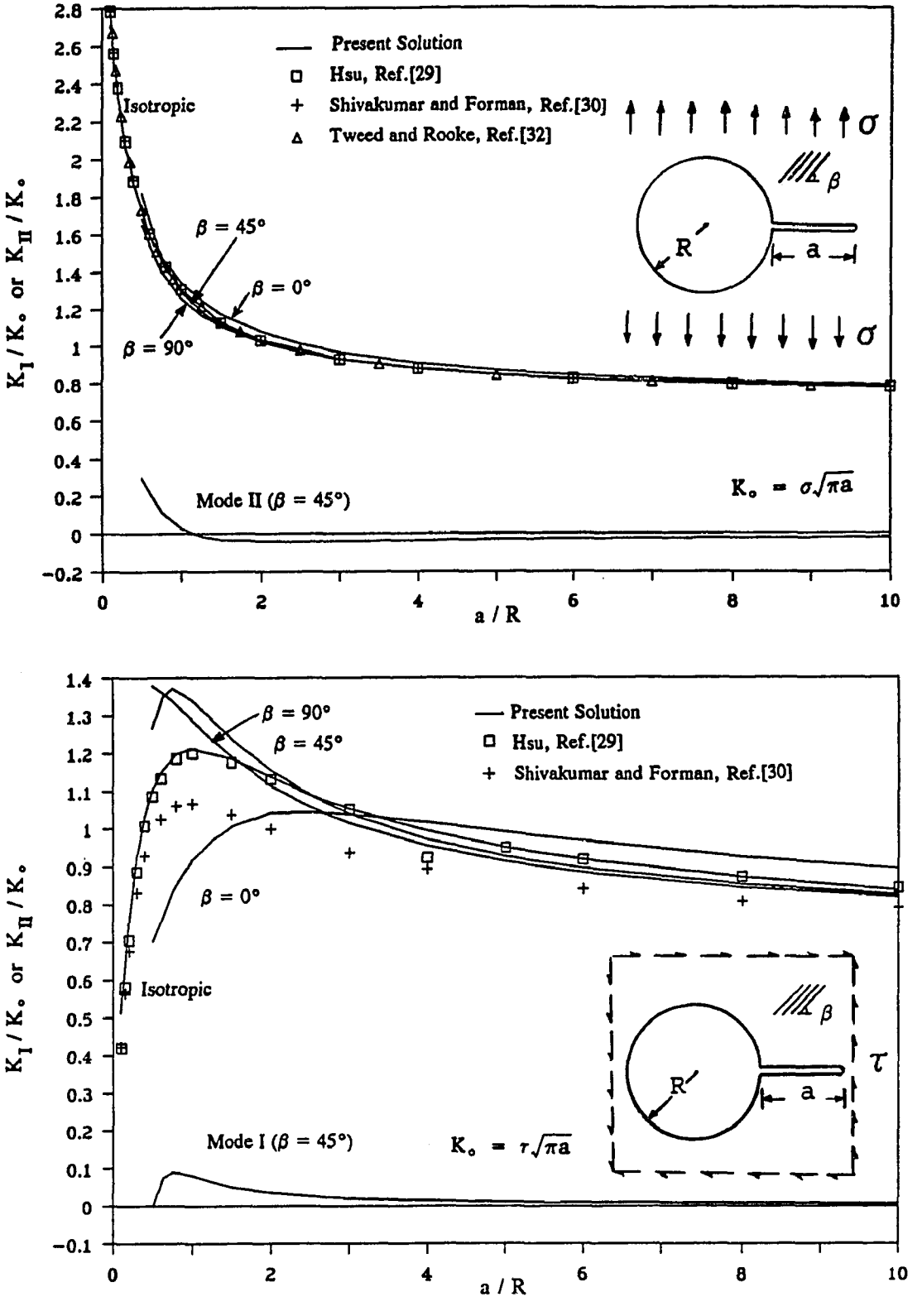

Figure 5.1.1. A radial crack emanating from a circular hole under uniaxial tension or uniform shear.

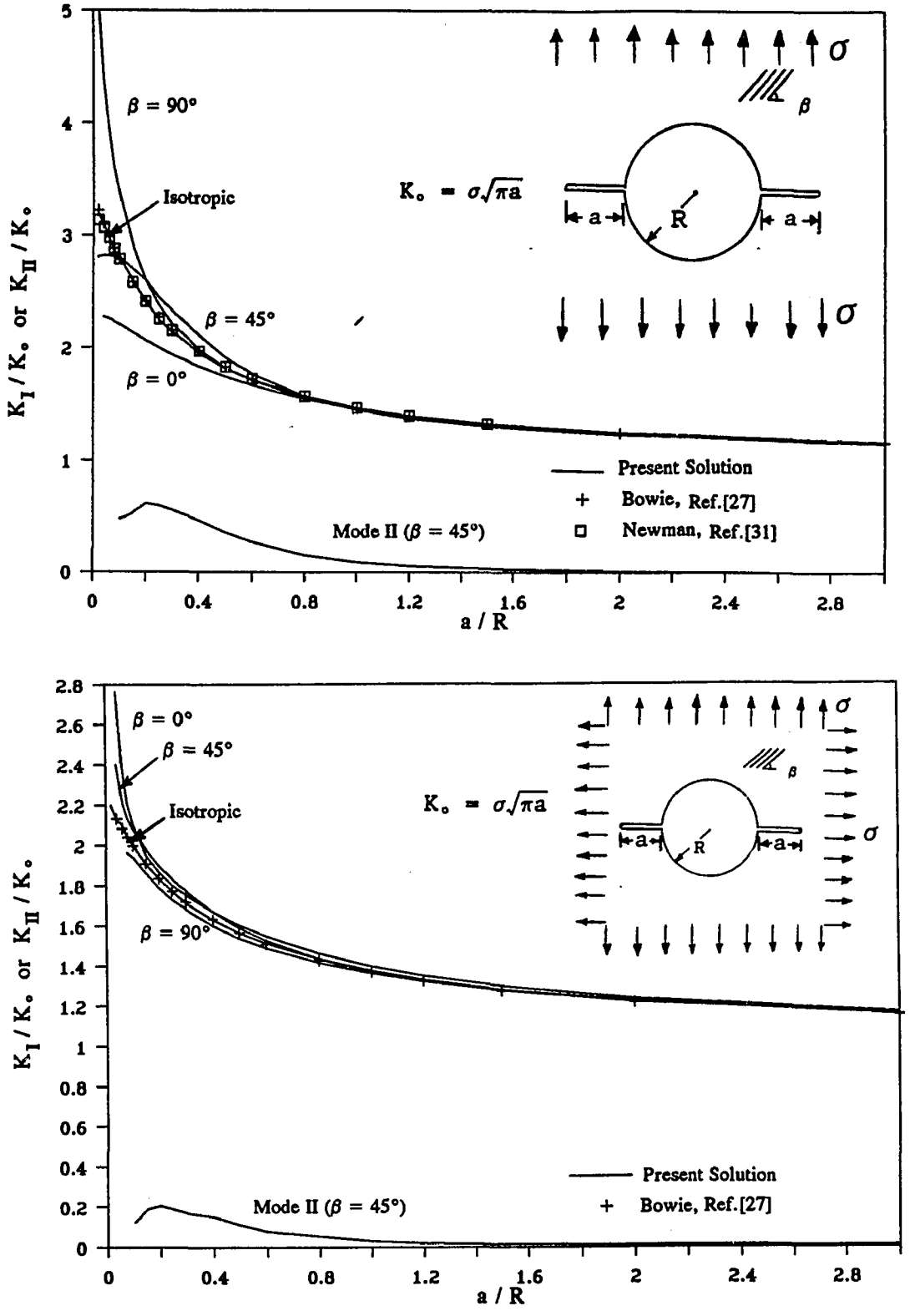

Figure 5.1.2. Two symmetric radial cracks emanating from a circular hole under uniaxial or biaxial tension.

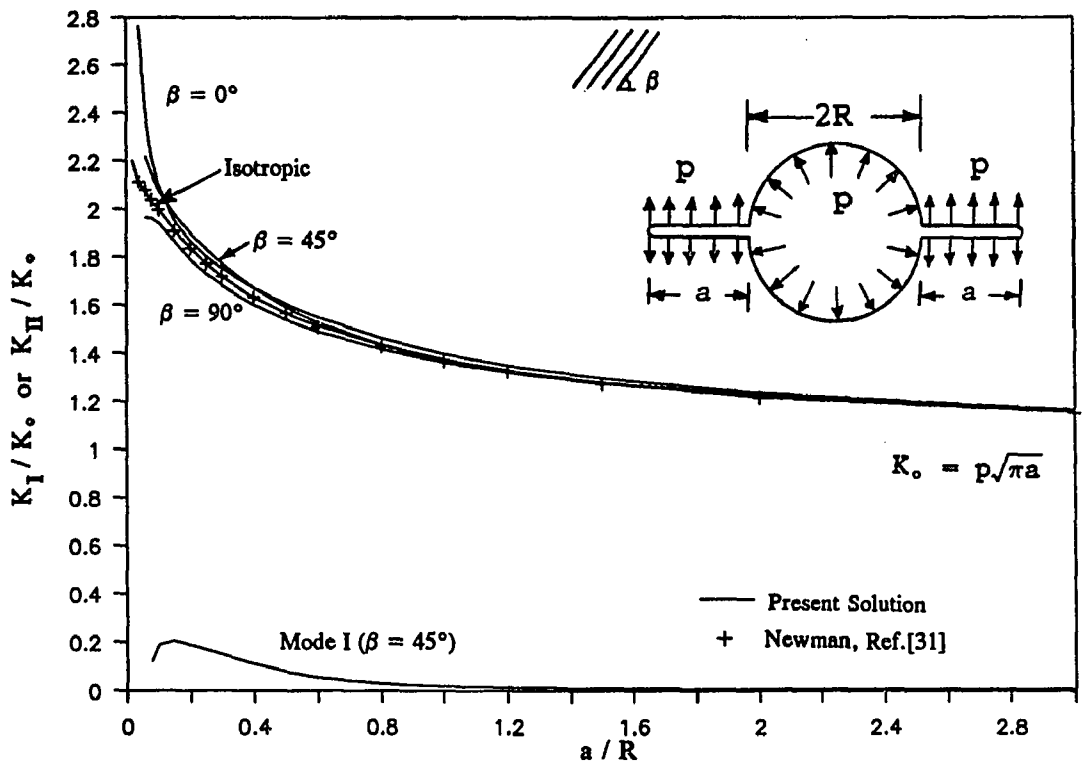

Figure 5.1.3. Two symmetric radial cracks emanating from a circular hole under internal pressure.

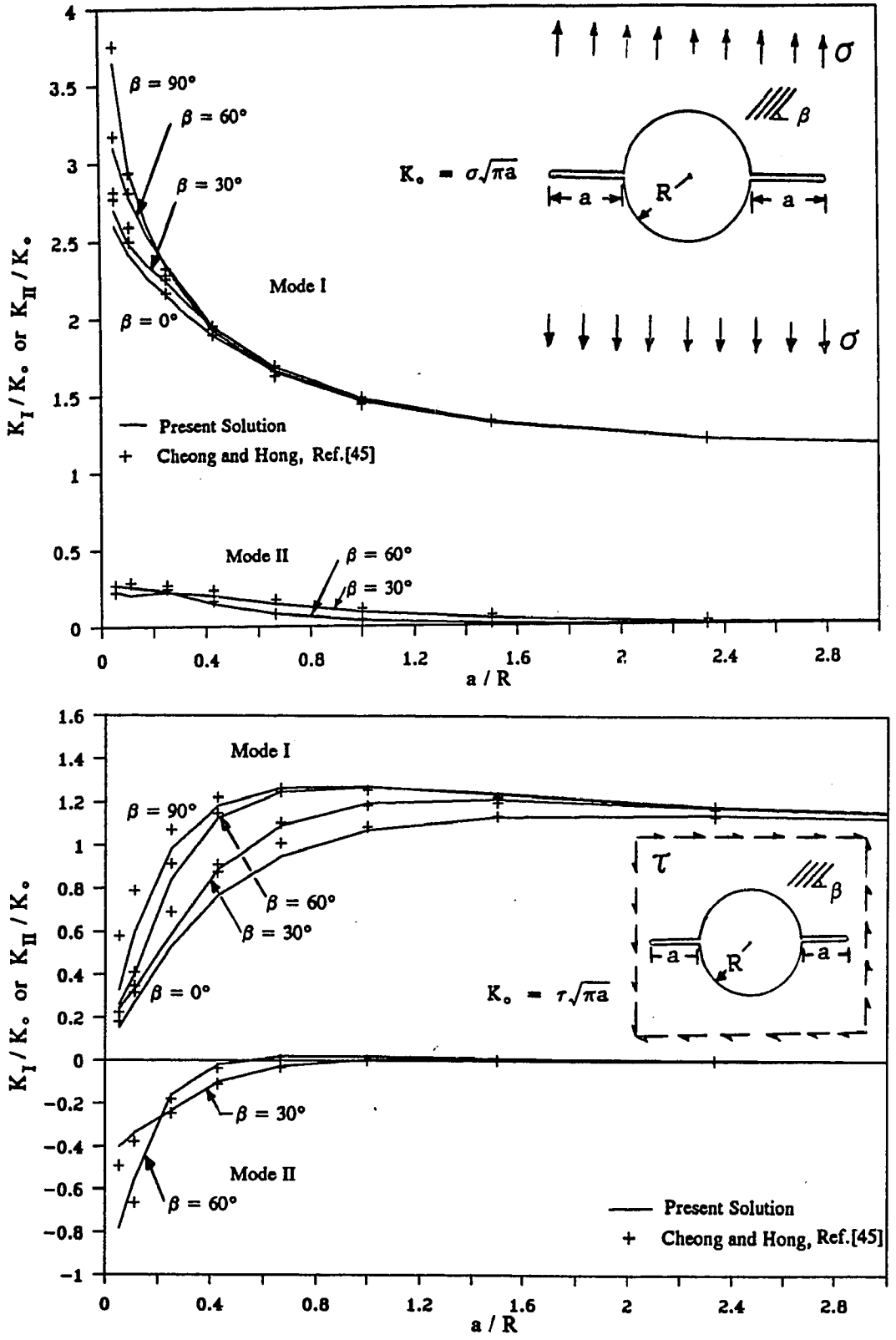

Figure 5.1.4. Two symmetric radial cracks emanating from a circular hole under uniaxial tension or uniform shear.

V.2 CRACKS AT A FASTENER HOLE IN AN ANISOTROPIC PLATE

V.2.1 Background

Like other structural members, components made of composites very often need to be joined together. Two of the most widely used methods of joining composites are mechanical fastening and adhesive bonding. The former approach, although being less expensive, has the disadvantage that the necessary hole drilled in the composite will create a high stress concentration, destroy fiber continuity, and form microcracks at the edge of the hole. These microcracks when loaded may propagate and coalesce to form a major crack and cause catastrophic structural failure. A pin-loaded hole in general is a major source of failure in the mechanically fastened joints and therefore plays an important role in designing safer and more reliable connections.

There have been quite a number of studies relating to the failure analysis of composites with bolted joints. Most of them, however, assumed the fastener hole to be flaw-free and used the elasticity approach to obtain the stress distribution in the vicinity of the hole. Linear elastic fracture mechanics (LEFM) approach was employed by Waszczak and Cruse [47], who conducted a two-dimensional stress analysis in conjunction with a fracture model to predict failure strength and location. Yet so far only a few researchers have obtained numerical values of the stress intensity factors for the isotropic case and currently no solution exists for the anisotropic counterparts. Ball [48] calculated the mode I stress intensity factors for finite width plates, lugs, and multi-fastener joints by superimposing individual solutions for various loading conditions. Grandt, et al. [37,49,50] applied the principle of

superposition to transform the problem to that of an edge crack with crack face pressure defined as the unflawed hoop stress surrounding the fastener. Cartwright and Ratcliffe [51] evaluated the stress intensity factors for a pair of symmetric cracks at the edge of a fastener hole in an infinite isotropic strip. Tweed and Rooke [36] used Mellin transform to reduce the cracked hole problem into a singular integral equation and solved it numerically for the stress intensity factors due to a radial force acting at the perimeter of the hole. This solution can then be used as a Green's function to construct the solutions due to an arbitrary distribution of radial forces, as demonstrated by Rooke and Tweed [35], who studied various loading conditions to simulate the pin load. Rooke and Hutchins [52] extended the solution in [36] to also include Green's function for a tangential force applied at the perimeter of the hole, thus allowing them to consider the effect of surface friction at the bolted holes. Their results are in good agreement with those reported by Shivakumar and Hsu [53]. Finally, the compounding technique was used by Rooke [38] to compute stress intensity factors for a row of cracked fastener holes. In all the fracture studies mentioned above, however, only fastener holes in an isotropic medium were considered. Their solutions, therefore, can not be applied to bolted joints in composite materials which should be considered as anisotropic. Consequently, there is an urgent need for a method to evaluate stress intensity factors for flawed fastener holes in anisotropic materials.

V.2.2 Numerical Results and Discussions

Here to simulate the pin load, the cases of point load, arc of uniform pressure, and cosine distribution of loading are considered. For purpose of comparison, the results of a double-cracked circular hole in an isotropic medium with two splitting vertical forces P are listed in Table 5.2.1. The crack on the right side of the hole is of length a and the one on the left λa. Therefore, $\lambda=0$ represents the case of a single-cracked hole. In Table 5.2.1, the values of mode I stress intensity factors with an asterisk symbol ("*") attached were read from a graph in [33], whereas the ones without the asterisk symbol were arrived at using the tables compiled in [52]. As shown in Table 5.2.1, the present results are very close to those obtained in [33,52] except for the very short cracks, a/R=0.01.

Figure 5.2.1 depicts the case of a single-cracked hole subjected to a vertical point load P at (0,R). The results are shown for isotropic case and for the orthotropic cases with fiber angle β equal to 0, 45, and 90 degrees with respect to the positive x-axis. As we can see from the figure, mode I stress intensity factor for the $\beta=45°$ case and mode II stress intensity factor for the $\beta=90°$ case tend to stabilize once a/R reaches 0.3. Also, the results for the isotropic case and the orthotropic cases are quite apart, indicating that the anisotropic effect can not be ignored. The results for the double-cracked hole are given in Fig. 5.2.2. It is apparent from comparing Figs. 5.2.1 and 5.2.2 that the second crack has almost no influence on the stress intensity factors for both isotropic and anisotropic cases. Also it is noticeable that both mode I and mode II stress intensity factors for $\beta=45°$ are much higher for the left crack tip than for the right tip. This is due to the in-plane normal-shear

coupling which occurs when the fibers are not directed symmetrically with respect to the symmetric axis of loading.

Next, the pin load is simulated by an arc of uniform pressure applied symmetrically with respect to the y-axis on the perimeter of the hole. The case where the span angle of loading 2θ=60° is given in Fig. 5.2.3, where a single-cracked hole with a/R varying between 0 and 1 is considered. For the isotropic case, a very good agreement exists between the stress intensity factors obtained in this study and the ones reported by Rooke and Hutchins [52]. As the graph indicates, much higher values of opening mode stress intensity factors are observed for β=90° case for short cracks (a/R less than 0.2). In Fig. 5.2.4 the loading span angle is increased to 120° and it is observed that other than an increase in the values of stress intensity factors, the basic trends of the graph remain the same. In Fig. 5.2.5, the uniform pressure is assumed to cover the upper half of the hole (2θ=180°). In this case, still larger values of mode I stress intensity factors are obtained for β=90°. But now, mode I values for β=45° become negative for crack length ratios smaller than a/R=0.1. This again indicates the effect of normal-shear coupling which tends to push the crack faces against each other. Finally, the pin load is simulated by the prevailing cosine distribution of loading. The results are depicted in Figs. 5.2.6 and 5.2.7 for one crack and two cracks, respectively. It is seen that the results in Fig. 5.2.6 are very close to the ones for 2θ=120° in Fig. 5.2.4. The effect of friction has been proven to be significant in some cases on the stress state near the hole and ultimately on the stress intensity factors [52]. Therefore, the correct stress intensity factors for cracks emanating from a fastener hole will be the combination of the

stress intensity factors due to normal and tangential loadings. To account for this fact, Fig. 5.2.8 depicts the stress intensity factors for a single cracked hole subjected to shear loading of the form $\tau(\theta) = \tau \cos(\theta)$ on its upper-half. A composite with the properties $E_1/E_2=10$ and $\nu_{12}=1/3$ was selected for this calculation. The isotropic results are in excellent agreement with the ones reported by Rooke and Hutchins [52]. Again as can be seen from the graph, effect of anisotropy on the stress intensity factors is substantial when the crack length is short.

So far, we have considered separately the effect of each loading case, i.e. point load, arc of uniform pressure and cosine distribution of loading. Tables 5.2.2 to 5.2.5 are intended to show the comparison between these loading conditions by making the resultant load of the distributed loading cases equal to that of the point load case P. Again a single-cracked circular hole is considered with a/R ratio varying between 0 and 1. In these tables the normalization factor K_o represents K_I or K_{II} for the corresponding point load case. Table 5.2.2 is for the isotropic case, while the values for their orthotropic counterparts with β equal to 0, 45 and 90 degrees are given in Tables 5.2.3, 5.2.4, and 5.2.5, respectively. It is seen that mode I values for the isotropic and the orthotropic cases are all fairly close to 1 except for $2\theta=180°$ with $\beta=45°$ in Table 5.2.4. This indicates that with the exception of this individual case, the mode I values for the other loading cases may be roughly estimated by the ones for the point load case. The deviation for the case of ($2\theta=180°$; $\beta=45°$) may be explained as follows. The uniform pressure in this case reaches the crack and therefore for short cracks there is a strong horizontal

component of loading in the vicinity of the crack tip, making the sliding mode stress intensity factor the dominant value over its opening mode counterpart. The normal-shear coupling effect due to the fiber orientation together with this large sliding force then tend to push the crack faces against each other. Once the crack is long enough (a/R > 0.1), this large sliding force is not close to the crack tip and the values of K_I/K_o tend to rebound towards 1. It is also noticed that for mode II of the same case there is an abrupt change of value at a/R=0.3. This is due to the fact that at this particular crack length, mode II stress intensity factor for the point load case changes sign and becomes very small, as shown in Fig. 5.2.1.

Table 5.2.1. Two cracks of unequal lengths emanating from a circular hole subjected to two splitting vertical forces in an isotropic plate.

	λ = 0.0		λ = 0.5		λ = 1.0		λ = 2.0	
a/R	Present	Ref.[33,52]	Present	Ref.[33]	Present	Ref.[33]	Present	Ref.[33]
0.01	0.01650	0.02199	0.01675	-	0.01674	-	0.01674	-
0.05	0.09016	0.10202	0.09104	-	0.09108	-	0.09133	-
0.10	0.17310	0.18660	0.17449	-	0.17494	-	0.17672	-
0.50	0.52314	0.53092	0.53273	-	0.55250	0.559*	0.58932	0.640*
1.00	0.63776	0.64088	0.67860	0.682*	0.72946	0.728*	0.80031	0.797*
2.00	0.64448	0.62832	0.75235	0.751*	0.84912	0.858*	0.94275	-
3.00	0.60559	0.598*	0.77333	0.770*	0.88442	-	1.00164	-
4.00	0.56680	0.552*	0.78358	0.828*	0.90859	-	1.03763	-
5.00	0.53305	0.536*	0.79061	-	0.92592	0.920*	1.06499	1.073*

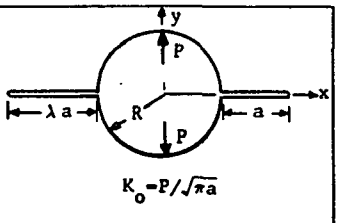

* Value Read From a Graph in Ref.[33]

Table 5.2.2. Mode I and mode II stress intensity factors for distributed loadings with an equal load resultant normalized by their point load counterparts (isotropic case).

	Uniform ($2\theta = 60°$)		Uniform ($2\theta = 120°$)		Uniform ($2\theta = 180°$)		Cosine Distribution	
a/R	K_I/K_o	K_{II}/K_o	K_I/K_o	K_{II}/K_o	K_I/K_o	K_{II}/K_o	K_I/K_o	K_{II}/K_o
0.01	1.272	-0.999	1.458	0.991	1.184	-51.876	1.474	0.264
0.02	1.183	0.998	1.351	0.982	0.997	-25.581	1.342	0.268
0.04	1.142	0.998	1.295	0.966	0.910	-12.857	1.261	0.276
0.06	1.128	0.993	1.269	0.945	0.880	-8.593	1.219	0.277
0.08	1.119	0.991	1.250	0.928	0.863	-6.511	1.188	0.280
0.10	1.112	0.990	1.234	0.911	0.852	-5.230	1.162	0.280
0.12	1.107	0.988	1.218	0.894	0.845	-4.371	1.141	0.282
0.14	1.102	0.986	1.204	0.877	0.839	-3.752	1.122	0.285
0.16	1.097	0.984	1.191	0.861	0.835	-3.285	1.106	0.287
0.18	1.093	0.982	1.178	0.845	0.832	-2.920	1.091	0.288
0.20	1.090	0.980	1.166	0.829	0.829	-2.627	1.078	0.290
0.25	1.082	0.975	1.139	0.793	0.826	-2.098	1.051	0.294
0.30	1.076	0.970	1.115	0.760	0.825	-1.742	1.030	0.300
0.35	1.069	0.965	1.094	0.731	0.825	-1.485	1.013	0.303
0.40	1.064	0.961	1.075	0.705	0.827	-1.292	0.999	0.328
0.45	1.059	0.956	1.059	0.682	0.829	-1.140	0.988	0.314
0.50	1.054	0.952	1.045	0.663	0.832	-1.018	0.979	0.318
0.60	1.046	0.945	1.023	0.631	0.839	-0.832	0.965	0.328
0.70	1.040	0.938	1.007	0.608	0.846	-0.697	0.957	0.337
0.80	1.035	0.933	0.994	0.591	0.855	-0.594	0.951	0.348
1.00	1.028	0.924	0.980	0.571	0.872	-0.443	0.946	0.366

Table 5.2.3. Mode I and mode II stress intensity factors for distributed loadings with an equal load resultant normalized by their point load counterparts (β=0° case).

	Uniform ($2\theta = 60°$)		Uniform ($2\theta = 120°$)		Uniform ($2\theta = 180°$)		Cosine Distribution	
a/R	K_I/K_o	K_{II}/K_o	K_I/K_o	K_{II}/K_o	K_I/K_o	K_{II}/K_o	K_I/K_o	K_{II}/K_o
0.01	1.169	1.060	1.405	1.316	1.678	-36.103	1.476	1.256
0.02	1.144	1.060	1.351	1.313	1.530	-16.901	1.407	1.262
0.04	1.114	1.059	1.296	1.306	1.392	-7.550	1.333	1.234
0.06	1.104	1.057	1.274	1.296	1.334	-4.548	1.301	1.215
0.08	1.100	1.056	1.262	1.287	1.299	-3.102	1.281	1.193
0.10	1.097	1.055	1.253	1.280	1.273	-2.266	1.266	1.171
0.12	1.095	1.056	1.246	1.273	1.252	-1.728	1.253	1.154
0.14	1.093	1.054	1.239	1.263	1.233	-1.350	1.241	1.136
0.16	1.091	1.053	1.232	1.254	1.217	-1.077	1.230	1.121
0.18	1.089	1.052	1.225	1.245	1.202	-0.869	1.220	1.105
0.20	1.088	1.051	1.219	1.235	1.188	-0.707	1.210	1.089
0.25	1.084	1.048	1.204	1.212	1.159	-0.427	1.189	1.057
0.30	1.080	1.045	1.189	1.189	1.134	-0.251	1.170	1.027
0.35	1.077	1.042	1.176	1.167	1.112	-0.133	1.153	1.002
0.40	1.073	1.039	1.163	1.146	1.093	-0.048	1.138	0.978
0.45	1.071	1.036	1.151	1.126	1.077	0.015	1.124	0.957
0.50	1.067	1.033	1.139	1.107	1.063	0.063	1.111	0.938
0.60	1.062	1.028	1.119	1.073	1.038	0.131	1.090	0.906
0.70	1.057	1.023	1.101	1.042	1.018	0.176	1.071	0.880
0.80	1.052	1.018	1.085	1.015	1.003	0.208	1.056	0.858
1.00	1.044	1.009	1.059	0.970	0.979	0.251	1.032	0.822

Table 5.2.4. Mode I and mode II stress intensity factors for distributed loadings with an equal load resultant normalized by their point load counterparts (β=45° case).

	Uniform (2θ = 60°)		Uniform (2θ = 120°)		Uniform (2θ = 180°)		Cosine Distribution	
a/R	K_I/K_o	K_{II}/K_o	K_I/K_o	K_{II}/K_o	K_I/K_o	K_{II}/K_o	K_I/K_o	K_{II}/K_o
0.01	1.099	0.945	1.126	0.815	-0.523	-34.380	0.960	-0.236
0.02	1.066	0.996	1.031	-0.949	-0.529	8.025	0.835	1.135
0.04	1.051	0.996	1.004	0.965	-0.265	5.410	0.814	1.184
0.06	1.046	1.001	0.991	0.990	-0.116	4.933	0.807	1.273
0.08	1.043	1.004	0.982	1.016	-0.010	4.789	0.806	1.362
0.10	1.041	1.009	0.976	1.050	0.073	4.808	0.807	1.457
0.12	1.039	1.016	0.971	1.092	0.140	4.936	0.810	1.562
0.14	1.038	1.023	0.968	1.142	0.196	5.154	0.814	1.680
0.16	1.037	1.032	0.965	1.205	0.246	5.492	0.819	1.823
0.18	1.036	1.046	0.963	1.291	0.289	6.036	0.825	2.020
0.20	1.035	1.066	0.962	1.415	0.328	6.897	0.831	2.296
0.25	1.035	1.197	0.962	2.210	0.410	12.835	0.848	4.070
0.30	1.035	-1.800	0.965	-15.871	0.476	-126.492	0.867	-36.305
0.35	1.036	0.728	0.968	-0.604	0.532	-9.051	0.885	-2.219
0.40	1.036	0.829	0.972	0.011	0.579	-4.397	0.902	-0.847
0.45	1.037	0.864	0.976	0.225	0.619	-2.808	0.918	-0.370
0.50	1.037	0.881	0.979	0.333	0.652	-2.021	0.932	-0.132
0.60	1.035	0.898	0.983	0.441	0.705	-1.251	0.953	0.107
0.70	1.034	0.906	0.985	0.495	0.745	-0.873	0.969	0.226
0.80	1.032	0.911	0.986	0.528	0.774	-0.647	0.981	0.299
1.00	1.025	0.916	0.989	0.568	0.815	-0.383	0.996	0.385

Table 5.2.5. Mode I and mode II stress intensity factors for distributed loadings with an equal load resultant normalized by their point load counterparts (β=90° case).

	Uniform (2θ = 60°)		Uniform (2θ = 120°)		Uniform (2θ = 180°)		Cosine Distribution	
a/R	K_I/K_o	K_{II}/K_o	K_I/K_o	K_{II}/K_o	K_I/K_o	K_{II}/K_o	K_I/K_o	K_{II}/K_o
0.01	1.190	0.822	1.351	0.148	0.696	-36.568	1.301	-1.370
0.02	1.149	0.838	1.290	0.128	0.622	-22.205	1.210	-1.381
0.04	1.124	0.833	1.238	0.087	0.599	-14.003	1.128	-1.344
0.06	1.111	0.830	1.202	0.051	0.600	-10.990	1.080	-1.313
0.08	1.101	0.825	1.173	0.019	0.608	-9.305	1.045	-1.280
0.10	1.093	0.821	1.148	-0.009	0.617	-8.210	1.020	-1.253
0.12	1.087	0.817	1.126	-0.035	0.627	-7.420	0.999	-1.225
0.14	1.081	0.814	1.107	-0.058	0.637	-6.819	0.983	-1.197
0.16	1.076	0.811	1.090	-0.078	0.646	-6.338	0.971	-1.172
0.18	1.071	0.807	1.075	-0.096	0.656	-5.943	0.960	-1.148
0.20	1.068	0.804	1.062	-0.113	0.666	-5.608	0.951	-1.124
0.25	1.060	0.797	1.037	-0.146	0.688	-4.960	0.936	-1.068
0.30	1.053	0.791	1.018	-0.171	0.709	-4.485	0.927	-1.018
0.35	1.048	0.786	1.004	-0.189	0.728	-4.113	0.921	-0.972
0.40	1.043	0.781	0.993	-0.202	0.746	-3.814	0.918	-0.929
0.45	1.038	0.777	0.985	-0.210	0.763	-3.565	0.917	-0.887
0.50	1.034	0.773	0.980	-0.215	0.778	-3.355	0.917	-0.849
0.60	1.027	0.767	0.973	-0.216	0.806	-3.012	0.920	-0.779
0.70	1.025	0.763	0.970	-0.210	0.831	-2.745	0.925	-0.717
0.80	1.024	0.761	0.970	-0.198	0.853	-2.527	0.930	-0.659
1.00	1.027	0.758	0.974	-0.167	0.889	-2.190	0.943	-0.547

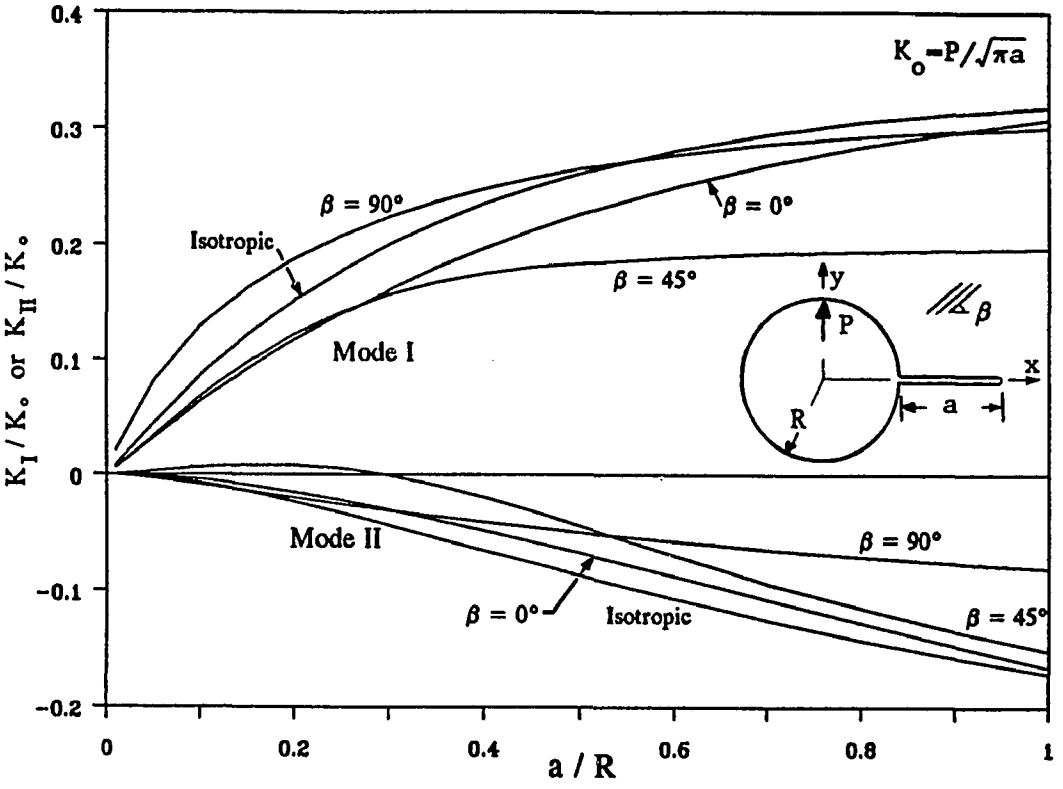

Figure 5.2.1. A single cracked circular hole loaded by a radial force in an anisotropic plate.

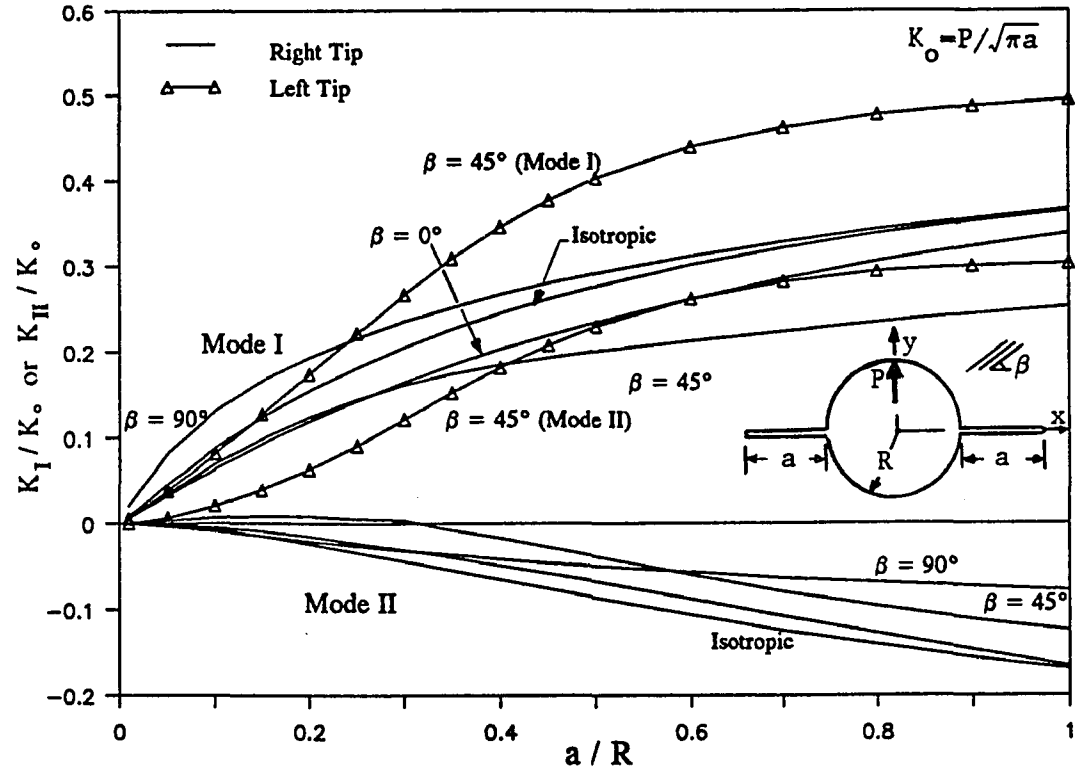

Figure 5.2.2. A double cracked circular hole loaded by a radial force in an anisotropic plate.

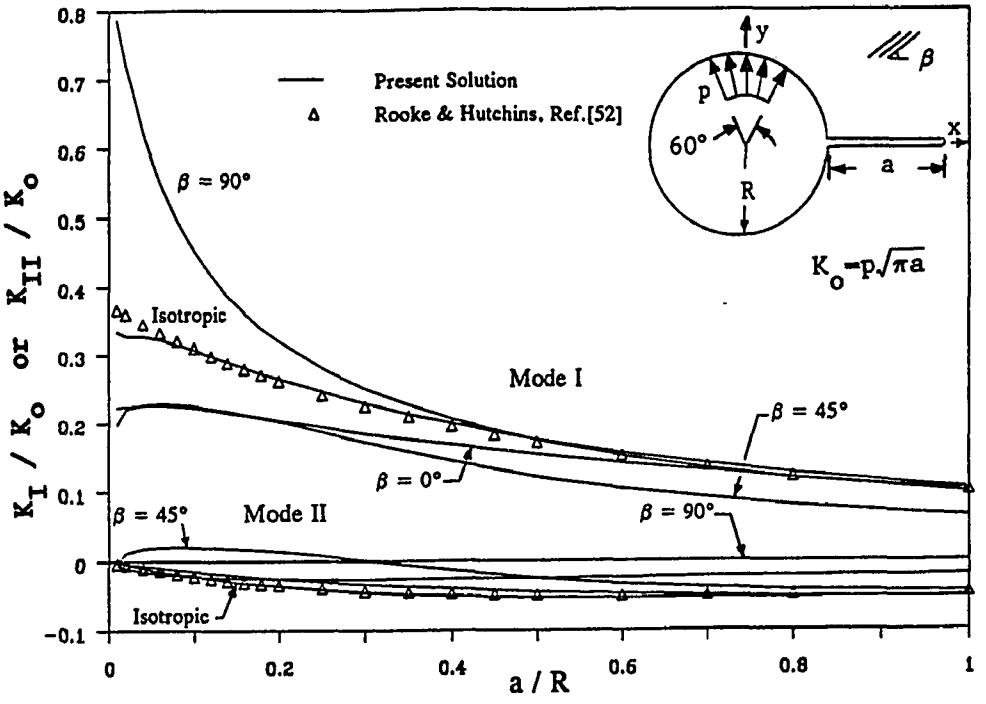

Figure 5.2.3. A single cracked circular hole loaded by an arc of uniform pressure of span 2θ=60° in an anisotropic plate.

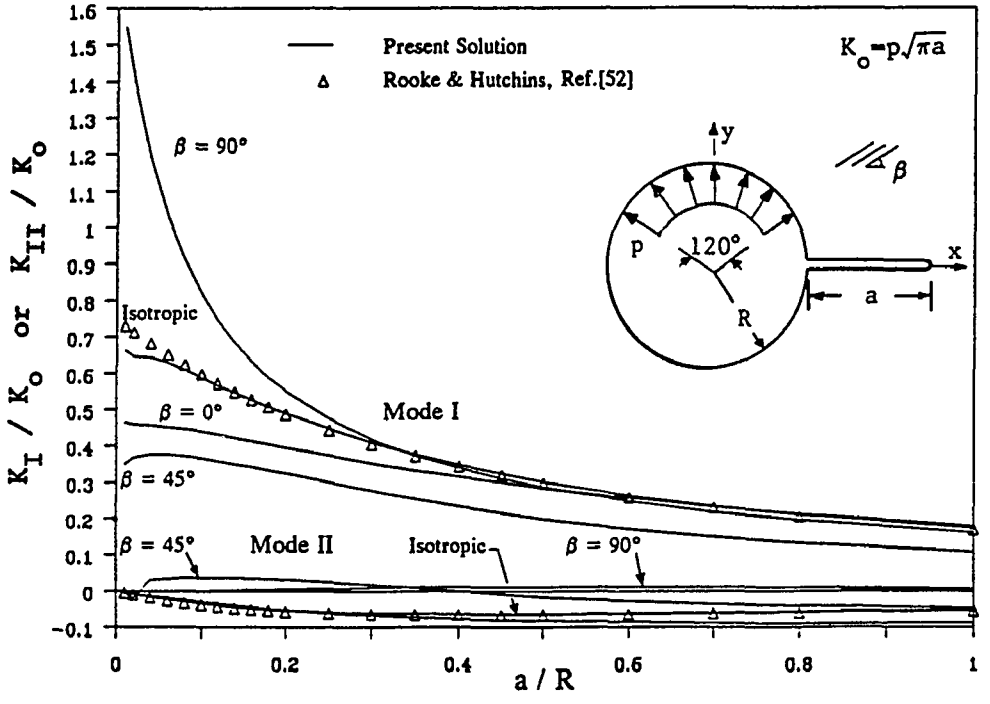

Figure 5.2.4. A single cracked circular hole loaded by an arc of uniform pressure of span 2θ=120° in an anisotropic plate.

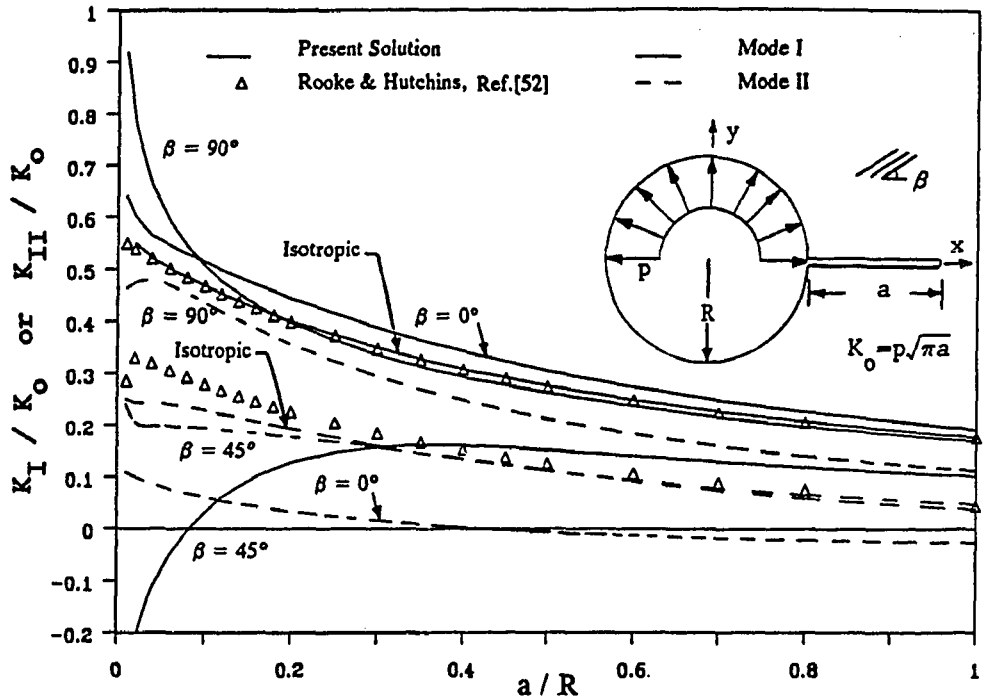

Figure 5.2.5. A single cracked circular hole loaded by an arc of uniform pressure of span 2θ=180° in an anisotropic plate.

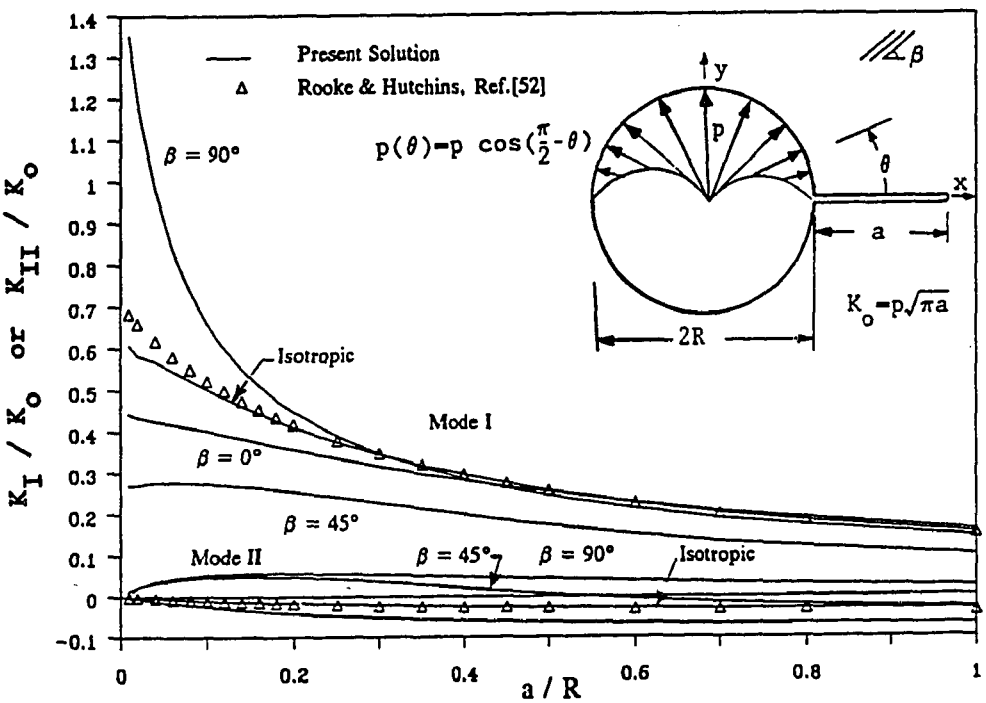

Figure 5.2.6. A single cracked circular hole loaded by a cosine distribution of pressure in an anisotropic plate.

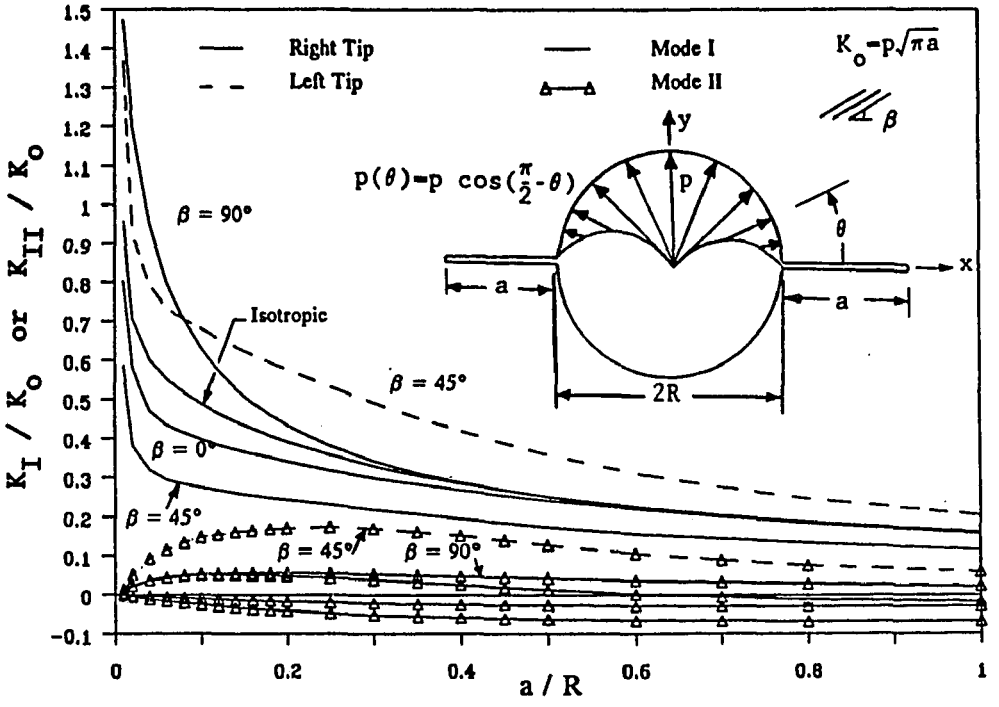

Figure 5.2.7. A double cracked circular hole loaded by a cosine distribution of pressure in an anisotropic plate.

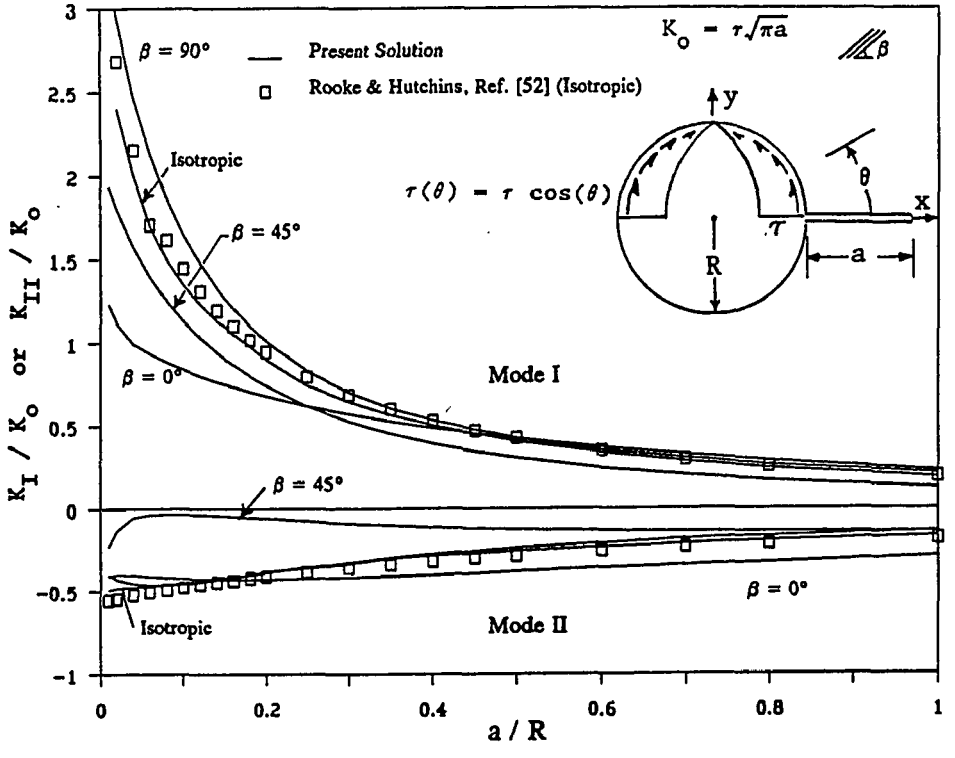

Figure 5.2.8. A single cracked circular hole loaded by a frictional type shear loading in an anisotropic plate.

V.3 AN ANISOTROPIC SOLID DISK CONTAINING A CRACK UNDER GENERAL LOADINGS

V.3.1 Background

The problem of stress intensity factors of cracks contained in an isotropic solid disk has been studied by various techniques. For instance, during the past two decades Tweed, Rooke and their associates [54-59] have used Mellin transform to reduce the cracked disk problems into Fredholm integral equations of the second kind which were then solved numerically. Concurrently a sequence of studies on the same topic has also been conducted in the Soviet Union using Muskhelishvili's method [12]. An excellent review on the Russian papers can be referred to Yarema [60]. The cracked disk problems were also investigated by Bowie and Neal [46] using modified mapping-collocation (MMC) method, by Isida [61] using Laurent series expansion, and by Shangchow [62] using Schwarz's alternating method. Both internal [46,54,55,58,60-62] or edge [56,57,59] cracks were considered and the loading types were uniform pressure [46,54,56,62], diametral tension/compression [58,60,61,62], pure shear [61], constant-speed rotation [55,57,59], or arbitrary loadings [60,61]. On the other hand research on the fracture of anisotropic solid disks is still very meager, despite of the advancements over the past decade on the use of composite materials in solid disks, such as flywheels [87].

V.3.2 Numerical Results and Discussions

The mixed-mode stress intensity factors due to a pair of horizontal forces Q, vertical forces P, or concentrated moments M acting on the surface of a central crack of length 2a in a circular disk of radius R are given in Figure 5.3.1. The computations assumed

a constant ratio of the crack length versus the disk diameter, i.e., a/R = 0.5. The loading point is located at a distance x_o away from the disk center. For the cases due to the horizontal and vertical forces, numerically higher stress intensity factors were found with higher fiber angle β. For the concentrated moment case, when the fiber angle β is high, numerically larger stress intensity factor was also found at the far-end crack tip C. However no consistent dependency on anisotropy can be found for the near-end crack tip D. Even though the loading and geometrical conditions are symmetrical, small but not negligible K_I for the horizontal force case and K_{II} for the vertical force and concentrated moment cases are present for the β=45° case which possesses asymmetrical anisotropy with respect to the loading and geometric conditions. This observation is true for all problems computed below.

The results for the case where two concentrated forces P are applied symmetrically along a diametral line normal to a central crack of length 2a inside a solid circular disk of radius R are shown in Tables 5.3.1 and 5.3.2 and Fig. 5.3.2. The normalized crack length is denoted as a/R and loading locations as y_o/R. The effect of y_o/R on stress intensity factors with a constant a/R equal to 0.5 is depicted in Table 5.3.1. The isotropic results computed by the proposed BIE method are first compared with those obtained respectively by Libatskii and Kovchik [63], Yarema [60], and an in-house finite element (FEM) program [64] which has been proved to have an accuracy within 3% when the crack length is moderate. As shown in Table 5.3.1 the BIE isotropic result is in excellent agreement with the FEM solution and quite comparable with Yarema's [60] result.

These results also can match in a reasonably well fashion with the earlier solution obtained by Libatskii and Kovchik [63] when y_o/R is greater than 0.4. For smaller y_o/R their results, however, tend to be underestimated substantially in comparison with the other three solutions. The Libatskii-Kovchik's result shown in Table 5.3.1 is computed according to the formula corrected by Rooke and Cartright [65]. Their original paper [63] was also checked and it was found that the results based on their original formula were even more erratic. For the isotropic case, the maximum stress intensity factor occurs when y_o/R is between 0.2 and 0.3. For the anisotropic cases, however, the maximum value may occur near the disk center (as in the β=0° case), near the edge (as in the β=90° case), or around y_o/R=0.2 (as in the β=45° case). It is also noticed that the isotropic case is closer to the β=45° case than to the other two cases. This may be explained by the fact that for β=45° the effect of anisotropy averages out along the directions perpendicular and parallel to the crack. In general, this observation is true when the loading and geometric conditions are symmetrical.

We next fix the loading locations at y_o/R=0.5 and vary the crack length. The isotropic results are tabulated in Table 5.3.2, which shows that the solutions obtained by BIE, FEM, Libatskii and Kovchik [63], and Yarema [60] are all in excellent agreement except when a/R is larger than 0.8. It should be noted that truncated power series in terms of a/R was used in [60] and [63]. Relatively large errors might have been introduced when a/R approached 1. The anisotropic effect is shown in Fig. 5.3.2 which also includes the results for an elliptical disk: $x^2/A^2 + y^2/B^2 = 1$. In general, the

case of smaller aspect ratio, B/A=0.5, has higher stress intensity factors. This may be due to the fact that, with the loading conditions specified above, the case with B/A=0.5 has its loading position closer to the crack than the other two cases do.

Figure 5.3.3 shows the variations of stress intensity factors when the central crack rotates about the disk axis while the loading locations are fixed at $y_o/R=0.7$ and the constant crack length is a/R=0.5. For all cases, whether isotropic or anisotropic, the maximum K_{II} stress intensity factor occurs in the neighborhood of $\alpha=45°$. Stress intensity factors of a central crack of length 2a inside an elliptical solid disk: $x^2/A^2 + y^2/B^2 = 1$ subjected to a uniform internal pressure σ is shown in Table 5.3.3. For a circular disk case (A/B=1) the isotropic results obtained by BIE, FEM, Tweed et al. [54] and Bowie and Neal [46] agree with each other within 3% error, except when a/A is very close to 1. Replacing the uniform pressure σ on the crack surface by a uniform shear τ, the results are listed in Table 5.3.4. The isotropic results are reasonably compatible to those reported in [62] up to a/R=0.7. As shown in Tables 5.3.3 and 5.3.4, the stress intensity factors, in general, increase for the elliptical disk case with A/B equals 2.

The normalized stress intensity factors of a uniformly-pressurized eccentric radial crack of length 2a within a circular disk of radius R are tabulated in Table 5.3.5 for the isotropic case and in Table 5.3.6 for the anisotropic case. For the problems considered, the normalized crack length a/R and crack location d/R were varied within 0.1 and 0.8. The present isotropic solutions, as shown in Table 5.3.5, differ from those obtained by Tweed et al. [54] only by a maximum of 2.5% for the inner crack tip C and 4.5% for the

outer crack tip D. The stress intensity factors at crack tip D, as expected, is higher than those at the crack tip C due to the presence of the circular boundary. Finally the problem of a circular disk of radius R containing an arbitrarily-positioned crack of length 2a which is subjected to a uniform pressure σ is considered. For the case when a/R equals 0.1, the normalized stress intensity factors are shown in Table 5.3.7 where d is the distance between the disk center and the crack. It can be seen that the stress intensity factors get higher when the crack approaches the circular boundary. For the isotropic, β=0°, and β=90° cases, the stress intensity factors are the same at both crack tips. However, they are quite different for the β=45° case where the anisotropy is no longer symmetrical with respect to the two crack tips. As a final note, it can be easily proved that the ove results obtained for a pressurized cracked solid disk remain valid when the uniform loading, instead of being applied on the crack surface, acts on the outer boundary of the same cracked disk.

Table 5.3.1. A cracked anisotropic circular disk loaded by a pair of symmetric diametral concentrated forces (effect of loading location).

	Ref.[63]	Ref.[60]	FEM	Isotropic	$\beta = 0°$	$\beta = 45°$		$\beta = 90°$
y_o/R	K_I/K_o	K_I/K_o	K_I/K_o	K_I/K_o	K_I/K_o	K_I/K_o	K_{II}/K_o	K_I/K_o
0.0	-	1.7888	1.7670	1.7558	1.4110	2.1263	0.3723	2.7738
0.1	1.2812	1.8122	1.7909	1.7781	1.4138	2.1493	0.3863	2.7789
0.2	1.4212	1.8290	1.8073	1.7944	1.3939	2.1571	0.4043	2.7826
0.3	1.6411	1.8294	1.8058	1.7945	1.3560	2.1536	0.4150	2.7843
0.4	1.7329	1.8113	1.7853	1.7761	1.3121	2.1231	0.3866	2.7839
0.5	1.7469	1.7798	1.7520	1.7445	1.2701	2.0279	0.2897	2.7816
0.6	1.7272	1.7417	1.7129	1.7063	1.2346	1.8940	0.1769	2.7796
0.7	1.6957	1.7026	1.6735	1.6672	1.2074	1.7827	0.1051	2.7888
0.8	1.6624	1.6663	1.6374	1.6308	1.1890	1.7108	0.0750	2.8682
0.9	1.6322	1.6349	1.6063	1.6040	1.1818	1.7064	0.0835	3.4206
1.0	1.6076	1.6098	1.5814	-	-	-	-	-

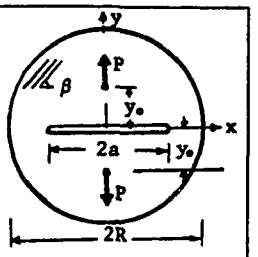

$a/R = 0.5$

$K_o = P/\sqrt{\pi a}$

Table 5.3.2. A cracked anisotropic circular disk loaded by a pair of symmetric diametral concentrated forces (effect of crack size).

a / R	BIE	FEM	Ref.[63]	Ref.[60]
0.000	0.0000	-	0.0000	0.0000
0.001	0.0040	-	0.0040	0.0040
0.025	0.1003	0.0739	0.1007	0.1007
0.050	0.2001	0.1680	0.2008	0.2008
0.100	0.3954	0.3763	0.3969	0.3969
0.200	0.7608	0.7452	0.7642	0.7644
0.300	1.0938	1.0817	1.0984	1.1008
0.400	1.4163	1.4070	1.4177	1.4289
0.500	1.7587	1.7520	1.7469	1.7798
0.600	2.1531	2.1502	2.1145	2.1852
0.700	2.6434	2.6471	2.5593	2.6778
0.750	2.9489	-	2.8293	2.9669
0.800	3.3221	3.3404	3.1460	3.2882
0.850	3.8107	-	3.5261	3.6410
0.900	4.5381	4.6311	3.9923	4.0186

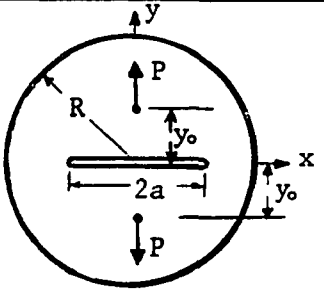

$y_o/R = 0.5$

$K_o = P/\sqrt{\pi a}$

Table 5.3.3. A centrally cracked anisotropic elliptical disk subjected to internal pressure.

A / B	a / A	Ref.[54] K_I/K_o	Ref.[46] K_I/K_o	F.E. K_I/K_o	Isotropic K_I/K_o	$\beta = 0°$ K_I/K_o	$\beta = 45°$ K_I/K_o	$\beta = 45°$ K_{II}/K_o	$\beta = 90°$ K_I/K_o
	0.1	1.015	1.020	-	1.015	1.007	1.028	0.012	1.059
	0.2	1.060	1.060	1.027	1.058	1.030	1.105	0.043	1.205
	0.3	1.136	-	1.106	1.131	1.068	1.221	0.087	1.395
	0.4	1.243	1.240	1.211	1.234	1.125	1.373	0.137	1.615
1	0.5	1.387	-	1.351	1.377	1.208	1.583	0.206	1.923
	0.6	1.578	-	1.533	1.561	1.325	1.830	0.278	2.256
	0.7	1.840	-	1.782	1.810	1.501	2.144	0.362	2.673
	0.8	2.238	2.240	2.157	2.181	1.800	2.577	0.460	3.225
	0.9	3.038	-	2.915	2.900	2.490	3.319	0.582	4.041
	0.1	-	-	-	1.046	1.021	1.067	0.024	1.181
	0.2	-	-	-	1.176	1.080	1.240	0.078	1.496
	0.3	-	-	-	1.370	1.170	1.481	0.144	1.809
	0.4	-	-	-	1.615	1.287	1.772	0.219	2.102
2	0.5	-	-	-	1.965	1.440	2.214	0.340	2.672
	0.6	-	-	-	2.362	1.627	2.670	0.451	3.050
	0.7	-	-	-	2.865	1.877	3.215	0.578	3.435
	0.8	-	-	-	3.519	2.244	3.865	0.720	3.855
	0.9	-	-	-	4.389	2.940	4.589	0.827	4.399

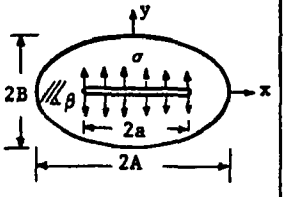

$K_o = \sigma\sqrt{\pi a}$

Table 5.3.4. A centrally cracked anisotropic elliptical disk subjected to uniform shear.

A / B	a / A	Ref.[62] K_I/K_o	Isotropic K_I/K_o	$\beta = 0°$ K_I/K_o	$\beta = 45°$ K_I/K_o	$\beta = 45°$ K_{II}/K_o	$\beta = 90°$ K_I/K_o
	0.1	1.0110	1.0097	1.0060	0.0078	1.0201	1.0200
	0.2	1.0399	1.0384	1.0241	0.0292	1.0746	1.0706
	0.3	1.0897	1.0861	1.0557	0.0610	1.1534	1.1389
	0.4	1.1608	1.1534	1.1032	0.1033	1.2512	1.2199
1	0.5	1.2575	1.2491	1.1774	0.1749	1.3879	1.3269
	0.6	1.3906	1.3749	1.2800	0.2665	1.5509	1.4506
	0.7	1.5862	1.5554	1.4354	0.4017	1.7778	1.6175
	0.8	1.9150	1.8466	1.6844	0.6082	2.1343	1.8794
	0.9	2.6626	2.4475	2.0938	0.9367	2.8436	2.4394
	0.1	-	1.0261	1.0091	0.0158	1.0520	1.0596
	0.2	-	1.0952	1.0356	0.0459	1.1714	1.1673
	0.3	-	1.1887	1.0784	0.0724	1.3083	1.2697
	0.4	-	1.2933	1.1379	0.0933	1.4392	1.3573
2	0.5	-	1.4258	1.2224	0.1368	1.6135	1.4966
	0.6	-	1.5638	1.3350	0.1745	1.7600	1.6060
	0.7	-	1.7384	1.4993	0.2372	1.9352	1.7528
	0.8	-	2.0029	1.7697	0.3679	2.2050	1.9919
	0.9	-	2.5694	2.3330	0.6896	2.8221	2.5191

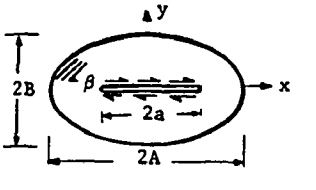

$K_o = \tau\sqrt{\pi a}$

Table 5.3.5. A eccentrically cracked anisotropic elliptical disk subjected to internal pressure.

		a / R = 0.1		a / R = 0.2		a / R = 0.3		a / R = 0.4		a / R = 0.5		a / R = 0.6		a / R = 0.7		a / R = 0.8	
	d / R	(1)	(2)	(1)	(2)	(1)	(2)	(1)	(2)	(1)	(2)	(1)	(2)	(1)	(2)	(1)	(2)
	0.1	1.015	1.015	1.059	1.060	1.132	1.134	1.233	1.238	1.365	1.375	1.535	1.551	1.754	1.783	2.059	2.112
	0.2	1.016	1.016	1.062	1.063	1.136	1.139	1.240	1.246	1.376	1.386	1.551	1.571	1.792	1.831		
Isotropic	0.3	1.017	1.018	1.067	1.068	1.148	1.152	1.261	1.269	1.413	1.428	1.630	1.662				
	0.4	1.020	1.020	1.077	1.079	1.170	1.175	1.304	1.315	1.504	1.530						
Tip C	0.5	1.024	1.025	1.093	1.096	1.209	1.216	1.392	1.413								
	0.6	1.032	1.033	1.123	1.128	1.288	1.303										
	0.7	1.047	1.049	1.187	1.196												
	0.8	1.085	1.090														
	0.1	1.016	1.016	1.062	1.063	1.140	1.143	1.256	1.261	1.414	1.425	1.636	1.658	1.977	2.022	2.654	2.773
	0.2	1.017	1.017	1.067	1.068	1.155	1.159	1.289	1.297	1.486	1.502	1.798	1.834	2.430	2.533		
Isotropic	0.3	1.018	1.019	1.077	1.078	1.182	1.186	1.351	1.362	1.629	1.657	2.203	2.290				
	0.4	1.022	1.022	1.093	1.095	1.228	1.235	1.468	1.488	1.976	2.045						
Tip D	0.5	1.027	1.028	1.121	1.124	1.316	1.329	1.752	1.804								
	0.6	1.038	1.039	1.177	1.184	1.534	1.570										
	0.7	1.060	1.063	1.324	1.346												
	0.8	1.129	1.138														

(1) Present Solution
(2) Tweed, Das, and Rooke, Ref.[54]

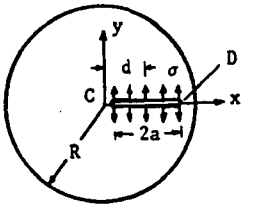

$K_o = \sigma\sqrt{\pi a}$

Table 5.3.6. A eccentrically cracked anisotropic circular disk subjected to internal pressure.

		a/R = 0.1		a/R = 0.2		a/R = 0.3		a/R = 0.4		a/R = 0.5		a/R = 0.6		a/R = 0.7		a/R = 0.8	
	d/R	Tip C	Tip D	Tip C	Tip D	Tip C	Tip D	Tip C	Tip D	Tip C	Tip D	Tip C	Tip D	Tip C	Tip D	Tip C	Tip D
β = 0°	0.1	1.008	1.008	1.030	1.033	1.067	1.077	1.121	1.146	1.194	1.250	1.293	1.410	1.437	1.685	1.676	2.292
	0.2	1.009	1.009	1.033	1.039	1.073	1.094	1.129	1.184	1.205	1.330	1.311	1.585	1.481	2.152		
	0.3	1.010	1.011	1.039	1.049	1.086	1.121	1.154	1.248	1.249	1.479	1.402	1.995				
	0.4	1.013	1.015	1.049	1.064	1.110	1.166	1.201	1.364	1.349	1.818						
	0.5	1.017	1.020	1.065	1.089	1.149	1.247	1.291	1.627								
	0.6	1.023	1.028	1.092	1.136	1.221	1.435										
	0.7	1.035	1.045	1.142	1.254												
	0.8	1.062	1.095														
β = 45°	0.1	1.029	1.029	1.109	1.109	1.231	1.231	1.389	1.393	1.584	1.602	1.823	1.876	2.117	2.264	2.491	2.964
	0.2	1.031	1.030	1.115	1.114	1.241	1.242	1.403	1.416	1.603	1.652	1.850	1.996	2.162	2.634		
	0.3	1.034	1.033	1.125	1.123	1.259	1.264	1.431	1.463	1.647	1.763	1.928	2.331				
	0.4	1.039	1.038	1.141	1.141	1.289	1.304	1.481	1.560	1.739	2.056						
	0.5	1.047	1.047	1.168	1.171	1.340	1.384	1.578	1.866								
	0.6	1.063	1.062	1.213	1.229	1.435	1.577										
	0.7	1.091	1.093	1.300	1.367												
	0.8	1.156	1.170														
β = 45°	0.1	0.013	0.012	0.049	0.042	0.099	0.083	0.159	0.131	0.229	0.186	0.311	0.247	0.406	0.318	0.513	0.413
	0.2	0.014	0.012	0.054	0.041	0.111	0.078	0.179	0.120	0.257	0.165	0.348	0.213	0.453	0.274		
	0.3	0.017	0.013	0.063	0.041	0.128	0.073	0.204	0.107	0.293	0.140	0.395	0.174				
	0.4	0.020	0.014	0.075	0.041	0.150	0.068	0.239	0.090	0.341	0.107						
	0.5	0.026	0.017	0.094	0.042	0.183	0.059	0.289	0.065								
	0.6	0.036	0.020	0.123	0.041	0.235	0.044										
	0.7	0.055	0.026	0.175	0.037												
	0.8	0.097	0.034														
β = 90°	0.1	1.061	1.062	1.212	1.216	1.409	1.422	1.640	1.668	1.908	1.965	2.227	2.335	2.616	2.828	3.108	3.587
	0.2	1.063	1.064	1.216	1.225	1.415	1.443	1.648	1.710	1.919	2.045	2.241	2.492	2.638	3.196		
	0.3	1.066	1.069	1.225	1.241	1.431	1.479	1.673	1.782	1.958	2.191	2.309	2.842				
	0.4	1.071	1.075	1.241	1.266	1.460	1.537	1.721	1.909	2.044	2.509						
	0.5	1.080	1.086	1.266	1.307	1.508	1.640	1.813	2.187								
	0.6	1.093	1.104	1.307	1.380	1.597	1.870										
	0.7	1.119	1.138	1.386	1.551												
	0.8	1.170	1.227														

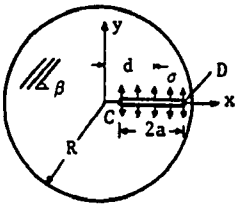

$K_o = \sigma\sqrt{\pi a}$

Table 5.3.7. An arbitrarily positioned crack in an anisotropic circular disk subjected to uniform pressure.

	Isotropic		$\beta = 0°$		$\beta = 45°$				$\beta = 90°$	
	Tip C		Tip C		Tip C		Tip D		Tip C	
d / R	K_I/K_o	K_{II}/K_o	K_I/K_o	K_{II}/K_o	K_I/K_o	K_{II}/K_o	K_I/K_o	K_{II}/K_o	K_I/K_o	K_{II}/K_o
0.0	1.015	0.000	1.007	0.000	1.028	0.012	1.028	0.012	1.059	0.000
0.1	1.015	0.000	1.008	0.000	1.029	0.013	1.029	0.012	1.063	0.001
0.2	1.017	0.001	1.008	0.000	1.032	0.015	1.030	0.012	1.069	0.002
0.3	1.020	0.001	1.010	0.000	1.036	0.018	1.033	0.013	1.080	0.004
0.4	1.025	0.002	1.012	0.001	1.043	0.022	1.039	0.014	1.099	0.006
0.5	1.033	0.003	1.015	0.001	1.055	0.030	1.048	0.016	1.128	0.010
0.6	1.049	0.005	1.022	0.002	1.077	0.045	1.064	0.020	1.174	0.017
0.7	1.081	0.012	1.036	0.005	1.121	0.075	1.096	0.025	1.250	0.031
0.8	1.157	0.033	1.073	0.016	1.227	0.153	1.165	0.030	1.377	0.060
0.9	1.388	0.132	1.208	0.081	1.544	0.406	1.370	0.026	1.528	0.137

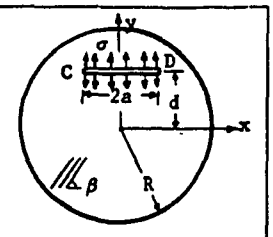

a/R = 0.1

$K_o = \sigma\sqrt{\pi a}$

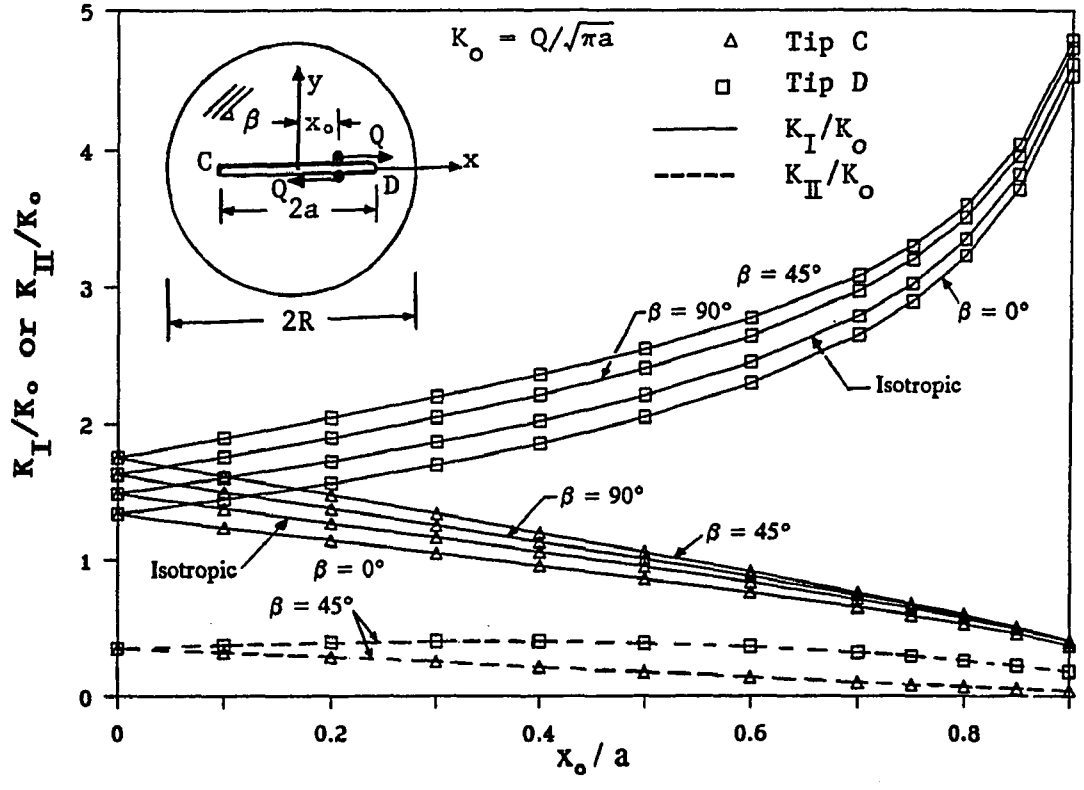

Figure 5.3.1. A centrally cracked circular anisotropic disk loaded by a pair of horizontal forces, vertical forces, or concentrated moments.

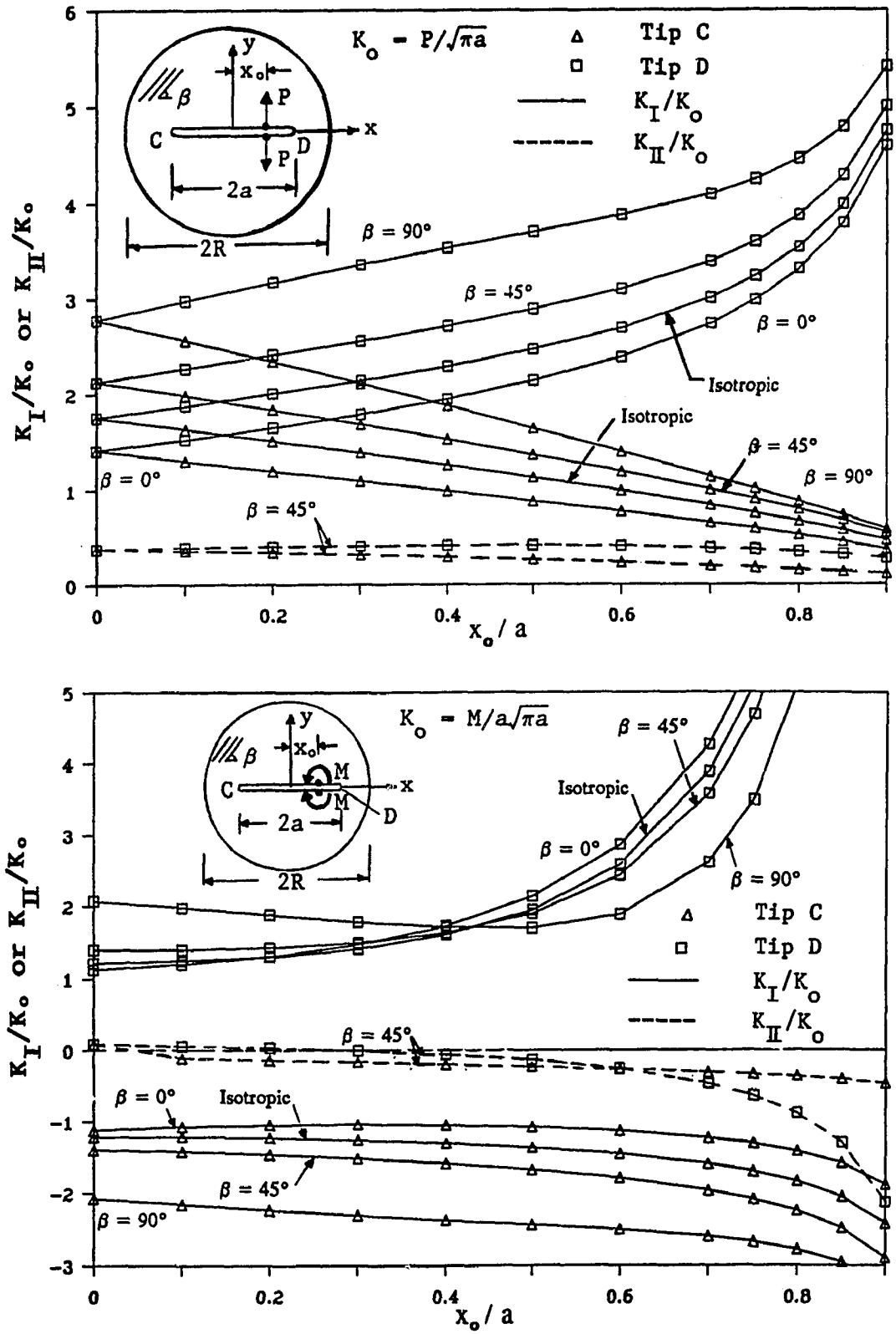

Figure 5.3.1. A centrally cracked circular anisotropic disk loaded by a pair of horizontal forces, vertical forces, or concentrated moments (continued).

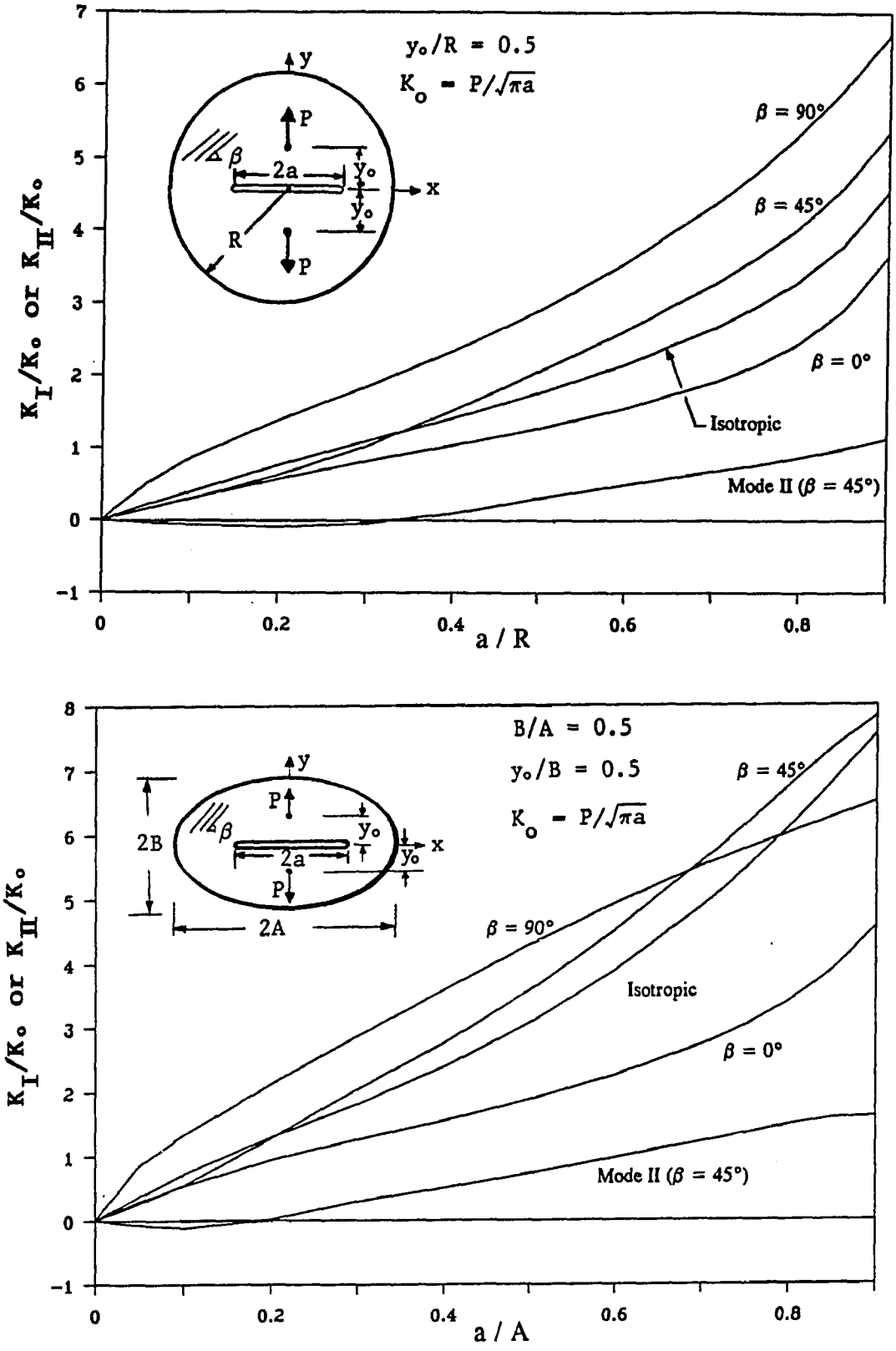

Figure 5.3.2. A centrally cracked circular or elliptical anisotropic disk loaded by a pair of symmetric point loads.

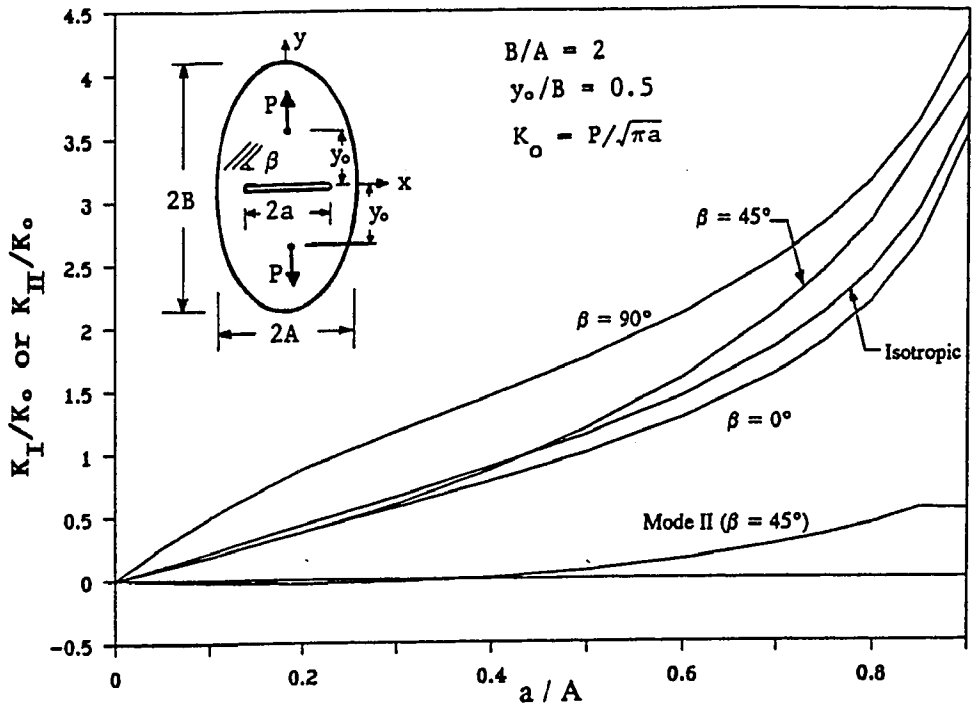

Figure 5.3.2. A centrally cracked circular or elliptical anisotropic disk loaded by a pair of symmetric point loads (continued).

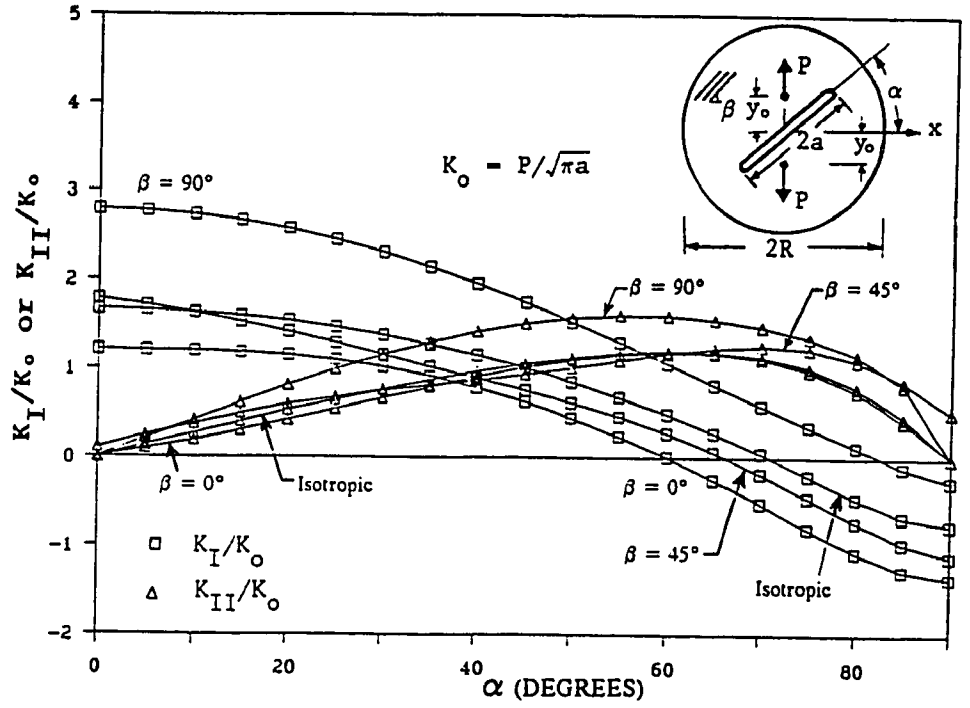

Figure 5.3.3. A circular anisotropic disk with a slant central crack loaded by a pair of symmetric point loads.

V.4 INTERACTION BETWEEN A CRACK AND A CURVILINEAR HOLE IN AN ANISOTROPIC PLATE

V.4.1 Background

The problem of a crack approaching a circular hole in an isotropic plate under biaxial loading was solved by Isida [67]. The solution was based on Laurent's expansions of complex stress potentials where the expansion coeffficients are determined from the boundary conditions. The solution given by Isida [67], though, is applicable to circular holes only and not to holes of general curvilinear shape. In addition, currently no solution exists for interaction between a crack and a curvilinear hole in an anisotropic domain. Using the present formulation, solution to the problem of a crack approaching a curvilinear hole in an anisotropic plate can be obtained under any type of loading.

V.4.2 Numerical Results and Discussions

For the current computations the values R/d=0.4 for the circular hole case and A/d=0.4 for the elliptical hole case have been assumed. Stress intensity factors for a crack interacting with a circular or an elliptical (B/A=0.5) hole in an anisotropic plate stretched by a uniaxial tension σ are shown in Figs. 5.4.1 and 5.4.2. The fiber direction β is varied to study the effect of anisotropy on the stress intensity factors. Consistently higher values of stress intensity factors are obtained when the fibers are parallel to the crack (β=0°). Small mode II stress intensity factors are also present for β=45° case. As can be expected, higher stress intensity factors are obtained for the crack tip closer to the hole (denoted as tip C) than that of the far tip (denoted as tip D). As can be seen from Figs. 5.4.1 and 5.4.2, relatively small differences in the

stress intensity factors exist between the circular and the elliptical hole results. The present isotropic stress intensity factors in Fig. 5.4.1 are accurate to within 1% of the results given by Isida [67] which are obtained by Laurent's series expansion.

Figure 5.4.3 depicts the stress intensity factors for the circular hole case under compression in the direction of the crack axis. It is interesting to note that the mode II stress intensity factor for the β=45° case at tip C changes sign at around a/d=0.35 and increase considerably afterward to be comparable and even higher than some of the mode I stress intensity factors at the same tip. This again might have been caused by the normal-shear coupling present for the β=45° case. If the loading is changed to pure shear, the results are given in Fig. 5.4.4. Consistently, higher values of mode I stress intensity factors are observed for the β=45° case at tip C. Much smaller values of mode I stress intensity factors are obtained for the β=0° case at the same tip.

Stress intensity factors for a crack approaching a pressurized circular hole in an anisotropic plate are shown in Fig. 5.4.5. As can be seen from Fig. 5.4.5 anisotropy has much less influence on the stress intensity factors for this case than when the loading is remote. When the internal pressure is moved to the crack the same observation is noted. The results for this case are depicted in Fig. 5.4.6.

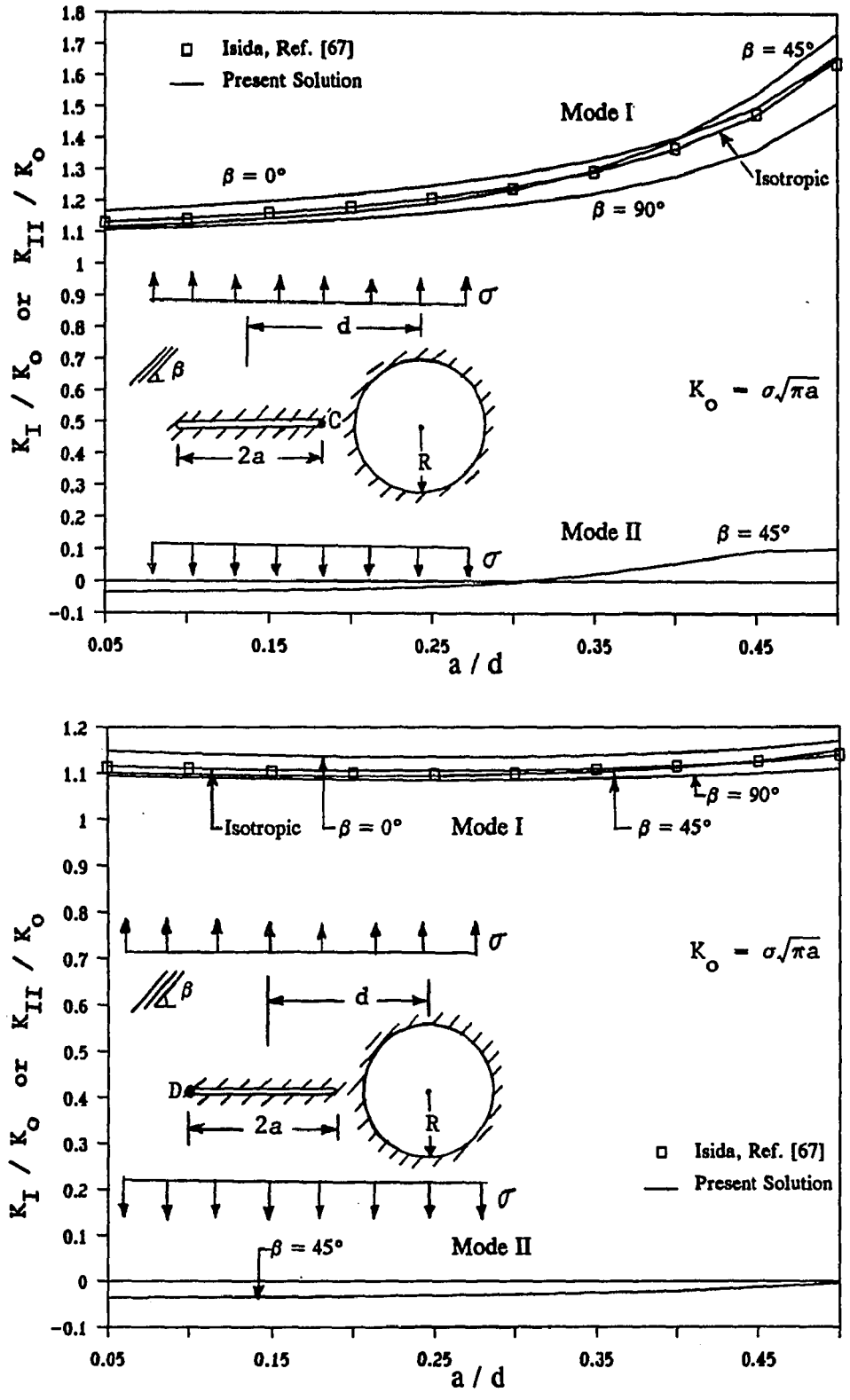

Figure 5.4.1. Interaction between a crack and a circular hole in an anisotropic plate under uniform tension.

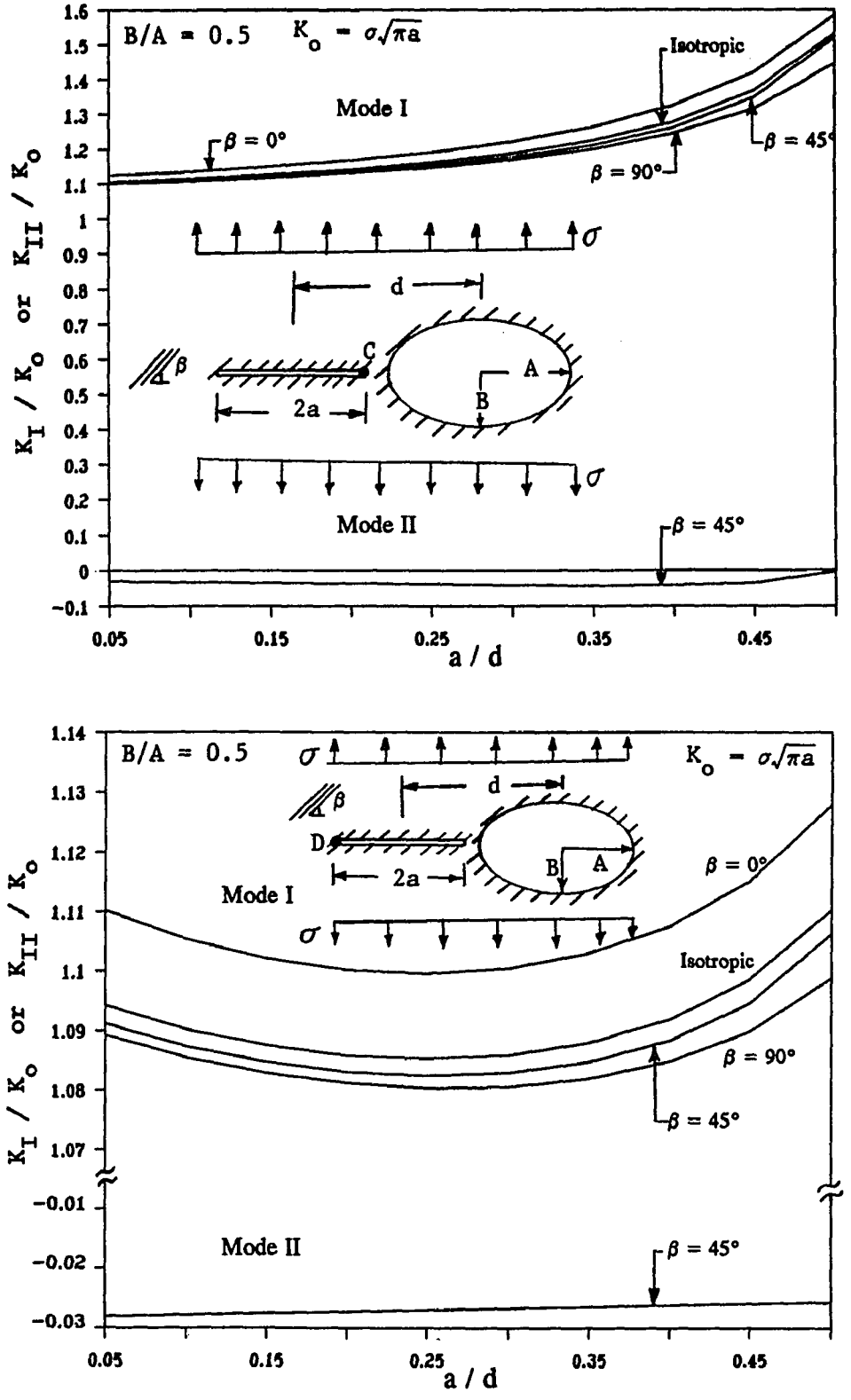

Figure 5.4.2. Interaction between a crack and an elliptical hole in an anisotropic plate under uniform tension.

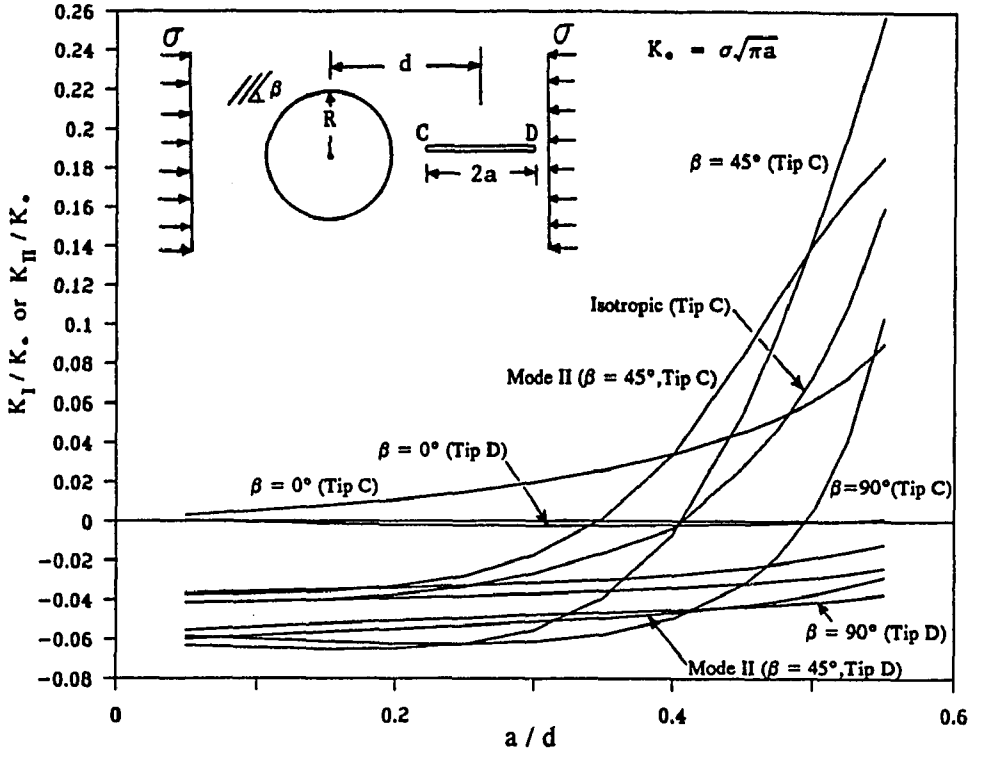

Figure 5.4.3. Interaction between a crack and a circular hole in an anisotropic plate under uniform compression.

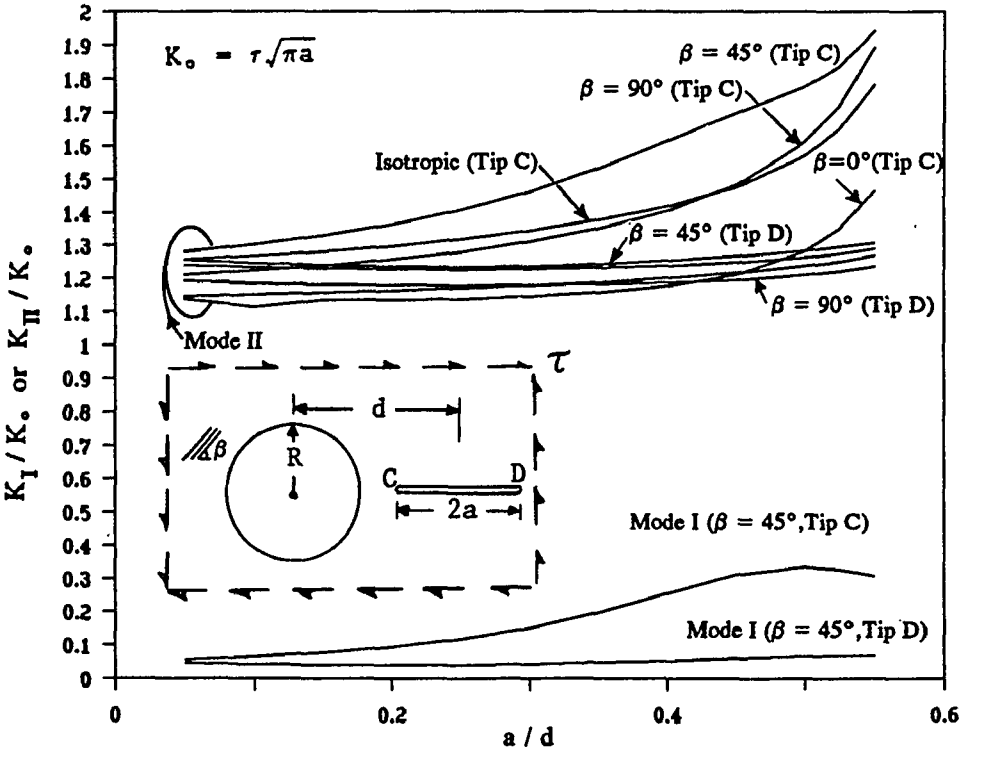

Figure 5.4.4. Interaction between a crack and a circular hole in an anisotropic plate under pure shear.

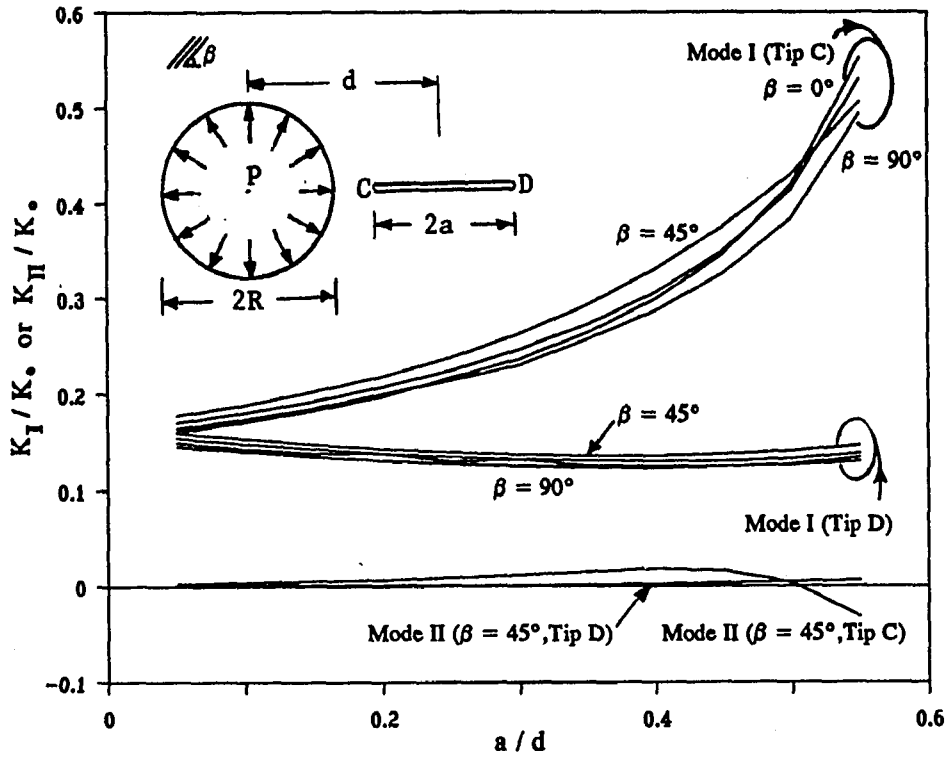

Figure 5.4.5. Interaction between a crack and a pressurized circular hole in an anisotropic plate.

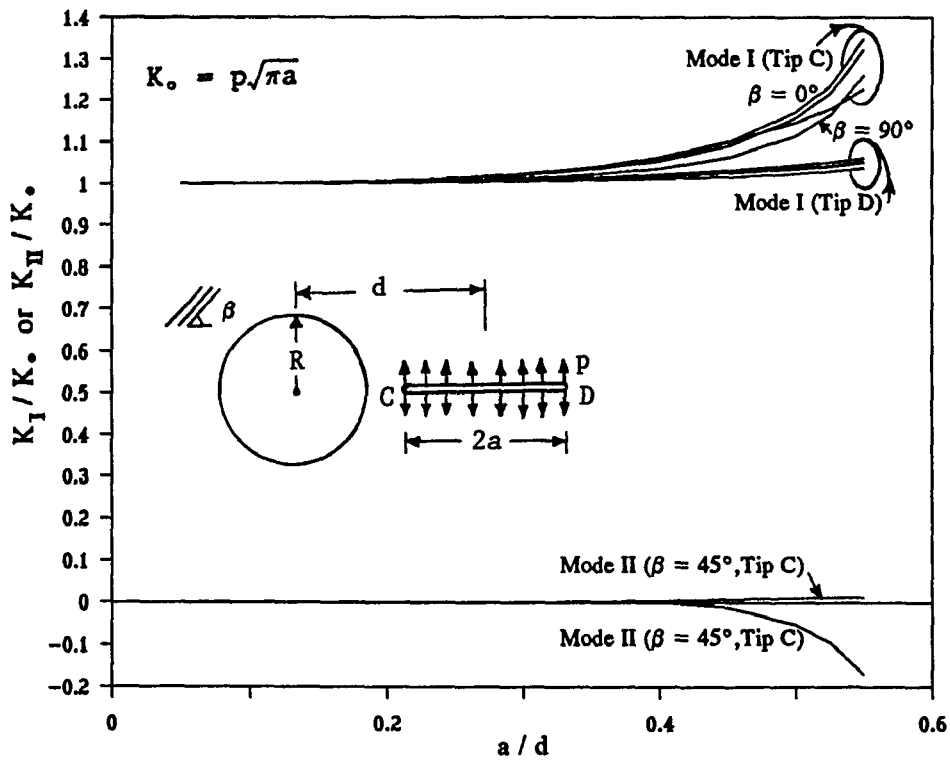

Figure 5.4.6. Interaction between a pressurized crack and a circular hole in an anisotropic plate.

CHAPTER VI

VERIFICATION OF THE DISPLACEMENT FIELDS

VI.1 MOTIVATION

Eventhough very accurate results have been obtained for the example problems which have been considered in this study, certain values obtained for the stress intensity factors seem to be physically awkward at first glance. This is in general due to the fact that the effect of anisotropy on the stress intensity factors are very difficult to predict as opposed to their isotropic counterparts. This is specially true, if the principal directions of orthotropy do not coincide with the coordinate directions that are geometrically natural to the problem. An example of this can be referred to Fig. 5.2.5, where a single-cracked fastener hole was subjected to a uniform pressure covering its upper-half. For this problem, mode I stress intensity factors for β=45° case become negative for crack length ratios smaller than a/R=0.1. In that section, this was explained as being the effect of normal-shear coupling which was said to push the crack faces against each other. But negative value for mode I stress intensity factor would mean penetration of the crack faces, which physically is impossible. Therefore, we are motivated here to explain this phenomenon and verify the results obtained. This is accomplished through the verification of the displacement fields and will be covered in this chapter.

VI.2 FURTHER ANALYSIS ON THE PROBLEM OF FIGURE 5.2.5

From Fig. 5.2.5, it is apparent that the negative value for mode I stress intensity factors occurs only for certain region of fiber angles β not including 0 and 90 degrees. Fig. 6.2.1 depicts this region of negative K_I, which is roughly between β=40° and β=75°. A crack length ratio of a/R=0.05 was selected here, which falls in the region of concern. Comparing Figs. 5.2.3, 5.2.4, and 5.2.5, it is noted that this phenomenon only occurs in the last figure where the pressure span is 2θ=180°. This might be due to the fact that the uniform pressure in this case (2θ=180°) reaches the crack and therefore for short cracks there is a strong horizontal component of loading in the vicinity of the crack tip, making the sliding mode stress intensity factor the dominant value over its opening mode counterpart. The normal-shear coupling effect due to the fiber orientation together with this large sliding force then tend to push the crack faces against each other. Once the crack is long enough (a/R>0.1), this large sliding force is not close to the crack tip and the values of mode I stress intensity factor change sign and stabilize. Proving this point, Fig. 6.2.2 shows the pressure spans for which the horizontal component is large enough for this phenomenon to occur (2θ>176.4°).

VI.3 NUMERICAL RESULTS AND DISCUSSIONS

In this section the displacement fields are presented for a few example problems to further ensure the validity of the results obtained in this study and also to further study the phenomenon occurring in Fig. 5.2.2. A well-known solution for displacements of a crack in the open literature is the Vertical Crack Opening

Displacements (VCOD) for a fully pressurized crack in an isotropic plate. Figure 6.3.1 shows the crack profiles for the isotropic and the orthotropic cases along with the horizontal displacements. As can be seen from Fig. 6.3.1 exact values of vertical displacements are obtained for the isotropic case. For the results given in this section, the Young's modulus of the isotropic case was chosen to be equal to the matrix value of the anisotropic cases.

Next, a single crack emanating from a fully pressurized circular hole is considered in Fig. 6.3.2. It is noticed that the VCOD for the β=45° case is not symmetric with respect to the crack axis and horizontal values of displacement are different for the upper crack face and the lower. This is again due to the normal-shear coupling. Adding a symmetric crack of the same length (a) to the pressurized hole, the crack displacement profiles are given in Fig. 6.3.3. The horizontal axis is denoted as x_r for the right crack tip and x_ℓ for the left crack, each starting from their corresponding crack mouths. The single cracked hole subjected to a uniform pressure of span 2θ=180 is considered next in Fig. 6.3.4. This is the problem which produces negative mode I stress intensity factors for crack length ratios of a/R<0.1. A penetration of crack faces is observed which is physically unrealistic. But negative values for mode I stress intensity factors can not be ignored. What they actually represent are the available load which closes the crack. Eventhough that alone represents a K_I value of zero, if some other loading is super-imposed on this problem which tends to open the crack in the vertical direction, the above-mentioned loading that tends to close the crack would actually negate the crack opening due to this added loading. Finally, Fig. 6.3.5 represents a single cracked hole subjected to

uniform pressures of total span 2θ=180° with fiber angles β=45° and 135°, and 2θ=360° with β=45°. The purpose of this figure is to show that the full pressure case (2θ=360°) with β=45° is actually the superposition of the half pressure cases (2θ=180°) with fiber angles equal to 45 and 135 degrees. What this in turn indicates is that an upper half pressure with β=135° is equivalent to a lower half pressure with β=45°. This is actually true for any two fiber angles symmetric about the y-axis.

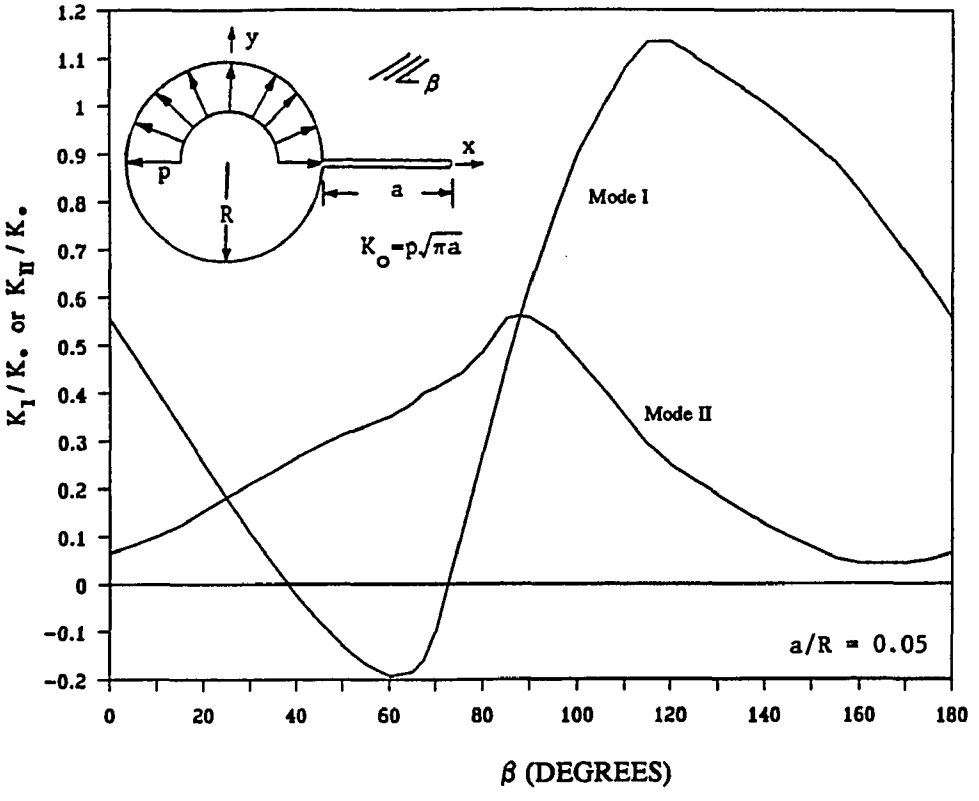

Figure 6.2.1. A single cracked circular hole loaded by an arc of uniform pressure in an anisotropic plate (effect of fiber direction).

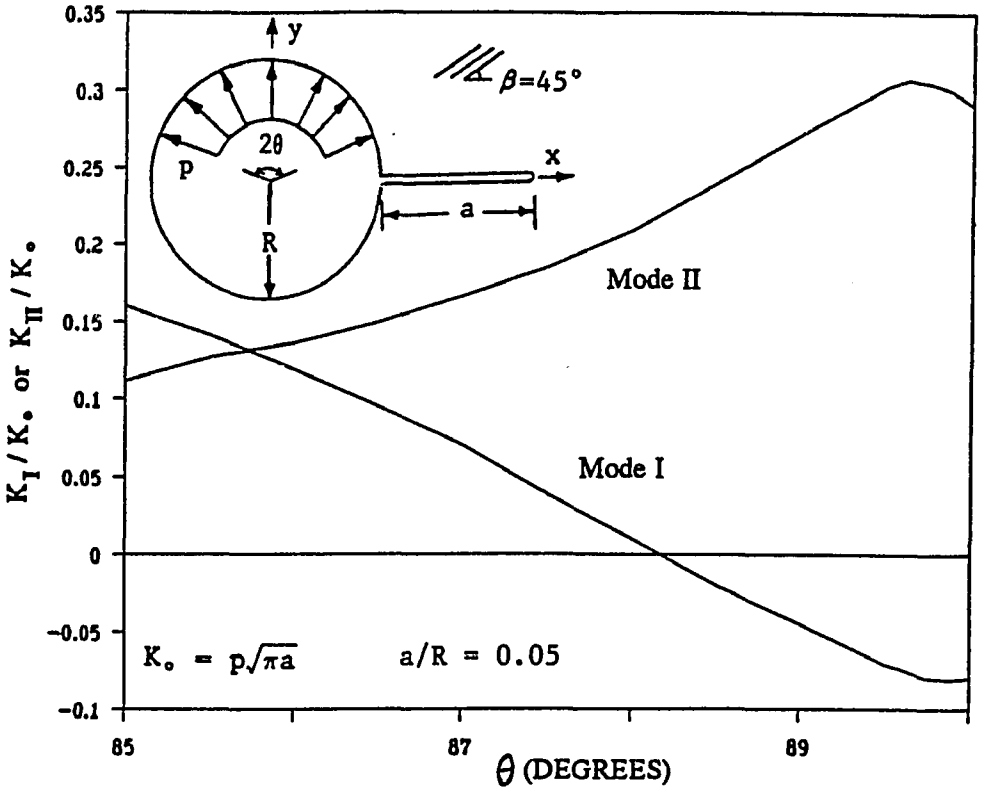

Figure 6.2.2. A single cracked circular hole loaded by an arc of uniform pressure in an anisotropic plate (effect of loading span).

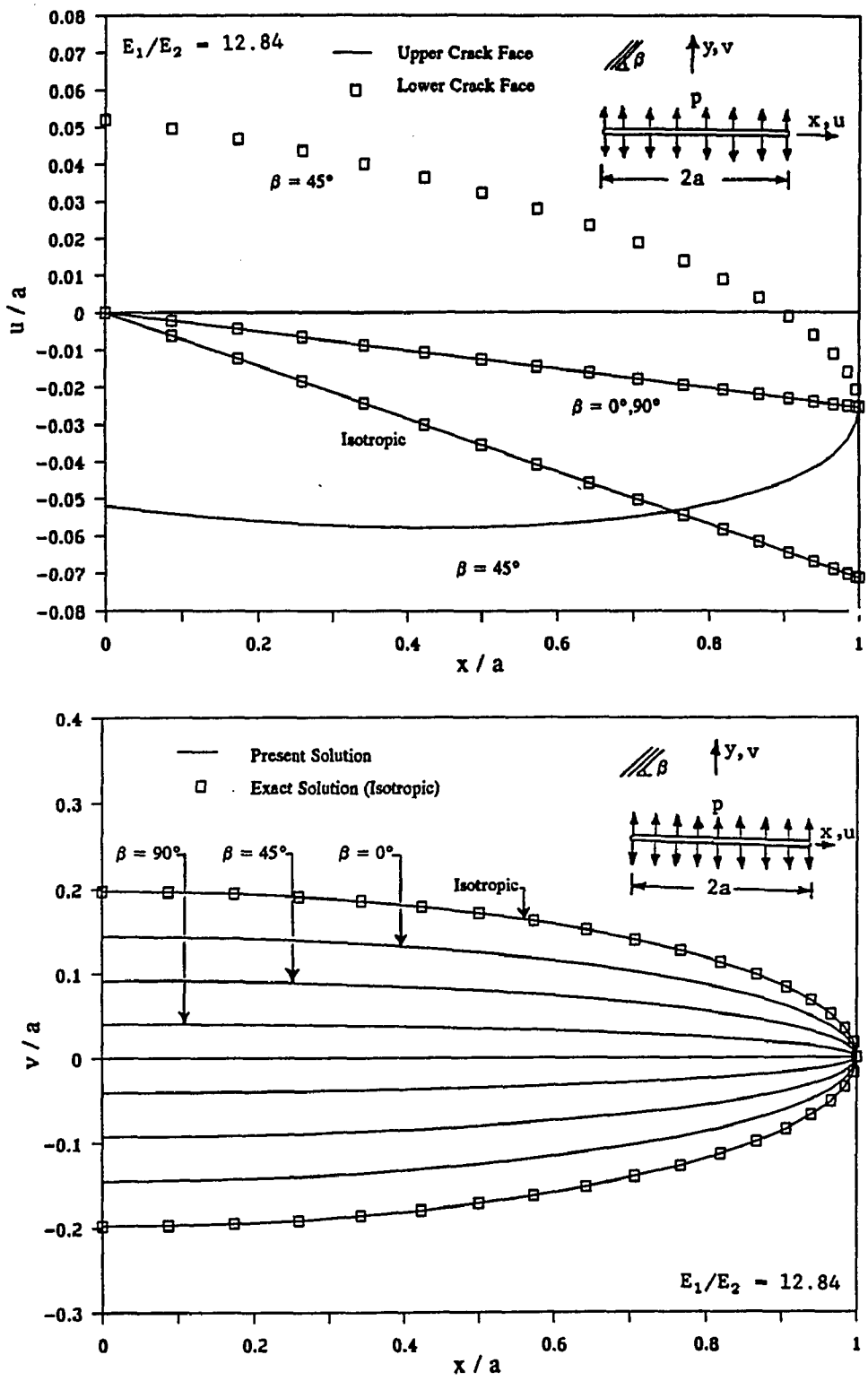

Figure 6.3.1. Displacement profiles for a pressurized crack in an anisotropic plate.

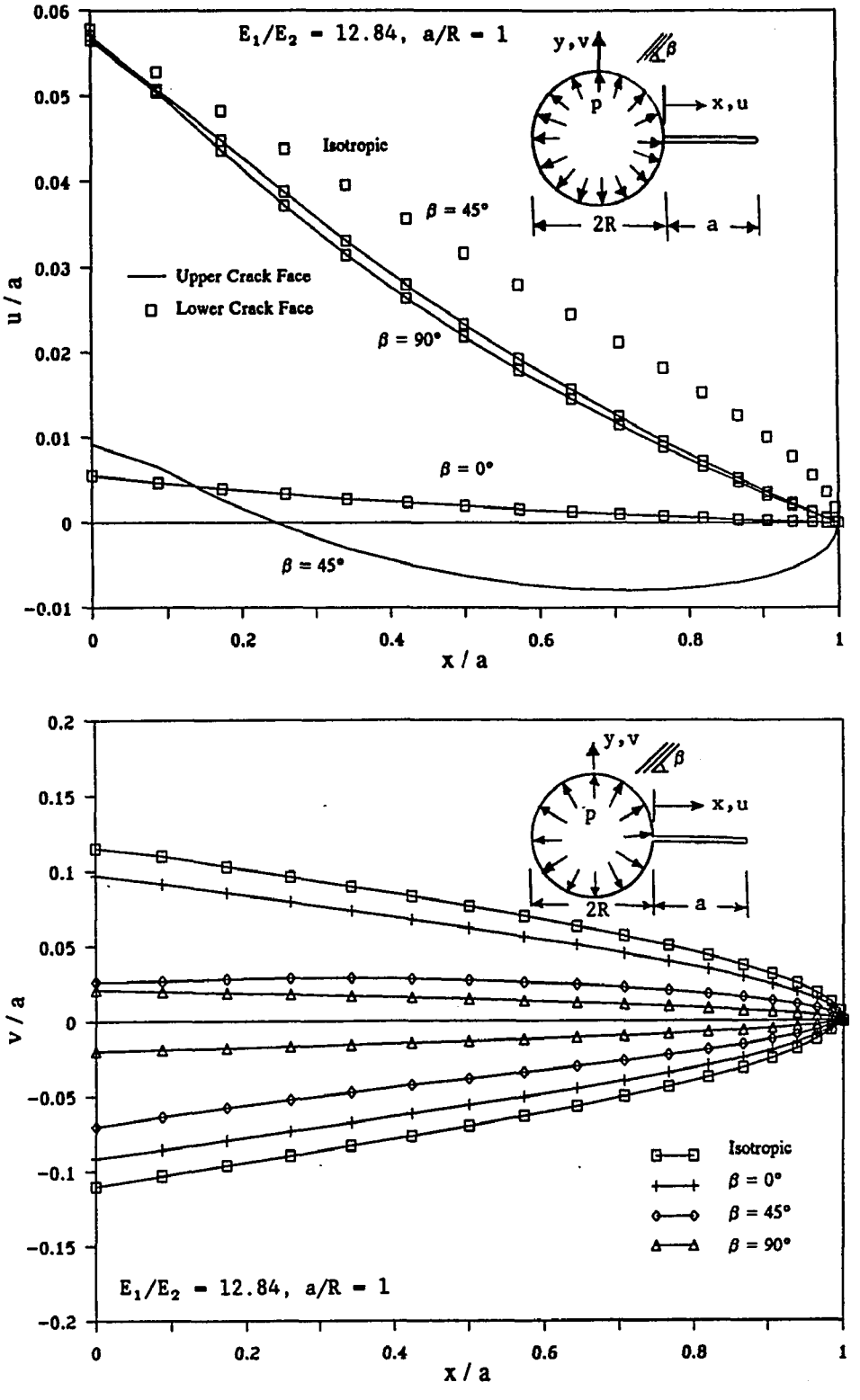

Figure 6.3.2. Displacement profiles for a crack emanating from a pressurized circular hole in an anisotropic plate.

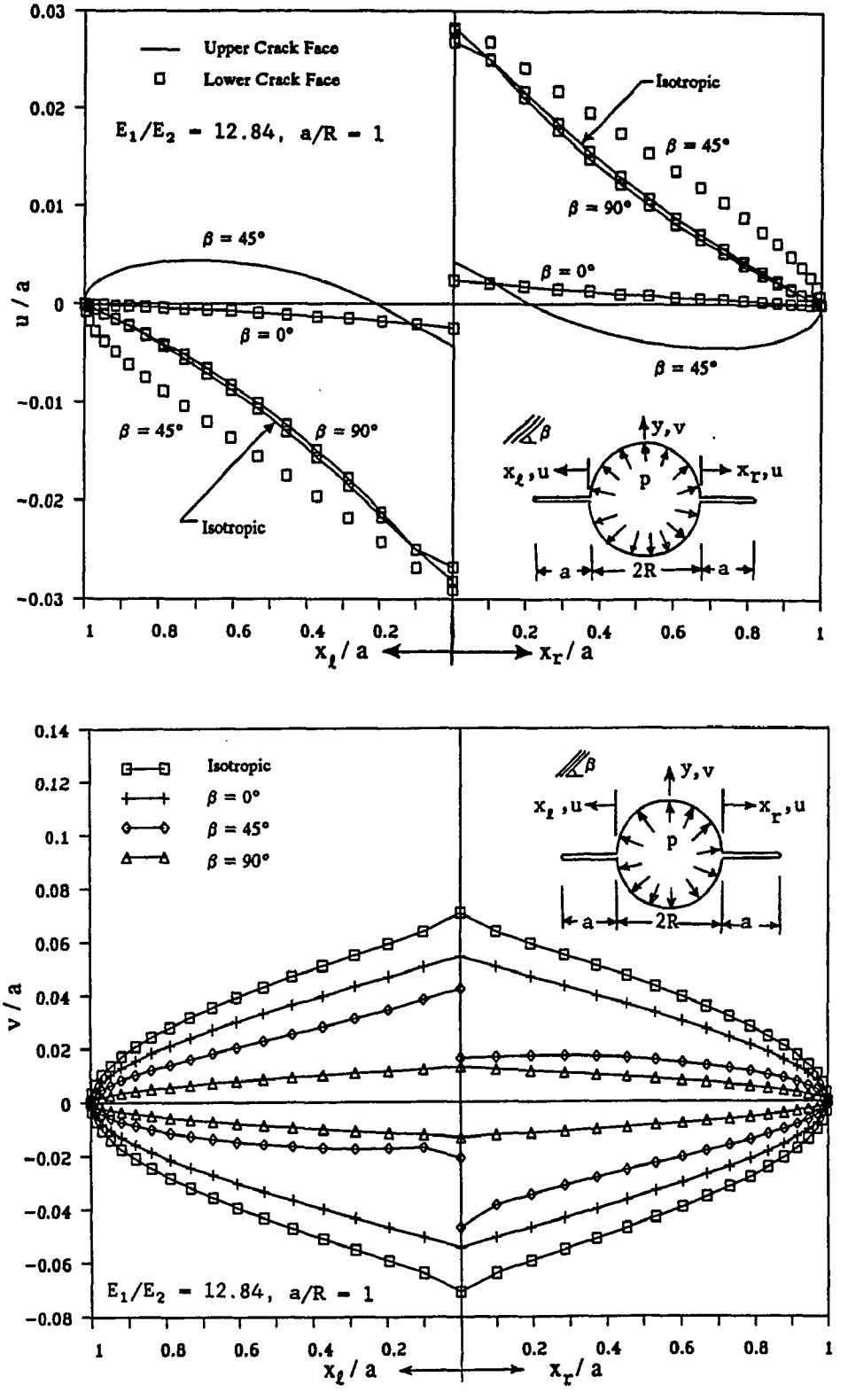

Figure 6.3.3. Displacement profiles for two symmetric cracks emanating from a pressurized circular hole in an anisotropic plate.

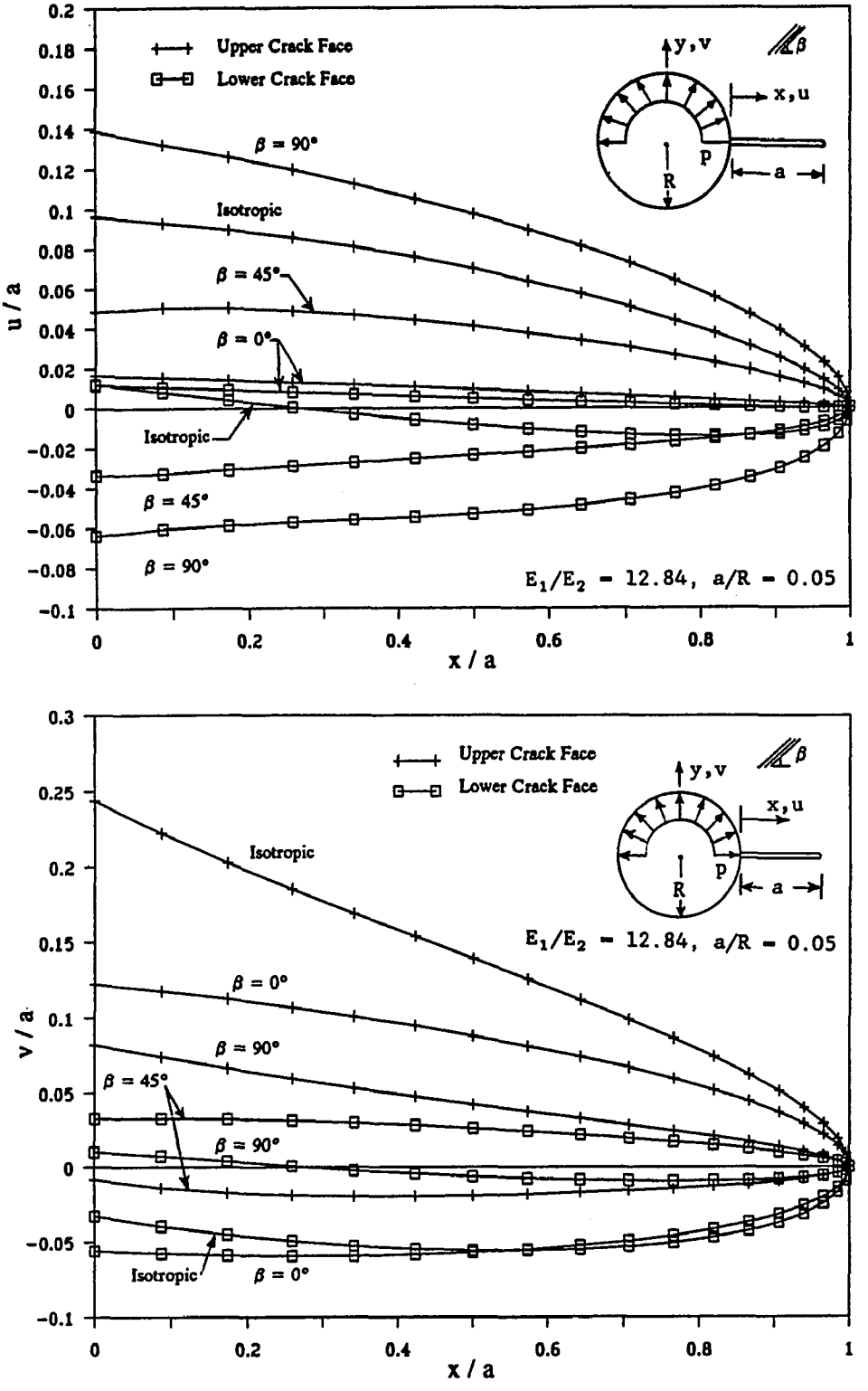

Figure 6.3.4. Displacement profiles for a crack emanating from a circular hole subjected to a uniform pressure of span 2θ=180° in an anisotropic plate.

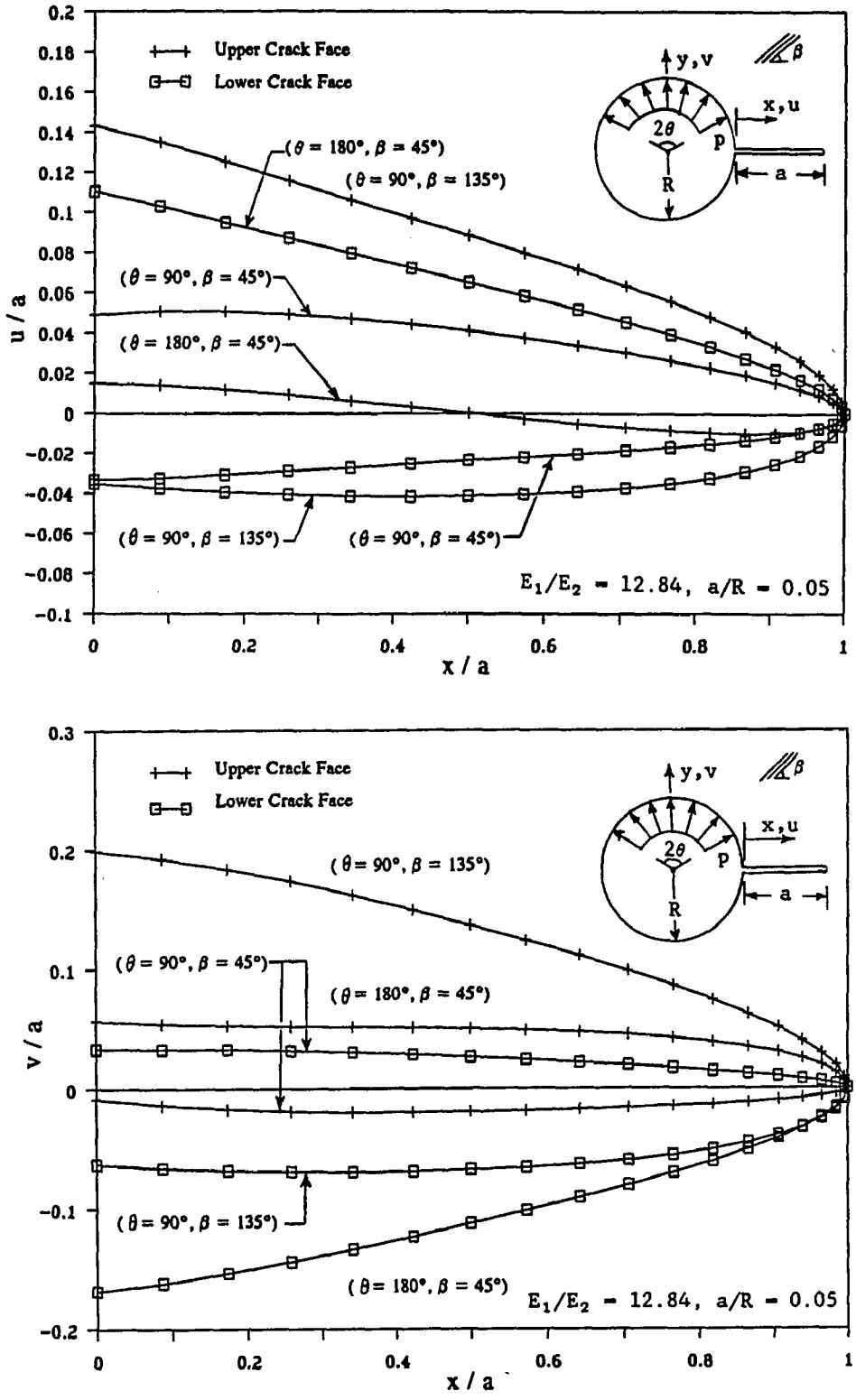

Figure 6.3.5. Verification of superposition principle for displacement profiles using symmetric fiber rotation.

CHAPTER VII

FUTURE APPLICATIONS

VII.1 APPLICATION TO LAMINATED COMPOSITE PANELS

Many of the structural elements are made of laminated composite plates or panels. A laminated panel is two or more panels bonded together to act as an integral structural element. Principal material directions for each individual panel is oriented to produce load resistance in several directions. In this chapter, a method is outlined, using which, we can proceed from the basic building block, the lamina, to the end result, the laminate. This method is called the classical lamination theory [68].

Laminated composites, in general, develop coupling between bending and extension. The coupling is influenced by the geometrical, loading, as well as material property characteristics of laminates. Therefore, knowledge of the variation of stress and strain through the laminate thickness is essential to the definition of the extensional and bending stiffnesses of a laminate.

The stress-strain relations for the k^{th} layer of a multilayered laminate can be written as:

$$\{\sigma\}_k = [\bar{Q}]_k \{\epsilon\}_k, \tag{7.1}$$

where $\bar{Q}_{ij}$ $(i,j = 1,2,6)$ are the transformed reduced stiffnesses for a lamina of arbitrary orientation. The following assumptions are made in the application of the lamination theory:

i) The displacements are continuous across the plate boundaries so that no plate can slip relative to another.

ii) Strain perpendicular to the middle surface is negligible (ϵ_z=0).

Thus, the stresses in the k^{th} layer can be expressed as:

$$\begin{Bmatrix} \sigma_x \\ \sigma_y \\ \sigma_{xy} \end{Bmatrix} = \begin{bmatrix} \bar{Q}_{11} & \bar{Q}_{12} & \bar{Q}_{16} \\ \bar{Q}_{12} & \bar{Q}_{22} & \bar{Q}_{26} \\ \bar{Q}_{16} & \bar{Q}_{26} & \bar{Q}_{66} \end{bmatrix}_k \left\{ \begin{Bmatrix} \epsilon_x \\ \epsilon_y \\ \gamma_{xy} \end{Bmatrix} + z \begin{Bmatrix} \kappa_x \\ \kappa_y \\ \kappa_{xy} \end{Bmatrix} \right\}, \tag{7.2}$$

where ϵ_x, ϵ_y, and γ_{xy} are the middle surface strains, κ_x, κ_y, and κ_{xy} are the middle surface curvatures, and z is any point through the laminate thickness. The resultant forces and moments acting on the laminate, then are obtained by integration of the stresses in each layer through the laminate thickness (h), i.e.,

$$N_x = \int_{-h/2}^{h/2} \sigma_x \, dz, \quad M_x = \int_{-h/2}^{h/2} \sigma_x z \, dz, \tag{7.3}$$

where N_x is the force per unit length and M_x is moment per unit length of the cross section of the laminate. Similar relations can be written for N_y, N_{xy}, M_y, and M_{xy}. Taking advantage of the fact that the stiffness matrix for each layer is constant through its thickness, we arrive at:

$$\begin{Bmatrix} N_x \\ N_y \\ N_{xy} \end{Bmatrix} = \begin{bmatrix} A_{11} & A_{12} & A_{16} \\ A_{12} & A_{22} & A_{26} \\ A_{16} & A_{26} & A_{66} \end{bmatrix} \begin{Bmatrix} \epsilon_x \\ \epsilon_y \\ \gamma_{xy} \end{Bmatrix} + \begin{bmatrix} B_{11} & B_{12} & B_{16} \\ B_{12} & B_{22} & B_{26} \\ B_{16} & B_{26} & B_{66} \end{bmatrix} \begin{Bmatrix} \kappa_x \\ \kappa_y \\ \kappa_{xy} \end{Bmatrix} \tag{7.4}$$

$$\begin{Bmatrix} M_x \\ M_y \\ M_{xy} \end{Bmatrix} = \begin{bmatrix} B_{11} & B_{12} & B_{16} \\ B_{12} & B_{22} & B_{26} \\ B_{16} & B_{26} & B_{66} \end{bmatrix} \begin{Bmatrix} \epsilon_x \\ \epsilon_y \\ \gamma_{xy} \end{Bmatrix} + \begin{bmatrix} C_{11} & C_{12} & C_{16} \\ C_{12} & C_{22} & C_{26} \\ C_{16} & C_{26} & C_{66} \end{bmatrix} \begin{Bmatrix} \kappa_x \\ \kappa_y \\ \kappa_{xy} \end{Bmatrix} \tag{7.5}$$

with

$$A_{ij} = \sum_{k=1}^{N} (\bar{Q}_{ij})_k (z_k - z_{k-1}), \qquad (i,j = 1,2,6), \tag{7.6a}$$

$$B_{ij} = \frac{1}{2} \sum_{k=1}^{N} (\bar{Q}_{ij})_k (z_k^2 - z_{k-1}^2), \qquad (i,j = 1,2,6), \qquad (7.6b)$$

$$C_{ij} = \frac{1}{3} \sum_{k=1}^{N} (\bar{Q}_{ij})_k (z_k^3 - z_{k-1}^3), \qquad (i,j = 1,2,6), \qquad (7.6c)$$

where N represents the total number of layers in the laminate. A_{ij}, in the above, are called extensional stiffnesses, B_{ij} are called coupling stiffnesses, and C_{ij} are called bending stiffnesses. The presence of the B_{ij} implies coupling between bending and extension of a laminate. This coupling can be avoided by stacking the laminate layers symmetric about the middle surface (B_{ij}=0).

To apply the above formulation to the fundamental solutions obtained in Chapter III, B_{ij} and C_{ij} (i,j=1,2,6) in Eqs. (7.4) and (7.5) should be set equal to zero to assure exclusion of bending and extension-bending coupling in the laminate. Then, the resulting expression of Eq. (7.4) can be used as a laminate counterpart for Eq. (2.1) of Chapter II.

VII.2 FURTHER APPLICATIONS

The fundamental solutions derived in this study can further be applied to other areas of mechanics of composite materials. The study of perforated or cracked composite panels stiffened with a planar and/or a linear stiffener is one example. These stiffeners in general may be attached to the sheet either continuously by welding or adhesion, or with discrete fasteners by spotwelding or riveting. Using the proposed fundamental solutions derived here as Green's functions to account for the adhesive shear stress (for adhesively bonded stiffeners) and/or the bolt load (rivetted stiffeners), the

governing equations for the problem can be obtained in integral and/or series form expressions which can be solved numerically.

Of other possible application areas for the proposed fundamental solutions, the study of fracture process zone (FPZ) ahead of a crack tip in a composite panel can be named. Using the fundamental solutions of Chapter III as Green's functions and integrating them ahead of the crack tip to account for the FPZ loading closing the crack, the size and the shape of the zone may be obtained.

Furthermore, the BIE formulation of Chapter IV can be combined with any of the solution procedures mentioned above to overcome the geometry limitations inherent to the problems. Then, as an example, cracks emanating from a hole in an stiffened composite panel and the FPZ ahead of a crack emanating from a hole in a composite panel can be studied.

APPENDIX A

FUNDAMENTAL SOLUTIONS FOR A LOADED ELLIPTICAL HOLE OR CRACK IN AN ANISOTROPIC PLATE

The fundamental solutions of Chapter III were derived using the principle of superposition such that the point load or the concentrated moment could locate anywhere in the domain. Therefore, the obtained solutions will remain valid if the loading is moved directly on the boundary of the hole or crack. Here, the fundamental solutions are given for an anisotropic plate containing an elliptical hole or a crack subjected to a point force and/or a concentrated moment at the edge of the hole or crack. Without the aid of an auxiliary problem, explicit solutions that satisfy exactly the prescribed surface-traction boundary conditions are obtained. The explicit solutions to be obtained are for the problem shown in Fig. A-1, and the notations used follow those of Chapter III.

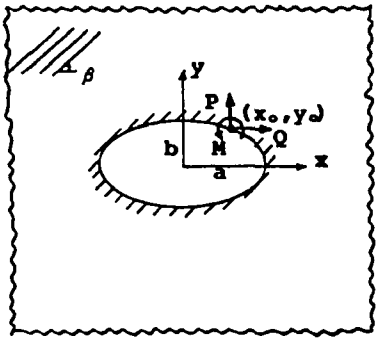

Figure A-1. An elliptical hole loaded by a concentrated force or a moment in an anisotropic plate.

A-1 POINT LOAD SOLUTION

The problem of an infinite anisotropic plate containing an elliptical hole part of which is subjected to normal pressure was solved by Savin [3]. Here an extended approach was used to also include shear traction. Taking the limiting values of the solutions

as the pressure and shear spans on the surface of the hole approached zero, the stress function Φ_j (j=1,2) for the concentrated load case is obtained in the form:

$$\Phi_j(\zeta_j) = \frac{D_{j1}Q+D_{j2}P}{4\pi D}\ell n(\zeta_j) - \frac{i(Q+s_kP)}{2\pi(s_j-s_k)}\ell n(t-\zeta_j)$$
$$+ \frac{1}{4\pi(s_j-s_k)(a^2+b^2-z_0\bar{z}_0)}\{[\frac{1}{\zeta_j}-\frac{t}{t-\zeta_j}((\zeta_j+\frac{1}{\zeta_j})-(t+\frac{1}{t}))]$$
$$[\frac{ia^2}{2}(t-\frac{1}{t})(Q+s_kP)-\frac{ab}{2}(t+\frac{1}{t})(s_kQ+P)]$$
$$+ [\frac{1}{\zeta_j}+\frac{t}{t-\zeta_j}((\zeta_j-\frac{1}{\zeta_j})-(t-\frac{1}{t}))]$$
$$[-\frac{ab}{2}(t-\frac{1}{t})(s_kQ+P)+\frac{ib^2}{2}(t+\frac{1}{t})(Q+s_kP)]\}, \qquad (A.1)$$

with (j=1,2; k=2,1). In the above, the definitions of D, D_{ij} (i,j=1,2), and ζ_j (j=1,2) follow those of Eqs. (3.4 to 3.8). Here again, the fundamental solution for the case of a concentrated load applied on the face of a crack can be obtained simply by setting the length of the semi-minor axis (b) in Eq. (A.1) equal to zero. The stress intensity factors then, may be obtained by using Eq. (2.21). For the tip (+a,0) we obtain:

$$K_I+\frac{K_{II}}{s_k} = \frac{1}{2\sqrt{\pi a}}[(\frac{s_j}{s_k}-1)(\frac{D_{j1}Q+D_{j2}P}{D})+(\frac{2i}{t-1})(\frac{Q}{s_k}+P)], \qquad (A.2)$$

with (j=1,2; k=2,1). In particular, when $s_1 = -\bar{s}_2 = s'+is"$,

$$K_I = \frac{1}{2\sqrt{\pi a}}[P(\frac{a+x_0}{a-x_0})^{1/2}+\frac{Q}{2s"}(1+\frac{a_{12}}{a_{22}}(s'^2+s"^2))]; \qquad (A.3a)$$

$$K_{II} = \frac{1}{2\sqrt{\pi a}}[Q(\frac{a+x_0}{a-x_0})^{1/2}-\frac{P}{2s"}(\frac{a_{12}}{a_{11}}+(s'^2+s"^2))]; \qquad (A.3b)$$

and when $s_1=is_1"$, and $s_2=is_2"$,

$$K_I = \frac{1}{2\sqrt{\pi a}}\left[P\left(\frac{a+x_0}{a-x_0}\right)^{1/2} + \frac{Q}{s_1''+s_2''}\left(\frac{a_{12}}{a_{22}}s_1''s_2''+1\right)\right]; \tag{A.4a}$$

$$K_{II} = \frac{1}{2\sqrt{\pi a}}\left[Q\left(\frac{a+x_0}{a-x_0}\right)^{1/2} - \frac{P}{s_1''+s_2''}\left(s_1''s_2''+\frac{a_{12}}{a_{11}}\right)\right]; \tag{A.4b}$$

which agree with the results obtained by Embley [9].

A-2 CONCENTRATED MOMENT SOLUTION

For the case of a concentrated moment applied on the boundary of the ellipse, the superposition of two oppositely directed point loads P is considered as shown in Fig. A-2.

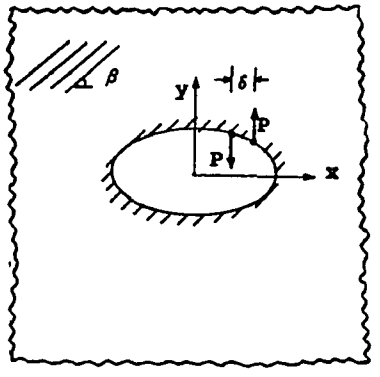

Figure A-2. Concentrated moment generated by an equivalent couple.

Taking the limit as δ approached zero and replacing $P\delta$ by M, we arrive at:

$$\Phi_j(\zeta_j) = \frac{M}{\pi a}\left(\frac{is_k}{s_j-s_k}\right)\left(\frac{t^2}{t^2-1}\right)\left(\frac{1}{t-\zeta_j}\right) - \frac{M}{4\pi(s_j-s_k)(a^2+b^2-z_0\bar{z}_0)}[A_1A_6+A_2A_5$$

$$+A_3A_8+A_4A_7+\frac{\bar{z}_0\left(1-\frac{b}{a}\frac{t^2+1}{t^2-1}\right)+z_0\left(1-\frac{b}{a}\frac{\bar{t}^2+1}{\bar{t}^2-1}\right)}{a^2+b^2-z_0\bar{z}_0}(A_1A_2+A_3A_4)], \tag{A.5}$$

where (j=1,2; k=2,1), and

$$A_1 = \frac{a}{2}\left[ias_k\left(t-\frac{1}{t}\right)-b\left(t+\frac{1}{t}\right)\right], \tag{A.6a}$$

$$A_2 = \frac{1}{\zeta_j} - \left(\frac{t}{t-\zeta_j}\right)\left[\left(\zeta_j+\frac{1}{\zeta_j}\right)-\left(t+\frac{1}{t}\right)\right], \tag{A.6b}$$

$$A_3 = \frac{ib}{2}\left[ia\left(t-\frac{1}{t}\right)+bs_k\left(t+\frac{1}{t}\right)\right], \tag{A.6c}$$

$$A_4 = \frac{1}{\zeta_j} + \left(\frac{t}{t-\zeta_j}\right)\left[\left(\zeta_j-\frac{1}{\zeta_j}\right)-\left(t-\frac{1}{t}\right)\right], \tag{A.6d}$$

$$A_5 = \frac{t^2}{t^2-1}\left[ias_k\left(1+\frac{1}{t^2}\right)-b\left(1-\frac{1}{t^2}\right)\right], \tag{A.6e}$$

$$A_6 = \frac{2}{a}\left(\frac{t^2}{t^2-1}\right)\left(\frac{1}{t-\zeta_j}\right)\left[\left(t-\frac{1}{t}\right)-\left(1-\frac{t}{t-\zeta_j}\right)\left(\left(\zeta_j+\frac{1}{\zeta_j}\right)-\left(t+\frac{1}{t}\right)\right)\right], \tag{A.6f}$$

$$A_7 = \frac{ib}{a}\left(\frac{t^2}{t^2-1}\right)\left[ia\left(1+\frac{1}{t^2}\right)+bs_k\left(1-\frac{1}{t^2}\right)\right], \tag{A.6g}$$

$$A_8 = \frac{2}{a}\left(\frac{t^2}{t^2-1}\right)\left(\frac{1}{t-\zeta_j}\right)\left[-\left(t+\frac{1}{t}\right)+\left(1-\frac{t}{t-\zeta_j}\right)\left(\left(\zeta_j-\frac{1}{\zeta_j}\right)-\left(t-\frac{1}{t}\right)\right)\right]. \tag{A.6h}$$

In Eqs. (A6a) to (A6h) the subscripts j and k range over 1 to 2 and 2 to 1, respectively. As before for the case of a crack with concentrated moment applied along its face, b is set equal to zero in Eq. (A.5) which becomes:

$$\begin{aligned}\Phi_j(\zeta_j) = {} & \frac{M}{\pi a}\left(\frac{is_k}{s_j-s_k}\right)\left(\frac{t^2}{t^2-1}\right)\left(\frac{1}{t-\zeta_j}\right) - \frac{M(ias_k)}{4\pi(s_j-s_k)(a^2-x_0^2)} \\ & \left\{\frac{t}{t-\zeta_j}\left[\left(t-\frac{1}{t}\right)-\left(1-\frac{t}{t-\zeta_j}\right)\left(\left(\zeta_j+\frac{1}{\zeta_j}\right)-\left(t+\frac{1}{t}\right)\right)\right]\right. \\ & \left.+\left[\frac{1}{\zeta_j}-\left(\frac{t}{t-\zeta_j}\right)\left(\left(\zeta_j+\frac{1}{\zeta_j}\right)-\left(t+\frac{1}{t}\right)\right)\right]\left[\frac{t^2+1}{t^2-1}+\frac{ax_0}{a^2-x_0^2}\left(t-\frac{1}{t}\right)\right]\right\},\end{aligned} \tag{A.7}$$

with (j=1,2; k=2,1). Using Eq. (2.21), the stress intensity factors are found to be:

$$K_I = \frac{Ma}{2\sqrt{\pi a}}\left[\frac{1}{(a-x_0)\sqrt{a^2-x_0^2}}\right] \quad \text{and} \quad K_{II} = 0. \tag{A.8}$$

Interestingly, these stress intensity factors are independent of material anisotropy and are identical to those of isotropic case [7].

APPENDIX B

A NON-JACOBIAN NUMERICAL QUADRATURE FOR SEMI-INFINITE INTEGRALS

Although in reality physical domains are all finite, many engineering problems have been solved in an unbounded domain due to its mathematical convenience. Most of the problems involving infinite domains require the evaluation of certain improper integrals over an infinite or semi-infinite range. In general, most of these improper integrals can only be estimated numerically.

In this appendix, a non-Jacobian numerical quadrature is proposed for evaluating improper integrals over a semi-infinite range. The quadrature first transforms the semi-infinite integration limit into a finite limit between -1 and 1. Standard numerical integration procedures such as Gauss-Chebyshev or Gauss-Legendre schemes can then be used to obtain the integral value. Unlike traditional methods using Laguerre or Hermite polynomials, numerical results show that no specific weight function is required for the proposed quadrature to converge as long as the integral exists. The transformation also includes a scale parameter which effectively expands the numerical-integration sampling points along its original semi-infinite integration path.

Without loss of generality the integrals to be computed can be expressed as:

$$I = \int_0^\infty f(x)dx. \tag{B.1}$$

This semi-infinite range of integration can be changed into a finite interval within -1 and 1 through the following transformation:

$$x = p\frac{(1+t)^c}{(1-t)^d} \qquad \text{where} \qquad p,c,d > 0, \tag{B.2}$$

then the Jacobian of the transformation is:

$$\frac{dx}{dt} = p[c(1+t)^{c-1}(1-t)^{-d} + d(1+t)^c(1-t)^{-d-1}], \tag{B.3}$$

and the integral becomes:

$$I = p[c\int_{-1}^{+1}(1+t)^{c-1}(1-t)^{-d}g(t)dt + d\int_{-1}^{+1}(1+t)^c(1-t)^{-d-1}g(t)dt], \tag{B.4}$$

where

$$g(t) = f[x(t)]. \tag{B.5}$$

It is noted that strong singularity occurs at the endpoint t=1 which corresponds to the original upper integration limit at infinity. Since the exponent of (1-t) term in the second integral of Eq. (B.4) is less than -1, the integrand cannot be expressed as a Jacobi orthogonal polynomial and the general Gauss-Jacobian quadrature formula cannot be applied. Here, the conventional Gauss-Legendre and Gauss-Chebyshev methods can be used instead to evaluate the transformed integral of Eq. (B.4). Using the Gauss-Legendre method the integral becomes:

$$I = p\int_{-1}^{+1} G_1(t)dt \approx p \sum_{i=1}^{n} w_i G_1(t_i), \tag{B.6}$$

where n is the Gauss-Legendre integration order, t_i the i^{th} root of the Legendre polynomial $P_n(t)$, w_i the weight factor corresponding to the root, and:

$$G_1(t) = [c(1+t)^{c-1}(1-t)^{-d} + d(1+t)^c(1-t)^{-d-1}]g(t). \tag{B.7}$$

Similarly for the Gauss-Chebyshev method, the integral becomes:

$$I = p\int_{-1}^{+1} \frac{1}{\sqrt{(1-t^2)}} G_2(t)dt \approx p\frac{\pi}{n} \sum_{i=1}^{n} G_2(t_i), \tag{B.8}$$

where n is the Gauss-Chebyshev integration order and

$$t_i = \cos \frac{(2i-1)}{2n}\pi, \qquad (i=1,2,\ldots,n), \tag{B.9}$$

$$G_2(t) = \sqrt{(1-t^2)}G_1(t). \tag{B.10}$$

The transformation shown in Eq. (B.2) involves three parameters. The first parameter p plays the role of scaling factor for the effective integration range, which is defined as the largest value corresponding to the farthest located sampling point of integration. The other two parameters c and d relate to the degree of singularity of the integrand. To test the valid ranges of these parameters and to check the validity of the proposed quadrature, the Gauss-Chebyshev method, as shown in Eq. (B.8), is used to evaluate the integral:

$$I = \int_0^{\infty} x^{m-1}e^{-x}dx, \tag{B.11}$$

which has an exact value of $\Gamma(m)$. This highly nonlinear integrand, $x^{m-1}e^{-x}$, has been used to estimate the accuracy of the classical Gauss-Laguerre quadrature. A few typical cases using a Gauss-Chebyshev integration order n=15, with c (or d) equal to 0.0001, 0.01, and 1 are shown in Fig. B-1. As can be seen from Fig. B-1 a very good agreement exists between the numerical results and the corresponding exact solution. Through parametric studies, it is found

that the optimized c and d, although depending on the exponential order m of the integrand, always occurs in the neighborhood of 1.

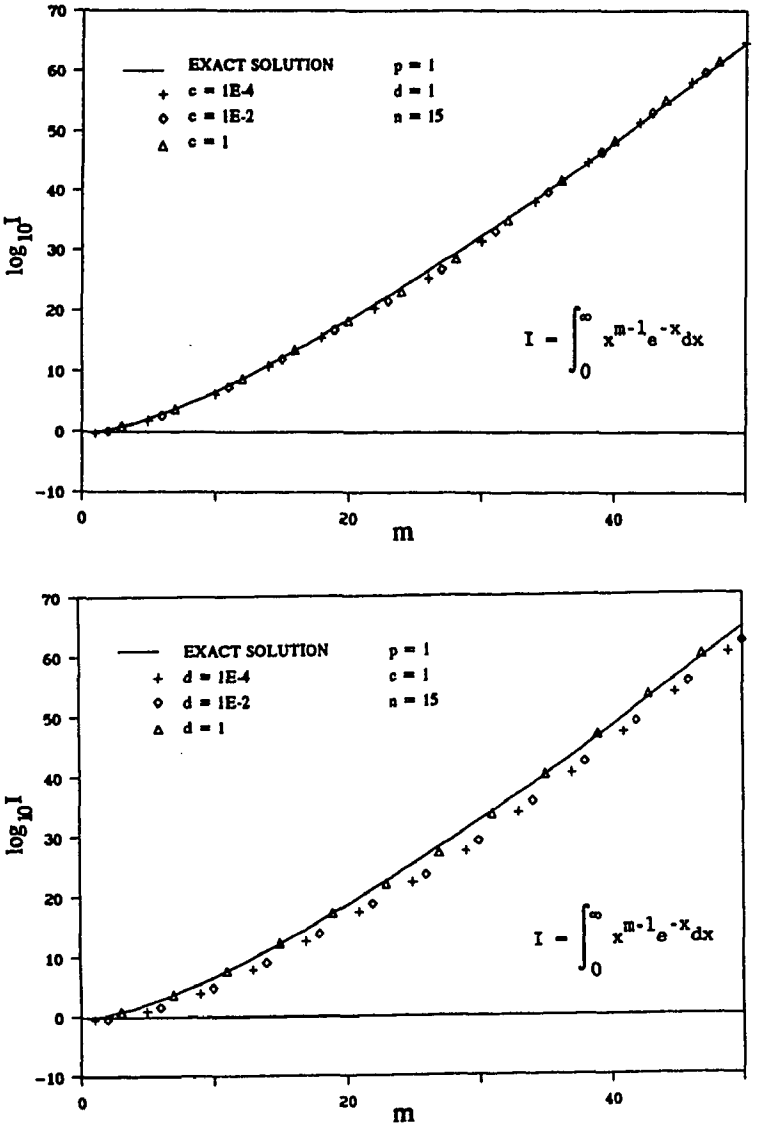

Figure B-1. Test integral evaluated by the proposed quadrature.

APPENDIX C

NUMERICAL RESULTS AND DISCUSSIONS FOR AN INFINITE ANISOTROPIC PLATE CONTAINING AN ELLIPTICAL HOLE OR A CRACK SUBJECTED TO GENERAL LOADINGS

To verify the proposed fundamental solutions, several problems with known exact solutions were compared. The first problem considered was the case when two vertical forces equal in value P and acting in opposite directions were applied at points (0,b) and (0,-b), respectively, as shown in Fig. C-1. The orthotropic material was assumed to have its fiber direction parallel to the x-axis. The circumferential stress $\sigma_{\theta\theta}$ along the elliptical hole and the Cartesian stress components σ_{xx}, σ_{yy} and τ_{xy} along a circle of radius a within the orthotropic medium were computed. As indicated in Fig. C-1 the results based on the proposed fundamental solutions are identical to those reported by Savin [3]. The second problem, as depicted in Fig. C-2, was concerned with an infinite anisotropic plate with an elliptical hole stretched by uniaxial tension σ normal to the major-axis of the hole. The proposed fundamental solutions were integrated within the range $(-\infty,+\infty)$ of two horizontal lines located far away from the elliptical hole. Numerical integrations involving infinite range were based on a numerical quadrature scheme given in Appendix B. Normalized circumferential stresses $\sigma_{\theta\theta}$ along the elliptical hole were computed. As shown in Fig. C-2, the numerical results are exact compared with those obtained analytically by Savin [3]. The third problem considered a vertical or a horizontal point load (P or Q) acting on a crack of length 2a in an orthotropic plane (β=0°). Figure C-3 shows the variation of mode I stress intensity factor K_I of the former case and of mode II stress

intensity factor K_{II} of the latter case. The results are identical to those reported by Embley [9]. Mode I and mode II stress intensity factors for an anisotropic plane with a crack of length 2a subjected to a concentrated moment located at various positions along the vertical axis of the crack are shown in Fig. C-4. The results for the corresponding isotropic case were also evaluated and shown to be in excellent agreement with Erdogan's [7] known solution. Effect of anisotropy on the stress intensity factors are illustrated by varying the fiber direction β. Figure C-5 shows the mode I and mode II stress intensity factors due to a vertical point load P or a horizontal point load Q acting along the vertical central line of a crack with length 2a. For the vertical point load case K_I decreases drastically as the loading point goes far away from the crack. For the horizontal point load case K_I becomes negative when y_o/a is larger than 0.4, where d is the y-coordinate of the loading point. This implies that the crack faces may stick to each other. The corresponding mode II stress intensity factors K_{II}, reduce drastically when the loads are away from the crack.

Now that the validity of the proposed fundamental solutions have been established, they can be applied directly to various mechanics problems involving elliptical holes or cracks. As an example, we consider a uniaxially stretched infinite ductile plate with a yield strength Y containing a crack of length 2a as shown in Fig. C-6. Following the classical Dugdale's strip yielding model [22], Tsai [23] showed that the size of strip yield zone a_Y for an infinite anisotropic plate can be expressed as:

$$a_Y/a = 2\sin^2(\pi\alpha/4), \qquad (C.1)$$

where α is the ratio p/Y. This equation states that anisotropy has no effect on the size of Dugdale zone a_Y. Figure C-6 shows the normalized crack opening displacements (COD) for various α values. In this graph W_{max} is the maximum COD at center of the crack. As shown in Fig. C-6 the results are in excellent agreement with Tsai's solution [23]. The final problem considered was that of a Dugdale crack with symmetric vertical point loads P applied at the center as shown in Fig. C-7(a), which also shows the numerically obtained Dugdale zone size a_Y as a function of Y and P. This problem can be important when cracks are initiated by a wedge or a split force. Again as shown in Fig. C-7(a), the size of Dugdale zone is not a function of anisotropy. It is worth mentioning that in Fig. C-7(a) as a_Y approaches zero, Y tends to infinity which indicates behavior of a brittle material. Knowing a_Y from Fig. C-7(a), the corresponding COD profiles were evaluated and are shown in Fig. C-7(b), which are quite different from those depicted in Fig. C-6, the uniaxial tension case.

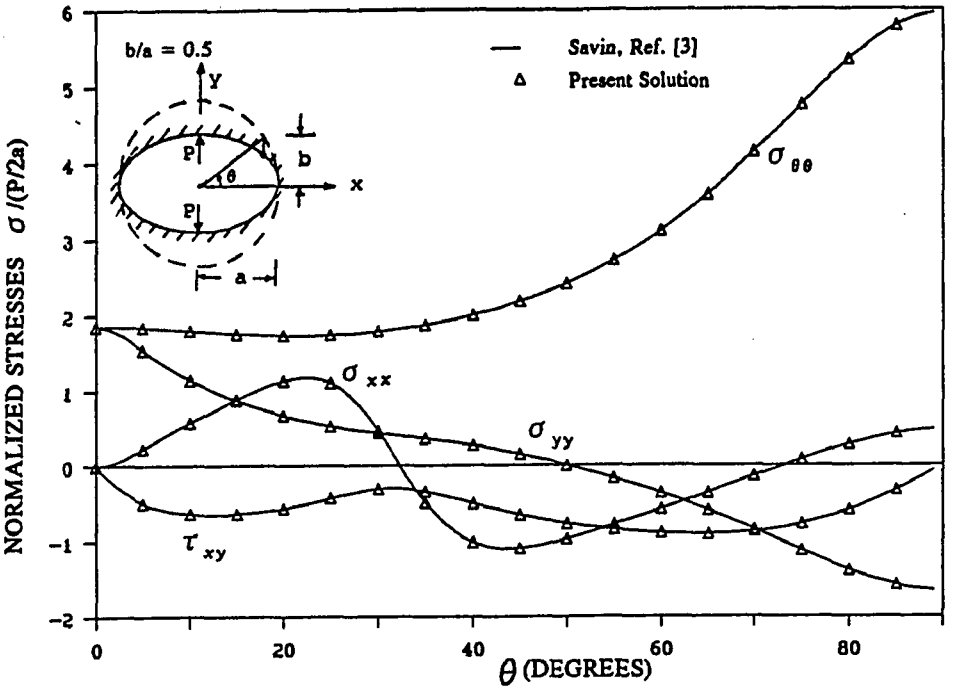

Figure C-1. Stress distributions due to symmetric vertical point loads on an elliptical hole.

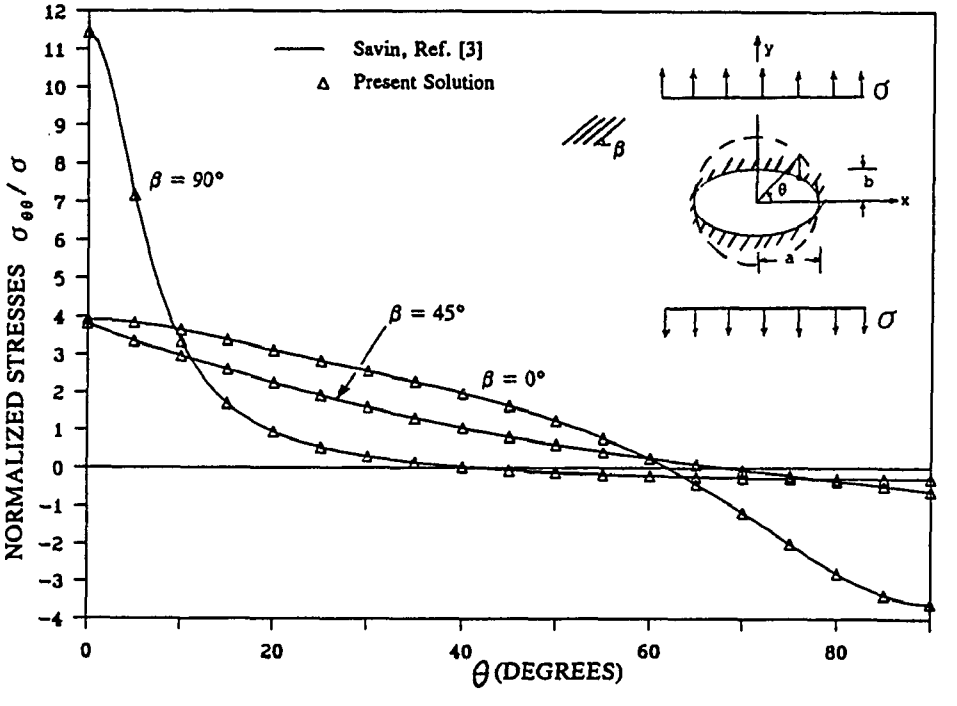

Figure C-2. Circumferential stresses of a uniformly stretched infinite anisotropic plate weakened by an elliptical hole.

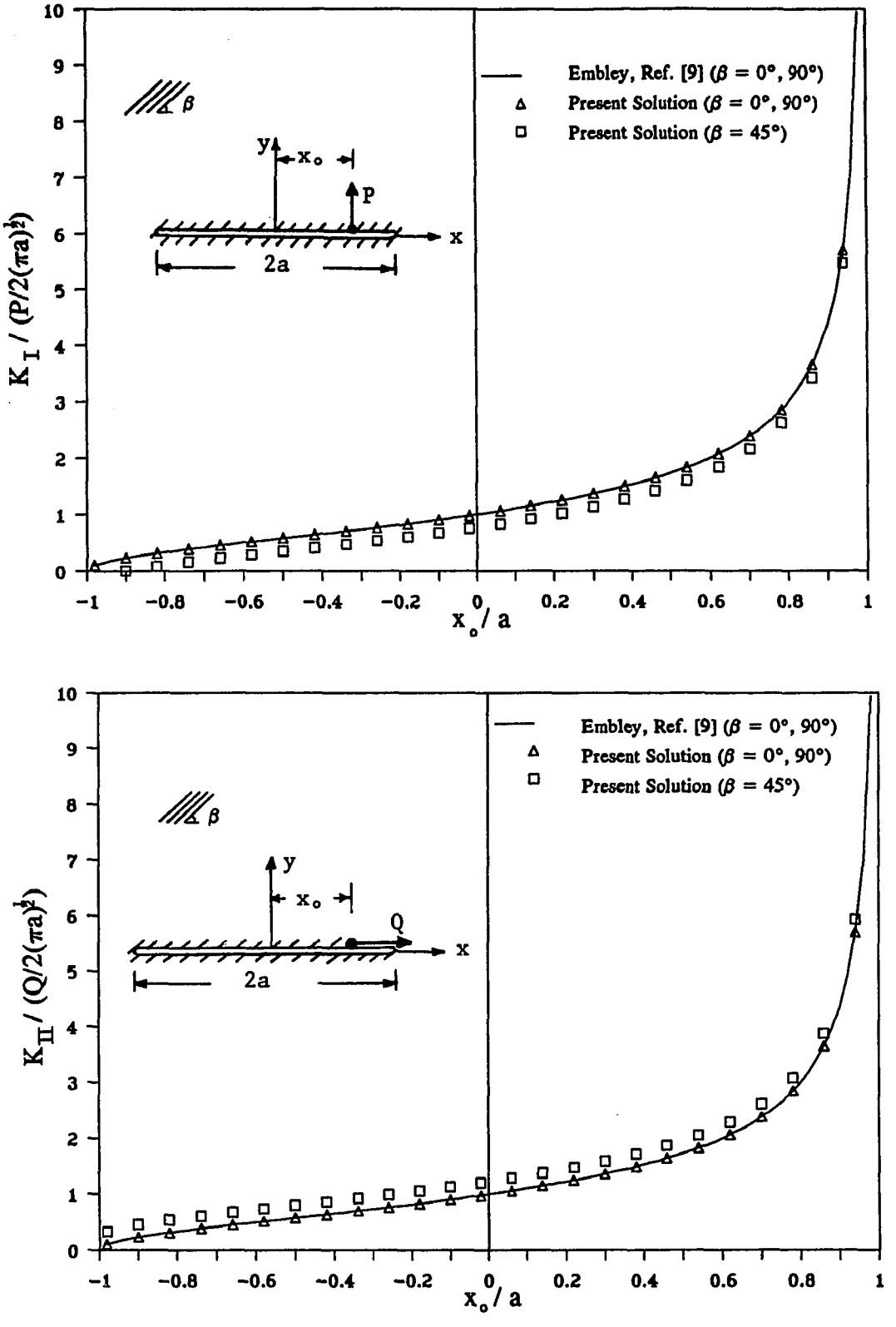

Figure C-3. Stress intensity factors due a point load acting on the face of a crack in an anisotropic plate.

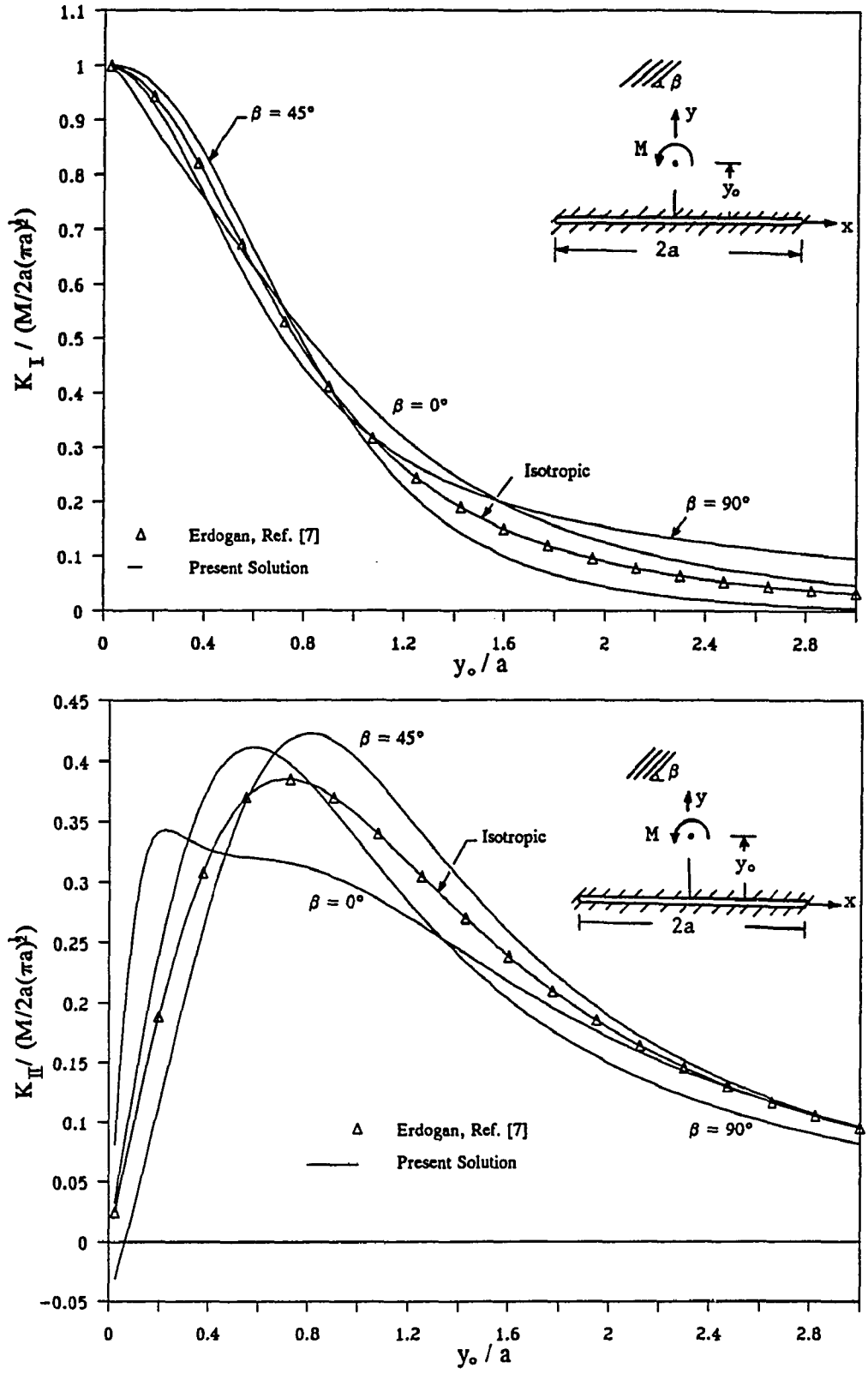

Figure C-4. Stress intensity factors due to a concentrated moment acting along the vertical central line of a crack in an anisotropic plate.

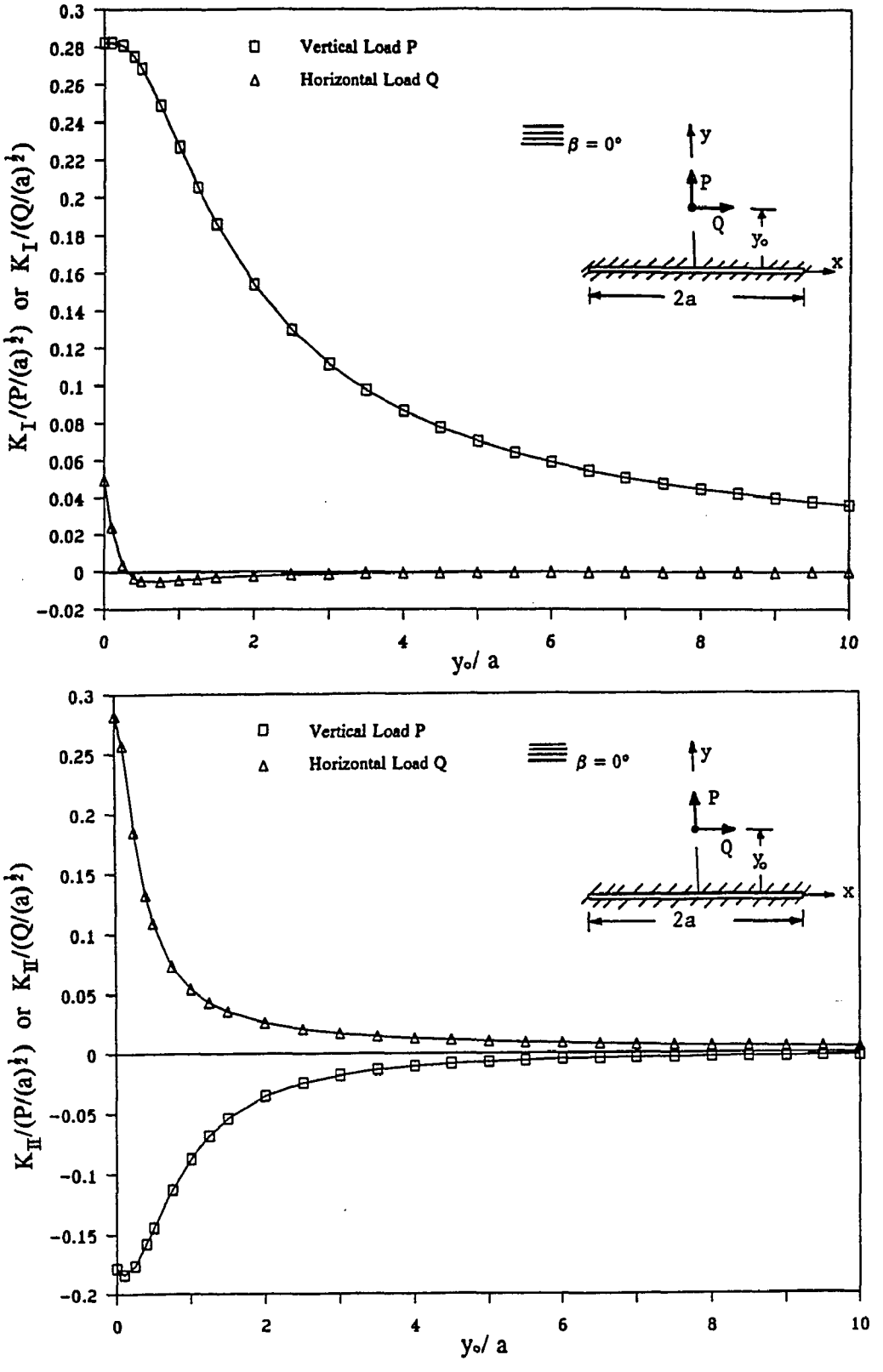

Figure C-5. Stress intensity factors due to point loads acting along the vertical central line of a crack in an anisotropic plate.

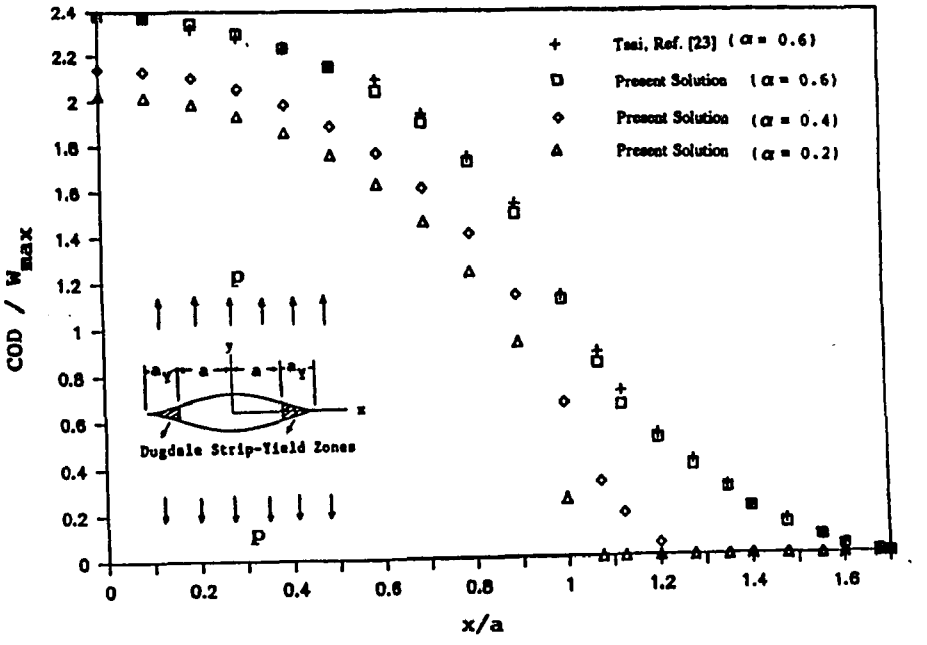

Figure C-6. Crack Opening Displacements of a Dugdale crack in an anisotropic plate under uniform tension.

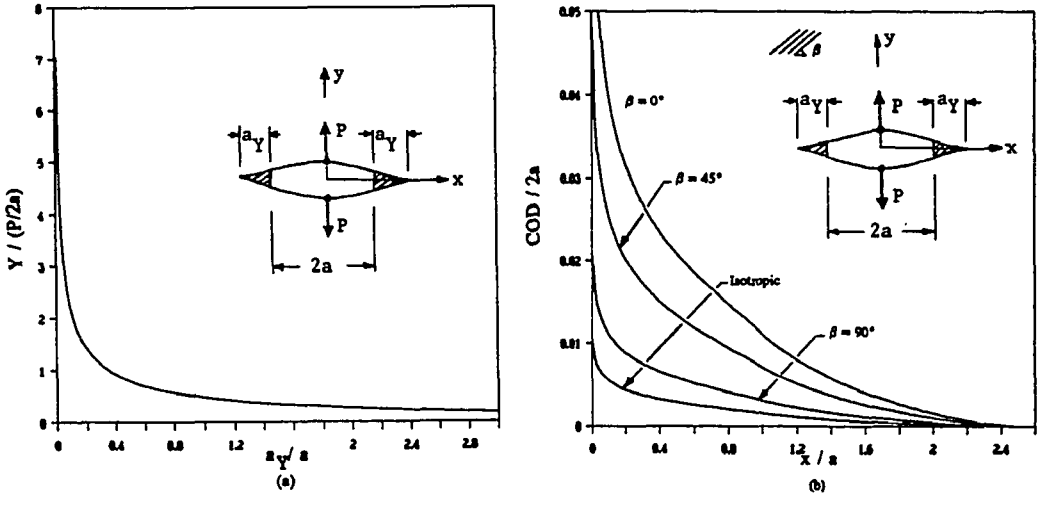

Figure C-7. A Dugdale crack in an anisotropic plate subjected to two central, symmetric, vertical point loads.

APPENDIX D

STRESS-STRAIN RELATIONS FOR A LAMINA OF ARBITRARY ORIENTATION

In Ch. II, the stress-strain relations were defined in the principal directions of orthotropy. However, the principal material directions often do not coincide with the geometrical coordinates natural to the problem. Given the stress-strain relations in the principal material directions 1-2, which are oriented at some finite angle β from the geometrical coordinates x-y, the stress-strain relations in the x-y system can be obtained by:

$$\begin{Bmatrix} \epsilon_x \\ \epsilon_y \\ \gamma_{xy} \end{Bmatrix} = \begin{bmatrix} \bar{a}_{11} & \bar{a}_{12} & \bar{a}_{16} \\ \bar{a}_{12} & \bar{a}_{22} & \bar{a}_{26} \\ \bar{a}_{16} & \bar{a}_{26} & \bar{a}_{66} \end{bmatrix} \begin{Bmatrix} \sigma_x \\ \sigma_y \\ \tau_{xy} \end{Bmatrix}, \tag{D.1}$$

where

$$\bar{a}_{11} = a_{11}\cos^4\beta+(2a_{12}+a_{66})\sin^2\beta\cos^2\beta+a_{22}\sin^4\beta, \tag{D.2a}$$

$$\bar{a}_{12} = a_{12}(\sin^4\beta+\cos^4\beta)+(a_{11}+a_{22}-a_{66})\sin^2\beta\cos^2\beta, \tag{D.2b}$$

$$\bar{a}_{22} = a_{11}\sin^4\beta+(2a_{12}+a_{66})\sin^2\beta\cos^2\beta+a_{22}\cos^4\beta, \tag{D.2c}$$

$$\bar{a}_{16} = (2a_{11}-2a_{12}-a_{66})\sin\beta\cos^3\beta-(2a_{22}-2a_{12}-a_{66})\sin^3\beta\cos\beta, \tag{D.2d}$$

$$\bar{a}_{26} = (2a_{11}-2a_{12}-a_{66})\sin^3\beta\cos\beta-(2a_{22}-2a_{12}-a_{66})\sin\beta\cos^3\beta, \tag{D.2e}$$

$$\bar{a}_{66} = 2(2a_{11}+2a_{22}-4a_{12}-a_{66})\sin^2\beta\cos^2\beta+a_{66}(\sin^4\beta+\cos^4\beta). \tag{D.2f}$$

Recall that the a_{ij} (i,j=1,2,6) were defined in terms of the engineering constants in Eq. (2.2).

APPENDIX E

NEAR-TIP STRESS AND DISPLACEMENT FIELDS FOR A CRACK IN A PLANE ANISOTROPIC MEDIUM

Knowledge of the stress and displacement fields in the vicinity of the crack tip plays an essential role in analyzing the fracture strength of cracked bodies. In this Appendix, the near field solutions (i.e., expressions for the stress and displacement fields near the crack tip in term of the mode I and mode II stress intensity factors) are given. Introducing the polar coordinates r-θ, where r is the radial distance from the crack tip and θ is the angle between the radius vector and the axis of the crack, the derivative of the stress functions can be approximated by [8]:

$$\Phi_j'(z_j) = \frac{s_k(K_I+\frac{K_{II}}{s_k})}{2\sqrt{2\pi r(\cos\theta+s_j\sin\theta)}(s_k-s_j)} + O(\sqrt{r}), \quad (j=1,2;k=2,1). \quad (E.1)$$

In the above, the higher order terms of r may be disregarded as r becomes small compared with other planar dimensions. The stress and displacement components in the vicinity of the crack tip may then be obtained as:

Mode I loading:

$$\sigma_x = \frac{K_I}{\sqrt{2\pi r}} \mathrm{Re}\left[\frac{s_1 s_2}{s_1-s_2}\left(\frac{s_2}{\theta_2} - \frac{s_1}{\theta_1}\right)\right], \quad (E.2a)$$

$$\sigma_y = \frac{K_I}{\sqrt{2\pi r}} \mathrm{Re}\left[\frac{1}{s_1-s_2}\left(\frac{s_1}{\theta_2} - \frac{s_2}{\theta_1}\right)\right], \quad (E.2b)$$

$$\tau_{xy} = \frac{K_I}{\sqrt{2\pi r}} \mathrm{Re}\left[\frac{s_1 s_2}{s_1-s_2}\left(\frac{1}{\theta_1} - \frac{1}{\theta_2}\right)\right], \quad (E.2c)$$

$$u = K_I\sqrt{2r/\pi}\ \mathrm{Re}\left[\frac{1}{s_1-s_2}\left(s_1 p_2 \theta_2 - s_2 p_1 \theta_1\right)\right], \quad (E.2d)$$

$$v = K_I\sqrt{2r/\pi}\ \mathrm{Re}\left[\frac{1}{s_1-s_2}\ (s_1q_2\theta_2-s_2q_1\theta_1)\right], \tag{E.2e}$$

Mode II loading:

$$\sigma_x = \frac{K_{II}}{\sqrt{2\pi r}}\ \mathrm{Re}\left[\frac{1}{s_1-s_2}\ (\frac{s_2^2}{\theta_2} - \frac{s_1^2}{\theta_1})\right], \tag{E.3a}$$

$$\sigma_y = \frac{K_{II}}{\sqrt{2\pi r}}\ \mathrm{Re}\left[\frac{1}{s_1-s_2}\ (\frac{1}{\theta_2} - \frac{1}{\theta_1})\right], \tag{E.3b}$$

$$\tau_{xy} = \frac{K_{II}}{\sqrt{2\pi r}}\ \mathrm{Re}\left[\frac{1}{s_1-s_2}\ (\frac{s_1}{\theta_1} - \frac{s_2}{\theta_2})\right], \tag{E.3c}$$

$$u = K_{II}\sqrt{2r/\pi}\ \mathrm{Re}\left[\frac{1}{s_1-s_2}\ (p_2\theta_2-p_1\theta_1)\right], \tag{E.3d}$$

$$v = K_{II}\sqrt{2r/\pi}\ \mathrm{Re}\left[\frac{1}{s_1-s_2}\ (q_2\theta_2-q_1\theta_1)\right], \tag{E.3e}$$

where $\theta_j=\sqrt{\cos\theta+s_j\sin\theta}$ (j=1,2) and p_j and q_j (j=1,2) are given in Eqs. (2.14a,b). The above expressions indicate that, similar to the isotropic case, an elastic stress singularity of the order $\frac{1}{\sqrt{r}}$ exists at the crack tip in an anisotropic domain.

APPENDIX F

JUMP CONDITION IN BIE

In the following, a simple method [21] is reviewed to evaluate the "jump" or the "free term" $\frac{1}{2}g_i(\hat{z})$ in Eq. (4.1). The "jump" condition is due to the strong -1 singularity in the first integral of Eq. (4.1) when $z=\hat{z}^0$. Figure F-1(a) shows a smooth portion of the boundary S near $\hat{z}^0$ which includes a small semi-circular path, of radius $\rho\to 0$, to envelope and thus avoid $\hat{z}^0$. It is intended to evaluate the singular portion of the first integral in Eq. (4.1) which arises when $z\to\hat{z}^0$ on S from inside the domain. If we consider $\hat{z}^0$ to be the origin of a local coordinate system ρ-θ, then one can prove easily:

$$T_{ijk}(\hat{z},\hat{\rho})n_j(\hat{z}) = \frac{(z-\hat{z}^0)_j}{2\pi\rho^2}n_j(\hat{z}) = \frac{\hat{z}_j n_j}{2\pi\rho^2} = \frac{1}{2\pi\rho}, \quad (i,j,k=1,2). \quad (F.1)$$

But $ds=\rho d\theta$ and whence

$$\int_{\Delta s} T_{ijk}(\hat{z}^0,\hat{\rho})n_j(\hat{z})g_k(\hat{\rho})ds(\hat{\rho}) = g_i(\hat{z})\int_0^{\pi}\frac{1}{2\pi\rho}\rho d\theta = \frac{1}{2}g_i(\hat{z}), \quad (F.2)$$

where n_j is taken as the outward normal to the boundary. Therefore, Eq. (4.1) has taken account of this "jump" or "free term" separately and the first integral in that equation is taken around the remaining boundary of S ($\hat{z}\neq\hat{\rho}$) as a Cauchy principal value. If on the other hand the boundary is not smooth (as in Fig. F-1(b)), i.e. S does not posses a unique tangent, then the limits of integration in Eq. (F.2) will not be 0 to π and the coefficient of $g_i(\hat{z})$ will not be 1/2. In

this case, the limits of integration are now 0 to α and the "jump" is $(\alpha/2\pi)g_i(\hat{z})$.

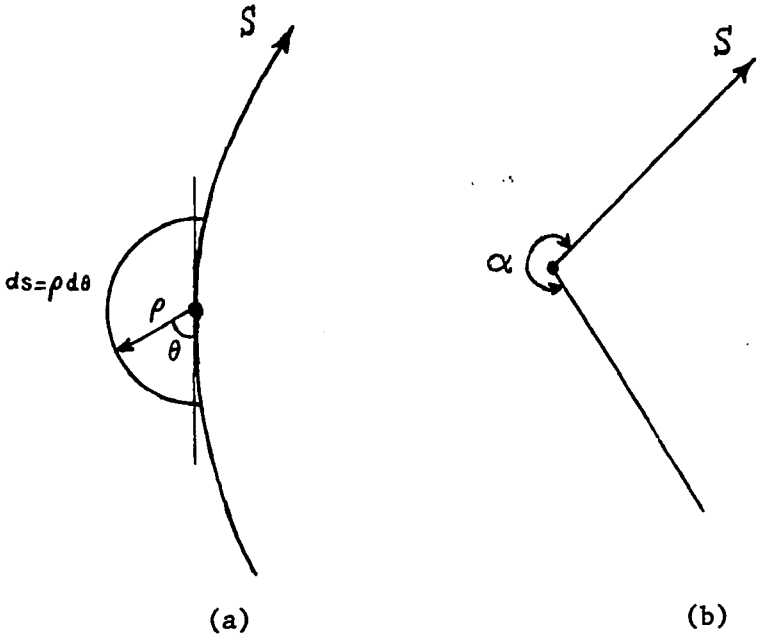

Figure F-1. Semi-circular path assumed on the boundary to avoid the singular point

APPENDIX G

EFFECT OF ELEMENT SIZE

As in other numerical methods of solution, there are several factors involved in obtaining accurate results using BIE. But generating the right mesh for the specific problem being considered is usually the most important one of them all. Obviously the larger the number of boundary elements specified, the higher the accuracy obtained. But a good engineering judgement involves using the least possible number of elements, i.e. the smallest computational time, to obtain a desired accuracy. For most practical engineering problems an accuracy of to within 3% relative error is acceptable.

Here to show the effect of variation of element size, we consider as an example the problem considered in Fig. 5.1.1, i.e. a crack emanating from a circular hole in an isotropic plate under uniform tension. A crack length ratio of a/R=1 was assumed and the number of elements varied between 4 and 70, which were assumed equal in length. The values for mode I stress intensity factor as compared with the value given by Shivakumar and Forman [30] (K_I/K_o=1.308) are depicted in Fig. G-1. As can be seen from Fig. G-1, even 20 elements produces results well within 3% difference with the value given in [30]. But from the results obtained in this study it was found that, on average, for all the problems considered a total number of boundary elements between 40 to 60 produces results within 3% difference with known solutions for moderate sized cracks.

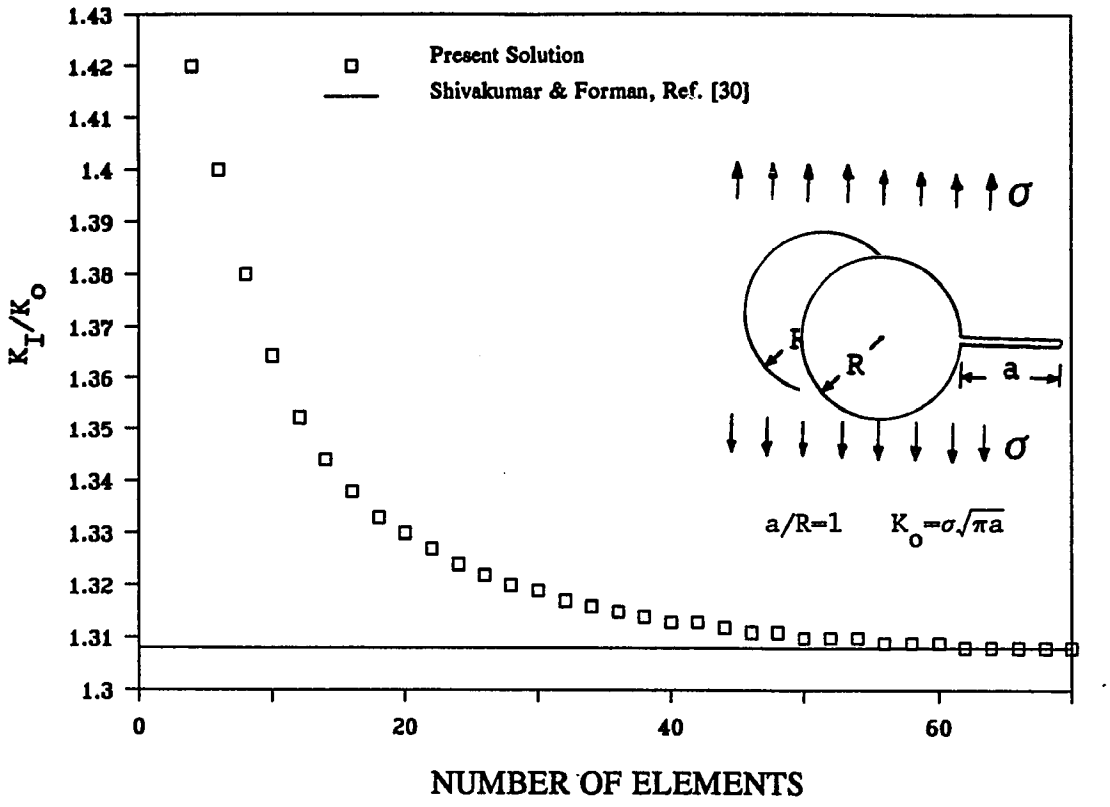

Figure G-1. Dependence of numerical accuracy on element size for an example problem

REFERENCES

[1] S. G. Lekhnitskii, "Theory of Elasticity of an Anisotropic Elastic Body," Holden-Day, Inc., San Francisco, 1963.

[2] S. G. Lekhnitskii, "Anisotropic Plates," Gordon and Breach Science Publishers, New York, 1968.

[3] G. N. Savin, "Stress Concentration Around Holes," Pergamon Press, New York, 1961.

[4] H. J. Konish and J. M. Whitney, "Approximate Stresses in an Orthotropic Plate Containing a Circular Hole," Journal of Composite Materials, Vol. 9, pp. 157-166, 1975.

[5] S. C. Tan, "Laminated Composites Containing an Elliptical Opening. I. Approximate Stress Analyses and Fracture Models," Journal of Composite Materials, Vol. 21, pp. 925-948, 1987.

[6] S. E. Ueng and J. K. Lin, "Stress Concentrations in Composite Laminates," Journal of Engineering Mechanics, ASCE, Vol. 113, pp. 1181-1193, 1987.

[7] F. Erdogan, "On the Stress Distribution on Plates with Collinear Cuts Under Arbitrary Loads," Proceedings of the Fourth U.S. National Congress of Applied Mechanics, ASME, pp. 547-553, 1962.

[8] G. C. Sih, P. C. Paris, and G. R. Irwin, "On cracks in Rectilinearly Anisotropic Bodies," International Journal of Fracture Mechanics, Vol. 1, pp. 189-203, 1965.

[9] G. T. Embley, "Cracks in Anisotropic Bodies in a State of Generalized Plane Deformation," M.S. Thesis, Lehigh University, 1968.

[10] M. D. Snyder and T. A. Cruse, "Boundary-Integral Analysis of Cracked Anisotropic Plates," International Journal of Fracture, Vol. 11, pp. 315-328, 1975.

[11] D. L. Clements and M. D. Haselgrove, "A Boundary Integral Equation Method for a Class of Crack Problems in Anisotropic Elasticity," International Journal of Computer Mathematics, Vol. 12, pp. 267-278, 1983.

[12] N.I. Muskhelishvili, "Some Basic Problems of the Mathematical Theory of Elasticity," 4th ed., Noordhoff, Groningen, The Netherlands, 1963.

[13] W. T. Ang, "A Boundary Integral Solution for the Problem of Multiple Interacting Cracks in an Elastic Material," International Journal of Fracture, Vol. 31, pp. 259-270, 1986.

[14] A. M. Sadegh, "On the Problem of a Plane, Finite, Linear Elastic Region Containing a Hole of Arbitrary Shape: A Boundary Integral Approach," Doctoral Dissertation, Michigan State University, 1978.

[15] M. Denda, "A dislocation and a point force in an anisotropic medium with an elliptical hole," Acta Mechanica, Vol. 74, pp. 221-225, 1988.

[16] L. M. Milne-Thomson, "Plane Elastic Systems," Springer-Verlag, 1960.

[17] A. E. Green and W. Zerna, "Theoretical Elasticity," Clarendon Press, 1954.

[18] T. A. Cruse, "Interactive Program in Advanced Composites Technology: Interim Technical Report," Report SM-72-31, Carnegie-Mellon University, Pittsburgh, Pennsylvania, 1972.

[19] G.C. Sih and H. Liebowitz, "Mathematical Theories of Brittle Fracture," In "Fracture: An Advanced Treatise," Vol. 2 (Edited by H. Liebowitz), Academic Press, New York, p. 67, 1968.

[20] T. A. Cruse, "Numerical Evaluation of Elastic Stress Intensity Factors by the Boundary-Integral Equation Method," In "The Surface Crack: Physical Problems and Computational Solutions," ASME, New York, pp. 153-170, 1972.

[21] P. K. Banerjee and R. Butterfield, "Boundary Element Methods in Engineering Science," McGraw-Hill, New York, 1981.

[22] D. S. Dugdale, "Yielding of Steel Sheets Containing Slits," Journal of Mechanics and Physics of Solids, Vol. 8, pp. 100-104, 1960.

[23] Y. M. Tsai, "Central Ductile Crack in an Orthotropic Strip of Finite Width," Journal of Composite Materials, Vol. 16, pp. 358-370, 1982.

[24] J. K. Lin and S. E. Ueng, "Stresses in a Laminated Composite With two Elliptical Holes," Composites & Structures, Vol. 7, pp. 1-20, 1987.

[25] J. M. Whitney and R. J. Nuismer, "Stress Fracture Criteria for Laminated Composites Containing Stress Concentrations," Journal of Composite Materials, Vol. 8, pp. 253-265, 1974.

[26] F. K. Chang, R. A. Scott, and G. S. Springer, "Failure of Composite Laminates Containing Pin Loaded Holes-Method of Solution," Journal of Composite Materials, Vol. 18, pp. 255-278, 1984.

[27] O. L. Bowie, "Analysis of an Infinite Plate Containing Radial Cracks Originating at the Boundary of an Internal Circular Hole," Journal of Mathematics & Physics, Vol. 25, pp. 60-71, 1956.

[28] H. K. Kutter, "Stress Analysis of a Pressurized Circular Hole With Radial Cracks in an Infinite Elastic Plate, "International Journal of Fracture Mechanics, Vol. 6, pp. 233-247, 1970.

[29] Y. C. Hsu, "The Infinite Sheet With Cracked Cylindrical Hole Under Inclined Tension or In-plane Shear," International Journal of Fracture, Vol. 11, pp. 571-581, 1975.

[30] V. Shivakumar and R. G. Forman, "Green's Function for a Crack Emanating From a Circular Hole in an Infinite Sheet," International Journal of Fracture, Vol. 16, pp. 305-316, 1980.

[31] J. C. Newman, Jr., "An Improved Method of Collocation for the Stress Analysis of Cracked Plates With Various Shaped Boundaries. NASA TN D-6376, 1971.

[32] J. Tweed and D. P. Rooke, "The Distribution of Stress Near the tip of a Radial Crack at the Edge of a Circular Hole," International Journal of Engineering Science, Vol. 11, pp. 1185-1195, 1973.

[33] J. Tweed and D. P. Rooke, "The Elastic Problem for an Infinite Solid Containing a Circular Hole With a Pair of Radial Edge Cracks of Different Lengths," International Journal of Engineering Science, Vol. 14, pp. 925-933, 1976.

[34] J. Tweed and D. P. Rooke, "The Stress Intensity Factor for a Crack in a Symmetric Array Originating at a Circular Hole in an Infinite Elastic Solid," International Journal of Engineering Science, Vol. 13, pp. 653-660, 1975.

[35] D. P. Rooke and J. Tweed, "Stress Intensity Factors for a Crack at the Edge of a Pressurized Hole," International Journal of Engineering Science, Vol. 18, pp. 109-121, 1980.

[36] J. Tweed and D. P. Rooke, "The Stress Intensity Factor for a Crack at the Edge of a Loaded Hole, International Journal of Solids & Structures, Vol. 15, pp. 899-906, 1979.

[37] A. F. Grandt, "Stress Intensity Factors for Some Through-cracked Fastener Holes," International Journal of Fracture, Vol. 11, pp. 283-294, 1975.

[38] D. P. Rooke, "Compounded Stress Intensity Factors for Cracks at Fastener Holes," Engineering Fracture Mechanics, Vol. 19, pp. 359-374, 1984.

[39] A. A. Rubinstein and A. M. Sadegh, "Analysis of a Crack Emanating From a Circular Hole in a Loaded Plane," International Journal of Fracture, Vol. 32, pp. 47-57, 1986.

[40] M. Isida, D. H. Chen, and H. Nisitani, "Plane Problems of an Arbitrary Array of Cracks Emanating From the Edge of an Elliptical Hole," Engineering Fracture Mechanics, Vol. 21, pp. 983-995, 1985.

[41] D. M. Neal, "Stress Intensity Factors for Cracks Emanating From Rectangular Cutouts," International Journal of Fracture Mechanics, Vol. 6, pp. 393-400, 1970.

[42] L. T. Berezhnitskii, "Propagation of Cracks Terminating at the Edge of a Curvilinear Hole in a Plate," Fiziko-Khimicheskaya Mekhanika Materialov (Soviet Materials Science) Vol. 2, pp. 21-31, 1966.

[43] A. A. Kaminskii, "Determination of the Critical Load Causing Crack Propagation Near a Curvilinear Hole," Fiziko-Khimicheskaya Mekhanika Materialov (Soviet Materials Science) Vol. 2, pp. 32-39, 1966.

[44] S. S. Wang and J. F. Yau, "An Analysis of Cracks Emanating From a Circular Hole in Unidirectional Fiber Reinforced Composites, Engineering Fracture Mechanics, Vol. 13, pp. 57-67, 1980.

[45] S. K. Cheong and C. S. Hong, "Analysis of Cracks Emanating From a Circular Hole in an Orthotropic Plate Under Mixed Mode Deformation," Engineering Fracture Mechanics, Vol. 31, pp. 237-248, 1988.

[46] O. L. Bowie and D. M. Neal, "A Modified Mapping-collocation Technique for Accurate Calculation of Stress Intensity Factors," International Journal of Fracture, Vol. 6, pp. 199-206, 1970.

[47] J. P. Waszczak and T. A. Cruse, "Failure Mode and Strength Predictions of Anisotropic Bolt Bearing Specimens," Journal of Composite Materials, Vol. 5, pp. 421-425, 1971.

[48] D. L. Ball, "The Development of Mode I, Linear-Elastic Stress Intensity Factor Solutions for Cracks in Mechanically Fastened Joints," Engineering Fracture Mechanics, Vol. 27, pp. 653-681, 1987.

[49] A. F. Grandt, Jr., "Stress Intensity Factors for Cracked Holes and Rings Loaded With Polynomial Crack Face Pressure Distributions," International Journal of Fracture, Vol. 14, pp. R221-R229, 1978.

[50] A. F. Grandt, Jr. and T. E. Kullgren, "Tabulated Stress Intensity Factor Solutions for Flawed Fastener Holes," Engineering Fracture Mechanics, Vol. 18, pp. 435-451, 1983.

[51] D. J. Cartwright and G. A. Ratcliffe, "Strain Energy Release Rate for Radial Cracks Emanating From a Pin Loaded Hole," International Journal of Fracture Mechanics, Vol. 8, pp. 175-181, 1972.

[52] D. P. Rooke and S. M. Hutchins, "Stress Intensity Factors for Cracks at Loaded Holes - Effect of Load Distribution," Journal of Strain Analysis, Vol. 19, pp. 81-96, 1984.

[53] V. Shivakumar and Y. C. Hsu, "Stress-Intensity Factors for Cracks Emanating From the Loaded Fastener Hole," in "Fracture Mechanics and Technology," (Edited by G. C. Sih and C. L. Chon) Sijthoff & Noordhoff, The Netherlands, pp. 1187-1200, 1977.

[54] J. Tweed, S. C. Das, and D. P. Rooke, "The Stress Intensity Factors of a Radial Crack in a Finite Elastic Disc," International Journal of Engineering Science, Vol. 10, pp. 323-335, 1972.

[55] D. P. Rooke and J. Tweed, "The Stress Intensity Factors of a Radial Crack in a Finite Rotating Elastic Disc," International Journal of Engineering Science, Vol. 10, pp. 709-714, 1972.

[56] J. Tweed and D. P. Rooke, "The Stress Intensity Factor of an Edge Crack in a Finite Elastic Disc," International Journal of Engineering Science, Vol. 11, pp. 65-73, 1973.

[57] D. P. Rooke and J. Tweed, "The Stress Intensity Factor of an Edge Crack in a Finite Rotating Elastic Disc," International Journal of Engineering Science, Vol. 11, pp. 279-283, 1973.

[58] D. P. Rooke and J. Tweed, "The Stress Intensity Factors of a Radial Crack in a Point Loaded Disc," International Journal of Engineering Science, Vol. 11, pp. 285-290, 1973.

[59] D. P. Rooke and J. Tweed, International Journal of Engineering Science, Vol. 26, pp. 1059, 1988.

[60] S. Y. Yarema, "Analysis of Cracked Disk Specimens," Engineering Fracture Mechanics, Vol. 12, pp. 365-375, 1979.

[61] M. Isida, "Arbitrary Loading Problems of Doubly Symmetric Regions Containing a Central Crack," Engineering Fracture Mechanics, Vol. 7, pp. 505-514, 1975.

[62] C. Shangchow, "An Equivalent Procedure for the Evaluation of the Stress Intensity Factors of a Radial Crack in a Disc," International Journal of Engineering Science, Vol. 21, pp. 1247-1252, 1983.

[63] L. L. Libatskii and S. E. Kovchik, "Fracture of Discs Containing Cracks," Fiz.-Khim. Mech. Mat. (Soviet Materials Science) Vol. 3, pp. 458-464, 1967.

[64] B. M. Liaw, A. S. Kobayashi, and A. F. Emery, "Double Noding Technique for Mixed Mode Crack Propagation Studies," International Journal for Numerical Methods in Engineering, Vol. 20, pp. 967-977, 1984.

[65] D. P. Rooke and D. J. Cartwright, "Compendium of Stress Intensity Factors," Her Majesty's Stationery Office, London, 1976.

[66] R. Bennison, "The use of Composite Fly Wheels for Braking Energy Recovery in Road Transport Vehicles," Composites, Vol. 8, pp. 137-138, 1977.

[67] M. Isida, "On the Determination of Stress Intensity Factors for Some Common Structural Problems," Engineering Fracture Mechanics, Vol. 2, pp. 61-79, 1970.

[68] R. M. Jones, "Mechanics of Composite Materials," McGraw-Hill Book Company, New York, 1975.